SIMULATION OF IRON CORROSION IN AERATED ACID SOLUTIONS

A Thesis

Submitted to the College of Engineering of

Nahrain University in Partial Fulfillment of the

Requirements for the Degree of Master of Science

in Chemical Engineering

by

Ethar Maqusod Jassar AL-Rawi

(B.Sc. in Chemical Engineering 2006)

Shawal 1430

September 2009

CERTIFICATION

We certify that this theses entitled **"SIMULATION OF MATALS CORROSION IN AREATED ACIDS"** was prepared by **Ethar Maqusod Jassar AL-Rawi** under our supervision at Nahrain University, College of Engineering, in partial fulfillment of the requirements for the degree of Master of Science in Chemical Engineering.

Signature:
Name: Prof Dr.
Qasim J. M. Slaiman
(**Supervisor**)

Date: 1 / 11 / 2009

Signature:
Name: Assistant Prof. Dr.
Basim O. Hasan
(**Supervisor**)

Date: 12/10/2009

Signature:
Name: Prof Dr. Qasim J. M. Slaiman
(Head of Department)
Date: 1 / 11 / 2009

CERTIFICATE

We certify, as an examining committee, that we have read the thesis entitled "**SIMULATION OF IRON CORROSION IN AERATED ACID SOLUTIONS**" examined the student **Ethar Maqusod Jassar AL-Rawi** in its content and found it meets the standard of thesis for the degree of Master of Science in Chemical Engineering.

Signature:
Name: Prof. Dr.
Qasim J. M. Slaiman
(Supervisor)
Date: 1 / 11/ 2009

Signature:
Name: Assistant Prof. Dr.
Basim O. Hasan
(Supervisor)
Date: 12 /10/ 2009

Signature: M. Sha
Name: Assistant Prof. Dr.
Muslet Sh. Hussain
(Member)
Date: 18 10/ 2009

Signature:
Name: Assistant Prof. Dr.
Mohammed Hliyil Hafiz
(Member)
Date: 20 /10/2009

Signature:
Name: Assistant Prof. Dr.
Sami I. AL– Rubaiey
(Chairman)
Date: 20 /10/ 2009

Approval of the College of Engineering

Signature: M. J. Jweeg
Name: Prof Dr. Muhsin J. Jweeg
(Dean)
Date: 1 /11/ 2009

Abstract

A theoretical study was carried out to analyze the corrosion of iron pipe and iron rotating cylinder in aerated hydrochloric acid using mixed potential theory equations under turbulent flow of Reynolds number of 5000, 10000, 20000, 40000, and 60000, temperature of 25 °C, 40 °C, and 60 °C, and pH 1, 2, and 4. The theoretical investigation included: the effect of Reynolds number, temperature, pH, relative roughness (e/d), and heat flux on corrosion rate and corrosion potential. The relation between the corrosion rate and corrosion potential in case of pipe flow and rotating cylinder was analyzed and discussed.

Polarization diagrams were constructed using theoretical equations that were proposed to describe the activation and concentration polarization of anodic and cathodic reaction for the whole investigated range of Reynolds number, temperature and pH.

The theoretical results showed that corrosion rate and corrosion potential increase with increasing velocity and temperature and decrease with increasing pH for both pipe flow and rotating cylinder. The corrosion rate of iron pipe increases with increasing relative roughness and the corrosion potential shifted to more positive as the relative roughness increases and with increasing velocity, temperature, and pH.

The corrosion rate and corrosion potential of iron smooth pipe increases with increasing the heat flux because of its effect on the wall temperature which in turn affect the fluid physical properties especially the diffusivity and solubility of oxygen.

The theoretical results showed good agreement with previous experimental works of other workers. For iron smooth pipe the following correlation was obtained with 6.51% error:

$$\mathrm{C.R(gmd)} = 10.20697\ \mathrm{Re}^{0.208226}\ \mathrm{T}^{0.312849}\ \mathrm{pH}^{-0.70156}$$

For rotating cylinder the folowing relation was obtained with 6.31% error:

$$\mathrm{C.R(gmd)} = 5.53953\ \mathrm{Re}^{0.260848}\ \mathrm{T}^{0.364818}\ \mathrm{pH}^{-0.68343}$$

For iron rough pipe flow the following relation was obtained with 3.74% error:

$$\mathrm{C.R(gmd)} = 18.2175\ \mathrm{Re}^{0.269075}\ \mathrm{T}^{0.300839}\ \mathrm{pH}^{-0.68342}\ f^{0.224908}$$

Theoretical correlation between Reynolds number of pipe and Reynolds number of rotating cylinder was attained:

$$Re_P = 247.889 \left(\frac{d_P}{d_R}\right)^{(8/7)} \frac{Re_R^{0.6971}}{Sc^{0.38095}}$$

The percentage error of this equation is 5.35%.

List of Content

CHAPTER TWO :CORROSION AND ACID CORROSION

CHAPTER THREE: REVIEW

CHAPTER FOUR :THEORATICAL WORK AND ANALYSIS

CHAPTER FIVE : RESULTS AND DISCUSSION

CHAPTER SIX: CONCLUSIONS AND RECOMMENDATIONS FOR FUTURE WORK

APPENDICES

Nomenclature

Symbols	Notations
A	Surface area of specimen, m^2
A_a ,A_c	Anodic and Cathodic electrode areas, m^2
A_T	The summations of Anode and Cathode area, m^2
f_a, f_c	Anodic and Cathodic electrode area fractions
a_{red}	Activities (concentration) of reduced species, mol/m^3
a_{oxid}	Activities (concentration) of oxidized species, mol/m^3
C	Concentration, $mole/m^3$
C_b	Bulk concentration, $mole/m^3$
C_p	Specific heat, $kJ/kg.^oC$
C_s	Surface concentration, $mole/m^3$
d	Pipe diameter, m
E, $E_{applied}$	Electrode potential, relative to (SHE), V
E°	Standard electrode potential, Volte
E_a	Anode potential, V
E_c	Cathode potential, V
E_{corr}	Corrosion potential, V
E_{eq}	Equilibrium potential, V

F	Faradays constant (96500 Columb/equivalent)
f	Friction factor
h	Heat transfer coefficient, $W/m^2.^\circ C$
I_a	Total anodic current, A
I_c	Total cathodic current, A
I_{corr}	Corrosion current, A
i	Current density, A/m^2
i_a	Anode current, A/m^2
i_c	Cathode current, A/m^2
i_{corr}	Corrosion current density, A/m^2
i_L	Limiting current density, A/m^2
J	the transport flux
K	Mass transfer coefficient, m/s
n	Number of electrons transfer
Nu	Nusselt number
P	Partial pressure, atm
Pr	Prandtl number
q_W	Wall heat flux, W/m^2
R	Gas constant
Re	Reynolds number

Sc	Schmidt number
Sh	Sherwood number
T	Temperature, ^{o}C or K
T_f	Film temperature, ^{o}C
x	distance, μm
α	symmetry coefficient for the anodic or cathodic reaction, close to 0.5
α_a	symmetry coefficient for the anodic reaction
α_c	symmetry coefficient for the cathodic reaction
β	Tafel slope
β_a	Anodic Tafel slope
β_c	Cathodic Tafel slope
δ	Thickness of this layer, μm
μ	Viscosity, kg/m.s^2
η	Polarization overpotential, V
η_{act}	Activation overpotential, V
η_{CONC}	Concentration overpotential, V
η_R	Resistance overpotential, V
ρ	Density, kg/m^2

Abbreviations

act.	Activation

conc.	Concentration
corr.	Corrosion
SHE	electrode potential relative to the standard hydrogen electrode, (V)
EMF	Electromotive force
ppb	Part per billion
ppm	Part per million

List of Tables

List of Figures

CHAPTER ONE

INTRODUCTION

"Corrosion is largely an electrochemical phenomenon, which may be defined as destruction by electrochemical or chemical agencies..." as defined by Evans **[Evans, 1948]**. Corrosion in an aqueous environment and in an atmospheric environment (which also involves thin aqueous layers) is an electrochemical process because corrosion involves the transfer of electrons between a metal surface and an aqueous electrolyte solution. It results from the overwhelming tendency of metals to react electrochemically with oxygen, water, and other substances in the aqueous environment. Fortunately, most useful metals react with the environment to form more or less protective films of corrosion reaction products that prevent the metals from going into solution as ions **[Kruger, 2001]**. Corrosion affects safety and health, safety is compromised by corrosion contributing to failures of bridges, aircraft, automobiles, gas pipelines etc. the whole complex of metal structures and devices that make up the modern world. In the handling of chemicals at high temperatures and pressures, explosive materials, and acids such as hydrofluoric and concentrated sulfuric demand materials of construction which minimize corrosion failures if severe injury or losses of life are to be avoided **[Brasunas, 1970]**.

Results of the study, entitled "Corrosion Costs and Preventive Strategies in the United States," show that the total annual estimated direct cost of corrosion in the U.S. is a staggering $276 billion approximately 3.1% of the nation's Gross Domestic Product (GDP). It reveals that, although corrosion management has improved over the past several decades, the U.S. must find more and better ways to encourage، support, and implement optimal corrosion control practices; this study is published recently in 2002

[Gerhardus, el, al., 2002]. Studies of the cost of corrosion in Australia, Great Britain, Japan, and other countries have also been carried out. In each of these countries studied, the cost of corrosion is approximately 3 – 4 % of the Gross National Product **[Uhlig and Winston 2008]**.

Uniform corrosion, or general corrosion, is a corrosion process exhibiting uniform thinning that proceeds without appreciable localized attack. It is the most common form of corrosion and may appear initially as a single penetration, but with thorough examination of the cross section it becomes apparent that the base material has uniformly thinned. Uniform chemical attack of metals is the simplest form of corrosion, occurring in the atmosphere, in solutions, and in soil, frequently under normal service conditions. Excessive attack can occur when the environment has changed from that initially expected. All metals are affected by uniform corrosion in some environments; the rusting of steel and the tarnishing of silver are typical examples of uniform corrosion. In some metals, such as steel، uniform corrosion produces a somewhat rough surface by the oxidation/reduction reaction, in which the end product (oxide) either dissolves in the environment and is carried away or produces a loosely adherent, porous coating now greater in thickness. Because of the porosity in the oxidation (rust), this metal is still considered active or able to continue degrading **[Kent, 1987]**. The application of protective coatings, cathodic protection, and material selection and the use of corrosion inhibitors usually serves to control uniform corrosion. Some of these methods are used in combination. For example, on buried oil and gas pipelines the primary corrosion protection is provided by organic coatings, with the cathodic protection system playing a secondary role to provide additional protection at coating defects or weaknesses **[Roberge, 2000]**.

Iron and steel are the most commonly used metals; corrode in many media including most outdoor atmospheres. Usually they are selected not for their corrosion resistance but for such properties as strength, ease of fabrication, and cost. These differences show up in the rate of metal lost due to rusting. Iron is a generic term that identifies a large family of ferrous alloys. Irons are primarily alloys of iron that contain more than 2% carbon and 1% or more silicon, which is generally not considered an alloying element in cast irons until levels exceed 3%. Low raw material costs and relative ease of manufacture make irons the least expensive of the engineering metals. Irons may often be used in place of steel at considerable cost savings **[Brasunas, 1970]**.

Environmental factors at normal atmospheric temperatures the moisture in the air is enough to start corrosive action. Oxygen is essential for corrosion to occur in water at ambient temperatures. Other factors that affect the tendency of a metal to corrode are **[Landrum, 1994]**:

1) Acidity or alkalinity of the conductive medium (pH factor).
2) Stability of the corrosion products.
3) Biological organisms (particularly anaerobic bacteria).
4) Variation in composition of the corrosive medium.
5) Temperature.

Metal ions go into solution at anodic areas in an amount chemically equivalent to the reaction at cathodic areas. At anodic areas, the following reaction takes place **[Uhlig and Winston 2008]**:

$$\underset{atom\ in\ metal\ surface}{M} \rightarrow \underset{ion\ in\ solution}{M^{n+}} + \underset{electron(s) in\ metal}{e} \quad \ldots (1.1)$$

The cathodic reaction proceeds rapidly in acids and can be accelerated by dissolved oxygen as in the following reaction:

$$O_2 + 4H^+ + 4e \rightleftharpoons 2H_2O \qquad \dots (1.2)$$

Dissolved oxygen reacts with hydrogen atoms adsorbed at random on the iron surface, independent of the presence or absence of impurities in the metal. The oxidation reaction proceeds as rapidly as oxygen reaches the metal surface **[Uhlig and Winston 2008]**.

The aim of present work is to investigate the effect of velocity, pH, temperature, heat flux and surface roughness on the corrosion rate and corrosion potential of carbon steel in aerated hydrochloride acid solution through theoretical simulation of the investigated system by using proposed equation describing this mixed control system in which both oxygen transport and hydrogen reduction control the system for pipe flow and rotating cylinder electrode which to be compared the results with available experimental of other workers. Also it is aimed to compare between the results of pipe flow and rotating cylinder to know the effect of electrode geometry on the corrosion rate and corrosion potential.

CHAPTER TWO

ACID CORROSION

2.1 Definitions of Corrosion

Corrosion has been defined as the undesirable deterioration of a metal or alloy, i.e. an interaction of the metal with its environment that adversely affects those properties of the metal that are to be preserved **[Uhlig, 1948]**. The scope of the term "corrosion" is continually being extended, and Fontana and Staehle in 1990 have stated that "corrosion" will include the reaction of metals, glasses, ionic solids, polymeric solids and composites with environments that embrace liquid metals, gases, non-aqueous electrolytes and other non-aqueous solutions. Vermilyea, 1962 who has defined "corrosion" as a process in which atoms or molecules are removed one at a time, considers that evaporation of a metal into vacuum should come within the scope of the term, since atomically it is similar to other corrosion processes. Evans, 1960 considers that corrosion may be regarded as a branch of chemical thermodynamics or kinetics, as the outcome of electron affinities of metals and non-metals, as short-circuited electrochemical cells, or as the demolition of the crystal structure of a metal. The definition of "corrosion" as the "unmaking of metals" seems to be particularly. In brief; it is descriptive; and it ties together the two subjects of corrosion and metallurgy, the studies of which have been mutually dependent upon one another. It does lack something of completeness, however; and there seems to be some justification for combining the two definitions and calling corrosion "the unmaking of metals by chemical action between the metal and the external agencies which constitute its environment" **[James Landrum, 1994]**.

2.2 Forms of Corrosion

It is convenient to classify corrosion by the forms in which it manifests itself, the basis for this classification being the appearance of the corroded metal. Each form can be identified by mere visual observation. In most cases the naked eye is sufficient, but sometimes magnification is helpful or required. Valuable information for the solution of a corrosion problem can often be obtained through careful observation of the corroded test specimens or failed equipment. Examination before cleaning is particularly desirable **[Fontana and Greene, 1984]**. In general, most types of corrosion، with some exceptions, occur by electrochemical mechanisms, but corrosion products are not necessarily observable and metal weight loss need not be appreciable to result in major damage. The five main types of corrosion classified with respect to outward appearance or altered physical properties are as follows **[Uhlig and Winston, 2008]**:

1. General Corrosion or Uniform Attack.
2. Pitting.
3. Dealloying, Dezincification, and Parting.
4. Intergranular Corrosion.
5. Cracking.

2.3 Uniform Attack

Uniform attack is the most common form of corrosion. It is normally characterized by a chemical or electrochemical reaction which proceeds uniformly over the entire exposed surface or over a large area. The metal becomes thinner and eventually fails. For example, a piece of steel or zinc immersed in dilute sulfuric acid will normally dissolve at a uniform rate over its entire surface. A sheet of iron roof will show essentially the same degree of rusting over its entire outside surface. Uniform attack, or general overall corrosion, represents the greatest destruction of metal on a tonnage basis. This form of corrosion, however, is not of too great concern from the technical standpoint, because the life of equipment can be accurately estimated on the basis of comparatively simple tests. Merely immersing specimens in the fluid involved is often sufficient. Uniform attack can be prevented or reduced by (1) proper materials, including coatings, (2) inhibitors, or (3) cathodic protection **[Fontana and Greene, 1984]**. Rates of uniform attack are reported in various units, with accepted terminologies being millimeters penetration per year (mm/y) and grams per square meter per day (gmd). Other units that are frequently used include inches penetration per year (ipy), mils (1 mil = 0.001 inch) per year (mpy), and milligrams per square decimeter per day (mdd). For handling chemical media whenever attack is uniform, metals are classified into three groups according to their corrosion rates and intended application. These classifications are as follows **[Uhlig and Winston, in 2008]**:

A. < 0.15 mm/y (< 0.005 ipy) ——Metals in this category have good corrosion resistance to the extent that they are suitable for critical parts, for example, valve seats, pump shafts, impellors, and springs.

B. 0.15 to 1.5 mm/y (0.005 to 0.05 ipy) ——Metals in this group are satisfactory if a higher rate of corrosion can be tolerated, for example, for tanks, piping, valve bodies, and bolt heads.

C. > 1.5 mm/y (> 0.05 ipy) ——Usually not satisfactory.

2.4 Acid Corrosion

The majority of corrosion reactions in aqueous environments occur by an electrochemical mechanism. So, many factors affect the distribution, rate, and mode of corrosion that selection of an appropriate material for particular application requires a sound understanding for the fundamental processes which occur during chemical attack **[Stern, 1957]**.

When discussing the ionic content of an aqueous medium, the question often arises as to how acid (or alkaline) is the solution. Quite simply, this refers to whether there is an excess of H^+ (hydrogen) or OH^- (hydroxyl) ions present. The H^+ ion is acid while the OH^- ion is alkaline or basic. The other ionic portion of an acid or alkali added to water can increase its conductivity or change other properties of the liquid, but does not increase or decrease its acidity. For instance, whether a given amount of H^+ ion is produced in water by introducing hydrochloric (HCl), sulfuric (H_2SO_4), or any other acid is immaterial. The pH of the solution will be the same for the same number of dissolved hydrogen atoms [**Roberge, 2006**]. Corrosion is the primary means by which metals deteriorate. Most metals corrode on contact with water (and moisture in the air), acids, bases, salts, oils, aggressive metal polishes, and other solid and liquid chemicals. Metals will also corrode when exposed to gaseous materials like acid vapors, formaldehyde gas, ammonia gas, and sulfur containing gases. The best known case is that of the **rusting of steel**. Corrosion processes are usually electrochemical in nature having the essential features of a battery. When metal atoms are exposed to an environment containing water molecules they can give up electrons, becoming themselves positively charged ions provided an electrical circuit can be completed. This effect can be concentrated locally to form a pit or, crack, or it can extend across a wide area to produce general wastage. Pitting corrosion also occurs much faster in areas where microstructural changes have occurred due to welding operations. The corrosion process (anodic reaction) of the metal dissolving as ions generates some electrons, as shown in Fig. 2-1, that are consumed by a secondary process (cathodic reaction). These two processes have to balance their charges. The sites hosting these two processes can be located close to each other on the metal's surface, or far apart depending on the circumstances **[Brasunas, 1970]**.

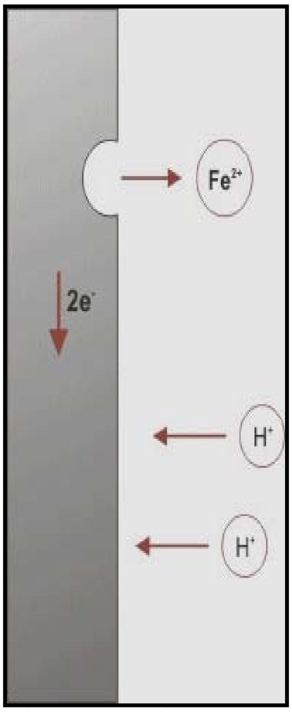

Figure 2-1: The simple shape **[Roberge, 1970]**.

Metallic corrosion is the result of basic chemical reaction. Like most other reactions, corrosion can be separated into two or more partial reactions. These partial reactions are divided into two classes: oxidation and reduction. Oxidation is the loss of electrons. This can be illustrated by the reaction of iron to produce ferrous irons.

$$Fe \rightleftharpoons Fe^{+2} + 2e \qquad \text{(Anodic reaction)} \qquad \ldots (2.1)$$

This reaction is the basis of the corrosion of iron. There are reduction reactions. The discharge of hydrogen ions is typical of such reactions **[Steigerwald, 1968]**:

$$H_2 \rightleftharpoons 2H^+ + 2e \qquad \text{(Cathodic reaction)} \qquad \ldots (2.2)$$

The anodic reaction is dissolution of the metal to form either soluble or insoluble ionic products or an insoluble compound of metal usually an oxide **[Steigerwald, 1968]**. Several cathodic reactions are possible depending on what reducible species are present in the solution. Typical reactions are the reduction of dissolved oxygen gas or the reduction of hydrogen ions

$O_2 + 2H_2O + 4e \rightleftharpoons 4OH^-$ (Neutral environment) $E^\circ = +0.401$ V ... (2.3)

$O_2 + 4H^+ + 4e \rightleftharpoons 2H_2O$ (Acidic environment) $E^\circ = +1.229$ V ... (2.4)

$2H^+ + 2e \rightleftharpoons H_2$ (Acidic environment) $E^\circ = 0.0$ V ... (2.5)

The flow of electrons between the corroding anodes and non-corroding cathodes forms the corrosion current, the value of which is determined by the rate of production of electrons by the anodic reaction and their consumption by the cathodic reaction. A driving force that causes the electrons to flow between anode and cathode is the difference in potential between the anodic and cathodic sites. This difference exists because each oxidation or reduction reaction has associated with it a potential determined by the tendency for the reaction to take place spontaneously. The potential is a measure of this tendency **[Kruger, 2001]**.

2.5 Effect of pH

The effect of pH may be different in hard water, in which a protective film of $CaCO_3$ forms on the metal surface **[Roberge, 2008]**. The effect of pH of aerated pure, or soft, water on corrosion of iron at room temperature is shown in Fig. 2-2. Within the range of about pH 4 - 10, the corrosion rate is independent of pH and depends only on how rapidly oxygen diffuses to the metal surface. The major diffusion barrier of hydrous ferrous oxide is continuously renewed by the corrosion process. Regardless of the observed pH of water within this range, the surface of iron is always in contact with an alkaline solution of saturated hydrous ferrous oxide **[Kruger, 2001]**.

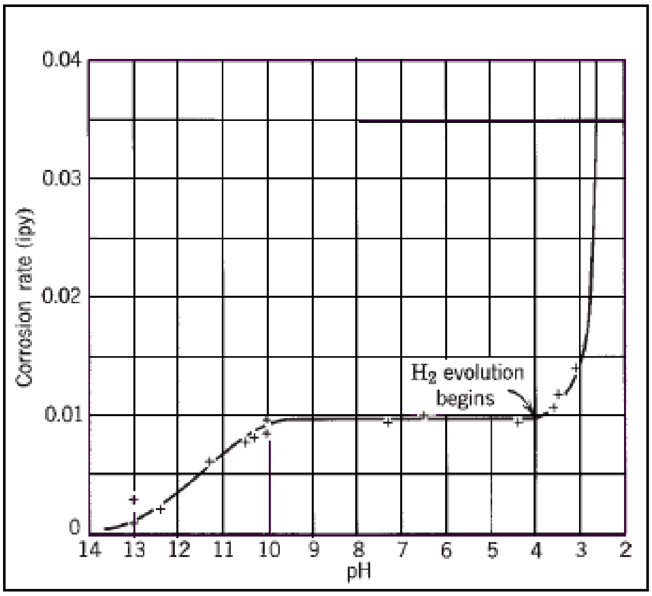

Figure 2-2: Effect of pH on corrosion of iron in aerated soft water, room temperature **[Uhlig and Winston, 2008]**.

On the other hand some investigators, using different natural waters and different chemicals to control pH, have observed that the corrosion rate does change with pH in the pH range 6 to 9. This behavior has been attributed to reduced buffer capacity of HCO_3 (an inhibitor) as pH increases, causing a pH at local sites that is lower than the pH that would otherwise exist in a solution of saturated hydrous ferrous oxide **[Peabody, 2001]**. Within the acid region pH < 4, the ferrous oxide film is dissolved, the surface pH falls, and iron is more or less in direct contact with the aqueous environment. The increased rate of reaction is then the sum of both an appreciable rate of hydrogen evolution and oxygen depolarization; above pH 10, an increase in alkalinity of the environment raises the pH of the iron surface. The corrosion rate correspondingly decreases because iron becomes increasingly passive in the presence of alkalis and dissolved oxygen. In the region of pH 4 – 10, the corrosion rate depends only on the rate of diffusion of oxygen to the available cathodic the extent of the cathodic surface is apparently not important. The corrosion rate of most metals is affected by pH **[Roberge, in 2008]**. Acid-soluble metals such as iron have a relationship as shown in Fig. 2-3. In the middle pH range (≈4 to 10), the corrosion rate is controlled by the rate of transport of oxidizer (usually dissolved O_2) to the metal surface. Iron is weakly amphoteric.

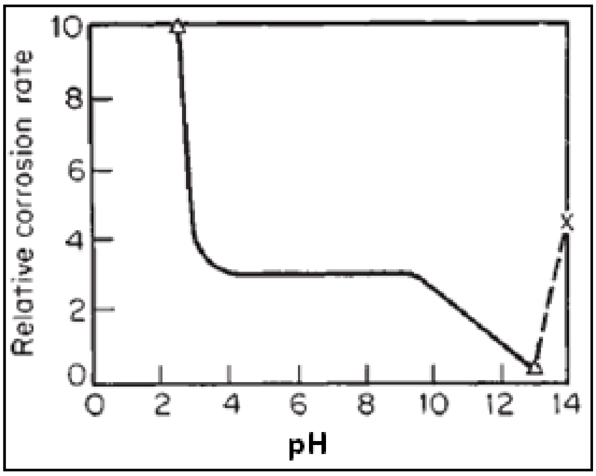

Figure 2-3: Effect of pH the on corrosion rate of iron

[Perry, 2008].

At very high temperatures such as those encountered in boilers, the corrosion rate increases with increasing basicity, as shown by the dashed line **[Uhlig, 1976]**. Charng and Lansing [1982] studied the corrosion rate of carbon steel in low velocity, room temprature, and pH range 2 to 10, in the acidic environment (HCl) and in alkaline environment (NaOH), their results are shown in Fig. 2-4.

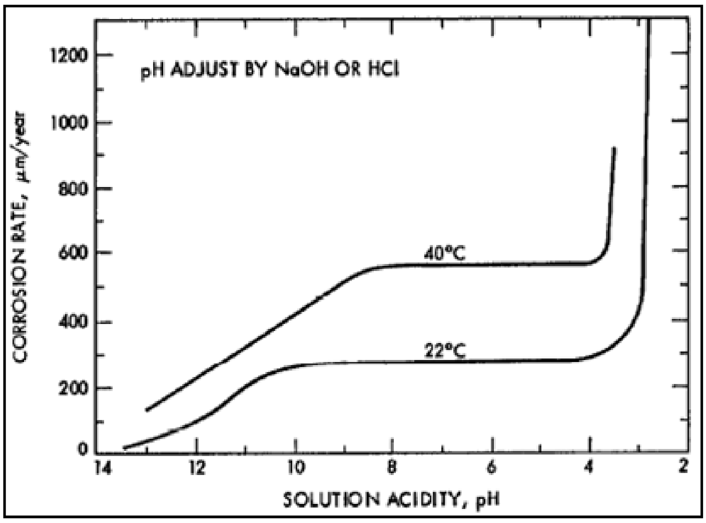

Figure 2-4: Effect of solution acidity on corrosion rate **[Charng and Lansing, 1982]**.

2.6 Dissolved Oxygen

In neutral or near - neutral water at ambient temperatures, dissolved oxygen is necessary for appreciable corrosion of iron in air-saturated water, the initial corrosion rate may reach a value of about 10 gmd. This rate diminishes over a period of days as the iron oxide (rust) film is formed and acts as a barrier to oxygen diffusion. The concentration of dissolved oxygen in air-saturated, natural fresh waters at ordinary temperatures is 8 to 10 ppm. In the absence of dissolved oxygen, the corrosion rate at room temperature is negligible both for pure iron and for steel. Higher partial pressures of oxygen although increase oxygen concentration at first accelerates corrosion of iron, it is found that, beyond a critical concentration, the corrosion drops again to a low value. In distilled water, the critical concentration of oxygen above which corrosion decreases again is shown in Fig, 2-5.This value (critical concentration of oxygen) increases with dissolved salts and with temperature and it decreases with an increase in velocity and pH **[Roberge, 2008]**.

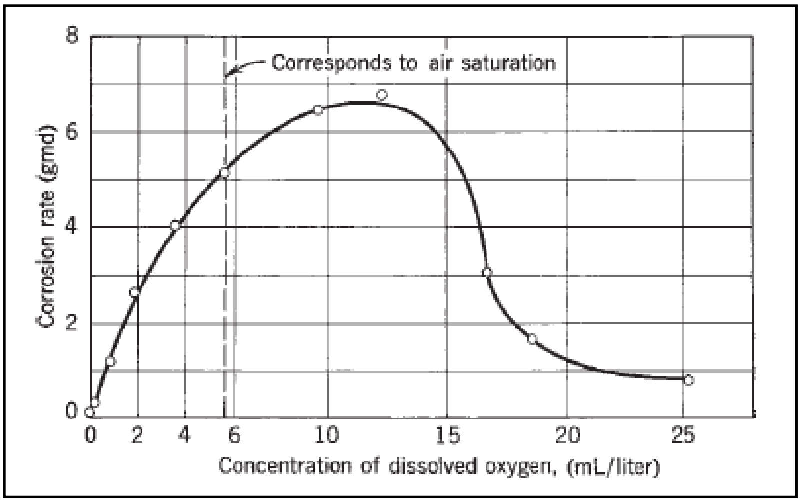

Figure 2-5: Effect of oxygen concentration on corrosion of mild steel in slowly moving distilled water Uhlig, **[Uhlig et. al., 1955**].

Dissolved oxygen can cause severe corrosion at very low concentrations (less than 100 ppb or 0.1 ppm) and if either or both CO_2 and/or H_2S are present, it further increases their corrosivity **[Uhlig et. al., 1955]**. Fig. 2-6 is a composite graph from results of three different studies showing corrosion rates as a function of oxygen concentration **[Frank, 1972]**. The solubility of oxygen in water is a function of pressure, temperature, and chloride content. Although it is not usually present in produced water, it is often introduced into oilfield water handling systems through failures to maintain oxygen free gas blankets on water handling vessels, vacuums created by positive displacement pumps or separator dump valves and/or exposure to the atmosphere. Water from lakes, streams, fresh water aquifers, rain or oceans usually will be oxygen saturated. Oxygen is more soluble at high pressures and lower temperatures and is less soluble in salt water than in fresh water. Oxygen accelerates corrosion under most circumstances because it is a strong and rapid oxidizing agent in cathodic reactions. It will easily combine with electrons at the cathode and allow the corrosion reactions to proceed at a rate limited by the rate at which oxygen can diffuse to the cathode.

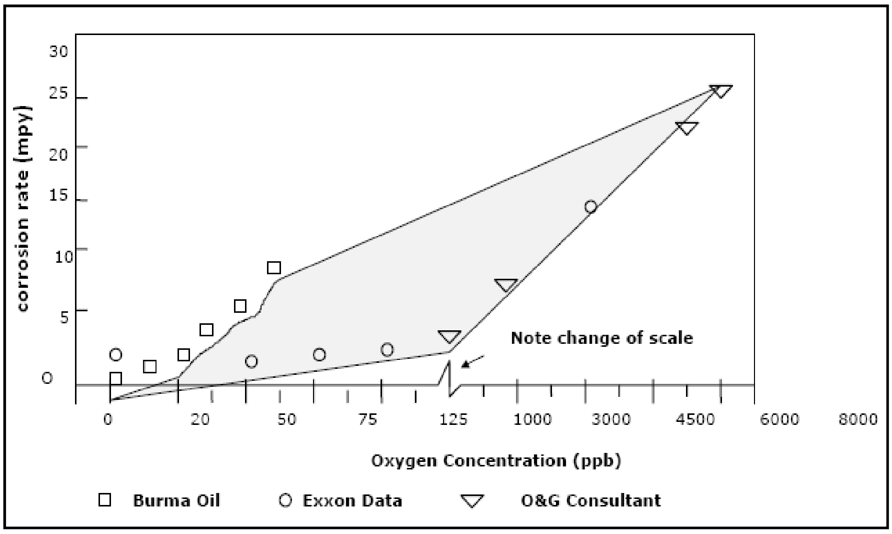

Figure 2-6: Relation of Dissolved Oxygen to the General Corrosion Rate of Steel [**Frank**, **1972**].

2.7 Physical Variables

The variables of temperature, pressure, and velocity need to be accounted for when designing and implementing a corrosion control program. Correct application of inhibitors and cathodic protection as corrosion control methods are very dependent on these variables. Temperature and pressure are interrelated, and the corrosivity of a system is further influenced by velocity **[Jones, 1988]**.

2.7.1 Temperature

As a general rule increasing temperature increases corrosion rates. This is due to a combination of factors- first; the common effect of temperature on the reaction kinetics themselves and the higher diffusion rate of many corrosive by-products at increased temperatures. This latter action delivers these by-products to the surface more efficiently. Occasionally, the corrosion rates in a system will decrease with increasing temperature. This can occur because of certain solubility considerations. Many gases have lower solubility in open systems at higher temperatures. As temperatures increase, the resulting decrease in solubility of the gas causes corrosion rates to go down. Like most chemical reactions corrosion rates generally increase with temperature, for example, in a system open to the atmosphere as shown in Fig. 2-7, the corrosion rate generally increases with increasing temperature until the concentration of dissolved gases decreases when corrosion is attended by hydrogen evolution **[Uhlig and Winston, 2008]**. And the corrosion rate continues to increase with temperature until all the oxygen is consumed **[Speller, 1951]**.

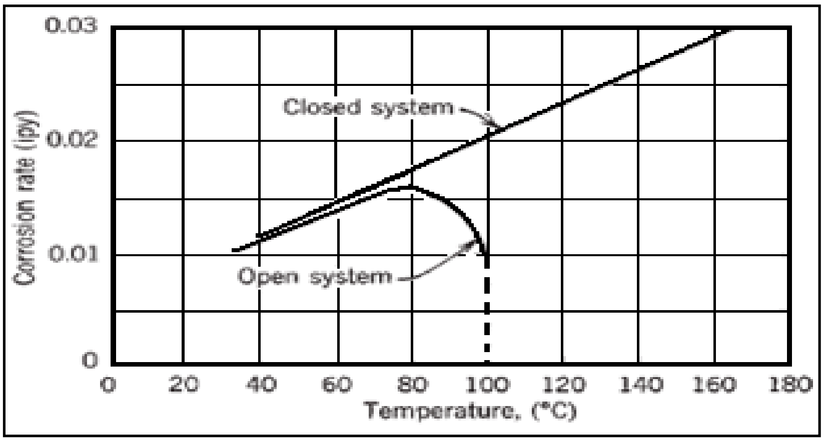

Figure 2-7: Effect of temperature on corrosion of iron in water containing dissolved oxygen **[Speller, 1951; Uhlig and Winston, 2008]**.

2.7.2 Pressure

Pressure also affects the rates of corrosion reactions. More gas goes into solution as the pressure increases, which may, depending on the dissolved gas, increase the corrosivity of the solution **[Jones, 1988]**.

2.7.3 Velocity

Velocity has a significant effect on corrosion rates. Stagnant or low velocity fluids usually give low general corrosion rates, but pitting rates may be high.

Corrosion rates generally increase with increasing velocity due to the depolarizing effect on the cathode. High velocities and the presence of suspended solids or gas bubbles can lead to erosion corrosion, impingement, or cavitations **[Jones, 1988]**.Velocity primarily affects corrosion rate through its influence on diffusion phenomena. It has little effect on activation controlled processes. The manner in which velocity affects the limiting diffusion current is a marked function of the physical geometry of the system. In addition the diffusion process is affected differently by velocity when the flow conditions are laminar as compared to a situation where turbulence exists. For most conditions the limiting diffusion current can be expressed by the equation:

$$i_L = Ku^n \qquad \dots (2.6)$$

where K is a constant, u is the velocity of the environment relative to the surface and n is a constant for a particular system. Values of n vary from 0.2 to 1**[Shreir, 1994]**. Fig. 2-8 shows the effect of velocity on the limiting current density **[Fontana and Greene, 1984]**.

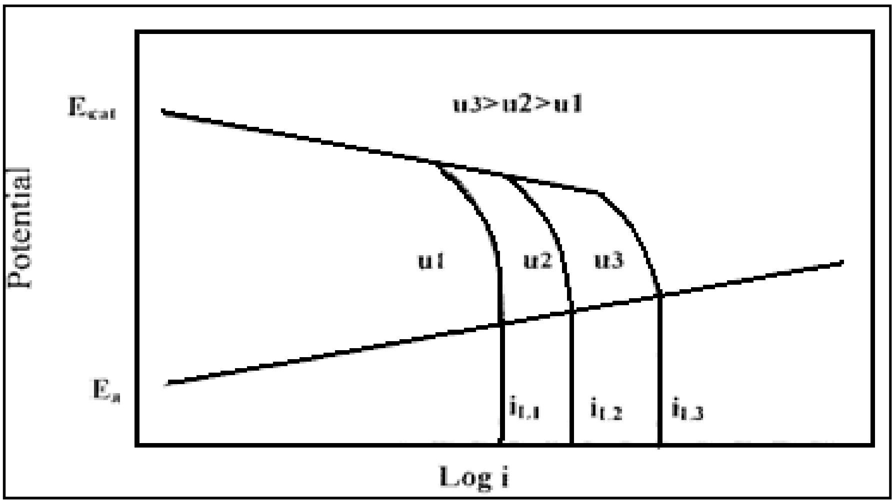

Figure 2-8: Effect of velocity on i_L **[Fontana and Greene, 1984].**

2.8 Polarization

Polarization methods such as potentiodynamic polarization, potentionstaircase, and cyclic voltammetry are often used for laboratory corrosion testing. These techniques can provide significant useful information regarding the corrosion mechanisms, corrosion rate and susceptibility of specific materials to corrosion in designated environments. Polarization methods involve changing the potential of the working electrode and monitoring the current which is produced as a function of time or potential **[Roberge, 2008]**. In practical situations polarization sometimes defined as the potential change away from some other arbitrary potential and in mixed potential experiments, this is the free corrosion potential **[Trethewey and Chamberlain, 1996]**. If equilibrium at an electrode is disturbed, a net current flows across its surface displacing the potential in a direction and to an extent depending on the direction and magnitude of the current. The shift in potential is called polarization and its value, η, is the overpotential. There are three distinct types of polarization in any electrochemical cell, activation, concentration, and resistance polarization **[David and James, 1998]**.

2.8.1 Activation Polarization (η_{act})

When some steps in a corrosion reaction control the rate of charge or electron flow, the reaction is said to be under activation or charge-transfer control. The kinetics associated with apparently simple processes rarely occur in a single step **[Roberge, in 2000]**. In the case of activation polarization, the rate of the corrosion reaction is limited by the electron transfer reaction at the metal surface. This electron transfer process has associated activation energy and the rate of this process is exponentially related to the free energy change. Since the free energy is directly related to the potential, and the rate is directly related to the electrical current, the relationship becomes equation 2.7:

$$\Delta \mathrm{I} \propto \mathrm{e}^{\eta/\mathrm{RT}} \qquad \ldots (2.7)$$

in which I is the corrosion current, R is the gas constant, and T is the absolute temperature. Upon taking the log of both sides of the equation 2.7, the relationship becomes the following:

$$\log(\Delta \mathrm{I}) \propto \frac{\eta}{\mathrm{RT}} \qquad \ldots (2.8)$$

Rather than using equations, a better way of visualizing the relationship between potential and current is by means of Evans diagrams (E-log i plots), where potential is plotted on the vertical (Y) axis and log current or log current density is plotted on the horizontal (X) axis, see Fig. 2-9. The equilibrium potentials for the reduction reaction, hydrogen reduction, and the metal oxidation reaction are indicated as E_{H^+/H_2} and $E_{M^{2+}/M}$, respectively **[Peabody, 2001]**.

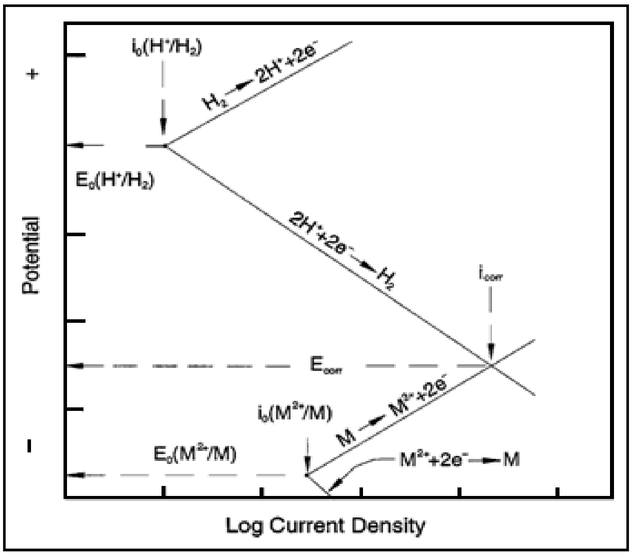

Figure 2-9: Evans diagram (potential versus logarithm of current density) for metal M in acid solution [**Peabody, 2001].**

There is an associated current; this current is referred to as an exchange current i_o. At equilibrium, the exchange current for the oxidation and reduction reactions are equal and the net rate is zero. The exchange current of a reaction is different depending on the type and nature of the surface on which it is occurring. The corrosion potential for a metal in an environment is established at a potential where the net sum of the reduction reactions is equal to the net sum of the oxidation reactions. This is because there can be no net accumulation of charge; all of the electrons liberated by the oxidation of the metal must be consumed by the reduction reactions. The value of the corrosion potential, E_{corr}, is indicated in Fig. 2-9. Note in the example in Fig.2-9 that the oxidation reaction for hydrogen and the reduction reaction for the metal are ignored in the summation process. This is because the current scale is logarithmic and the rates for these reactions are negligible near the free corrosion potential. The curves in Fig. 2-9 show the current-potential relationships of the individual oxidation and reduction reactions.

2.8.2 Concentration polarization (η_{conc})

When the cathodic reagent at the corroding surface is in short supply, the mass transport of this reagent could become rate controlling. A frequent case of this type of control occurs when the cathodic processes depend on the reduction of dissolved oxygen, because the rate of the cathodic reaction is proportional to the surface concentration of the reagent, the reaction rate will be limited by a drop in the surface concentration. For a sufficiently fast charge transfer, the surface concentration will fall to zero, and the corrosion process will be totally controlled by mass transport **[Roberge, 2000]**. Concentration polarization refers to electrochemical reactions which are controlled by the diffusion in the electrolyte.

It is the slowing down of a reaction due to an insufficiency of the desired species or an excess of the unwanted species at the electrode **[Fontana and Greene, 1984]**. This type of polarization occurs at the cathode when reaction rate or the cathode current is so large that the substance being reduced cannot reach the cathode at a sufficiently rapid rate. Since the rate of reaction is determined by the slowest step, the diffusion rate will be the rate determining step. At very high reduction rates, the region adjacent to the electrode surface will become depleted of ions. If the reduction rate is increased further, a limiting rate will be reached which is determined by the diffusion rate of ions to the electrode surface. This limiting rate is the limiting diffusion current density i_L. It represents the maximum rate of reduction possible for a given system; the expressing of this parameter is:

$$i_C = i_L = \frac{DnFC_B}{\delta} \qquad \ldots (2.9)$$

where i_L is the limiting diffusion current density, D is the diffusion coefficient of the reacting ions, C_B is the concentration of the reacting ions in the bulk solution, and δ is the thickness of the diffusion layer. When the cathodic current is smaller than i_L, η_{conc} can be evaluated using an expression derived from Nernst equation **[Uhlig, 1976]**. Fig.2-10 illustrates the concentration- distance profile at the electrode surface approximated by a simple gradient. In this diagram the metallic surface is positioned at the ordinate axis while the x-axis expresses the distance away from the electrode and the y-axis the concentration of the chemical species being reacted **[Roberge, 2008]**.

$$E_i - E_{eq} = \eta_{conc} = \frac{2.303RT}{nF}\log\left(1 - \frac{i}{i_L}\right) \qquad \ldots (2.10)$$

Equation 2.10 is shown in Fig. 2-11.

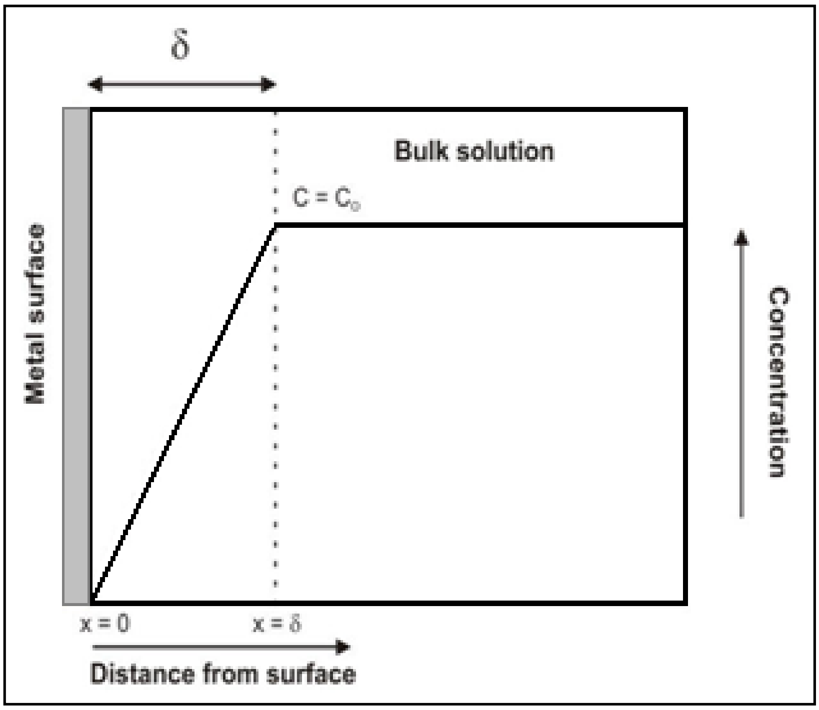

Figure 2-10: Nernst diffusion layer for a limiting current situation **[Roberge, 2008].**

2.8.3 Resistance Polarization

In corrosion the resistance of the metallic path for charge transfer is negligible. Resistance overpotential η_R is determined by factors associated with the solution or with the metal surface. Resistance polarization η_R is only important at higher current densities or in higher resistance solution. It may be defined as **[Fontana and Greene, 1984; Uhlig and Winston, 2008]**:

$$\eta_R = I\left(R_{soln} + R_f\right) \qquad \ldots (2.11)$$

where R_{soln} is the electrical resistance of solution, which is dependent on the electrical resistivity (Ω cm) of the solution and the geometry of the corroding system, and R_f is the resistance produced by films or coatings formed on the surface of the sites, which block contact between the metal and the solution, and increase the resistance overpotential.

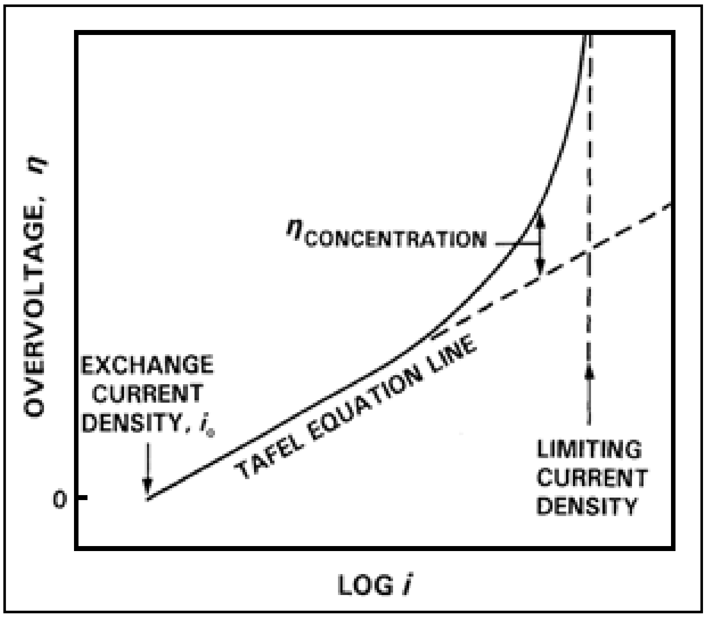

Figure 2-11: Concentration Polarization Curve (Reduction Process)

[David Talbot and James Talbot, 1998].

2.9 Combined Polarization

Both activation and concentration polarization usually occur at an electrode. At low reaction rates activation polarization usually controls, while at higher reaction rates concentration polarization becomes controlling **[Fontana and Greene, 1984]**. The total polarization of an electrode is the sum of the contribution of activation polarization, concentration polarization, and resistance polarization **[David and James, 1998]**:

$$\eta_{\text{total}} = \eta_{\text{act}} + \eta_{\text{conc}} + \eta_R \qquad \ldots (2.12)$$

The effects of these forms of polarization are illustrated by the characteristics of hydrogen evolution and oxygen reduction reactions that feature prominently in corrosion processes shown in Fig. 2-12.

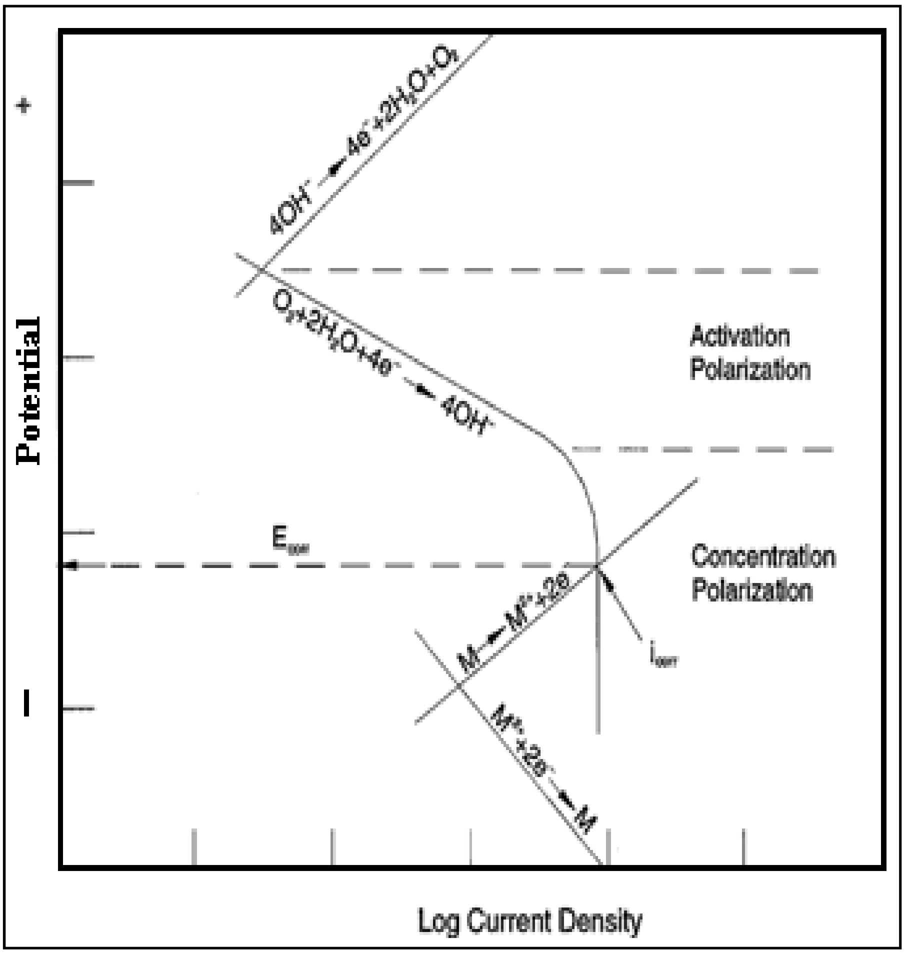

Figure 2-12: Evans diagram for Combined Polarization (Activation and Concentration) **[Peabody, 2001]**.

CHAPTER THREE

REVIEW

3.1 Corrosion in History

Interest in the corrosion science and engineering has been increasing for many years. This has inspired investigators and writers to such an extent that it is now difficult to follow the voluminous technical literature relating to this subject and select that which is useful. The wastage of metals due to corrosion has become an important engineering problem. Probably no other source of waste, except that affecting human life, is of greater concern to all **[Speller, 1935]**. For many centuries there seems to have been little curiosity regarding the causes of corrosion, although a few significant observations were made. As early as 1788, Austin noticed that water, originally neutral, tends to become alkaline when it acts on iron. The belief that corrosion is an electrochemical phenomenon was expressed in a paper published in 1819 by an anonymous French writer, thought to be Thenard. Faraday's researches, especially those conducted between 1834 and 1840, afforded evidence of the essential connection between chemical action and the generation of electric currents. One of the most interesting chapters of Faraday's work was concerned with the study of passivity-the subject of a famous correspondence in 1836 with Schonbein. Schools of Ostwald and Nernst and culminating in an important paper by Wilsmore (1900). Between 1888 and 1908 the view was frequently advanced that acids were the agents mainly responsible for corrosion; particularly it was held that the rusting of iron would only take place if carbonic acid was present. It was shown, however, by Dunstan, Jowett and Goulding in 1905, by Tilden in 1908, and by Heyn and Bauer in the same year, that iron exposed to water and oxygen, with exclusion of carbon dioxide, underwent rusting **[Evans, 1948]**.

3.2 Review of Previous Work

Butler and Ison [1960] computing the diffusional flow of dissolved oxygen in a corrosion reaction under flow conditions, have assumed the transferring surface to be smooth, in practice, due to the deposition of the corrosion product, the transferring surface becomes very rough with time, changing the nature of the flow vary materially.

Brenan and Trass [1964] studied the effect of surface roughness on the dissolution rate of cinnamic acid, benzoic acid and succinic acid, with the specific variables and their ranges being: temperature, 10-50°C; roughness height, 100-400 micro-in.; Reynolds number, 8000-60000, and Schmidt number, 294-1884. The observed mass transfer rate increased by about four times with the increase in roughness.

Were made by Mahato et. al., [1980] Corrosion tests of commercial steel pipe in aerated natural water under variable flow isothermal conditions by weight loss determinations over periods up to 210 days. They concluded that dissolved oxygen acts as a depolarizer, transfer phenomena under flowing conditions were very complex due to such unsteady process characteristics of the system as (i) building up of corrosion product on the surface; (ii) growth of surface roughness; (iii) changing physico-chemical properties of the corrosion products; and (iv) changing mechanics of flow.

Poulson [1983] studied the influence of fluid flow on the corrosion rate for different geometries (rotating disk, rotating cylinder, impinging jet, nozzle, and tube) using electrochemical technique. For pipe flow he obtained a correlation for fully developed turbulent flow using rotating cylinder electrode.

Silverman [1984] studied the effect of fluid flow on the corrosion rate. Experiments were carried out at room temperature on mild steel sample at rotation rate of 500 and 5000 rpm, weight loss was measured for 30 min, 60 min, 1hr, and 24hr. The purpose was to estimate the degree of mass transfer control. He found that the current density at anodic nose increases with fluid velocity. Thus the corrosion rate is highly depended on fluid velocity.

Speller [1951] showed that the initial corrosion rate of Fe in water at constant O_2 concentration increased linearly with temperature, and that the corrosion reaction was mainly influenced by the rate of transfer of O_2 to the metal surface. In a pipe corrosion process under turbulent flow conditions, the rate of transfer of dissolved O_2 will be determined largely by the nature of (i) the damped turbulence layer near the solid product surface and (ii) the corrosion product layer through which O_2 must diffuse to reach the reaction zone. With increase in temperature the solubility of O_2 decreases and the diffusion coefficient of O_2 increases, with the net effect that the corrosion of mild steel in aerated water goes through a maximum at about 80°C.

Wang and Postlethwaite [1997] studied effects of the mass transfer on the corrosion of metals throughout the mass transfer entry lengths in turbulent flow in pipes. Profiles of corrosion rate, surface metal ion concentration and surface pH for corrosion under charge transfer control; oxygen-mass transfer control; and anodic partial mass transfer control were presented. They found that the corrosion is solely controlled by the mass transfer of oxygen from bulk solution to the metal/solution interface, the corrosion rate increases with Reynolds number and decrease along the mass transfer entrance length.

Cox and Roetheli [1931] obtained data for steel specimens in aerated natural water (Cambridge, Mass., U.S.A.) by varying the rotational speed of the specimen and the O content in the water, and found that corrosion rate increased with the increased O content (up to 6 ppm) and increased peripheral velocity (up to 1.2 ft/s). Roetheli and Brown [1931] further reported that the corrosion rates increased to a maximum, as the rotational velocities of their steel specimens, in oxygenated water, increased, then decreased to a very low value and increased again to a somewhat higher value at very high velocities.

The model of Nesic et. al. [1996] takes into account the electrochemical reactions of hydrogen ion H^+ reaction, carbonic acid (H_2CO_3) reaction, direct water reaction, oxygen reduction, and anodic dissolution of iron. The corrosion process was monitored using polarization resistance, potentiodynamic sweep, electrochemical impedance, and weight-loss measurements. The model was calibrated for two mild steels over a range of parameters: temperature 20 °C to 80 °C, pH 3 to 6, velocity 0 to 5,000 rpm (u = 0 m/s to 2.5 m/s). The model was applicable for uniform corrosion with no protective films present, the model gave clearer picture of the corrosion mechanisms by considering the effects of pH, temperature and solution flow rate on the participating anodic and cathodic reactions.

Under controlled conditions of heat and mass transfer, asset of experiments using deionizer water containing 1,000 ppm of chloride ions, pH=7.5, and in presence and absence of different inhibitors were carried out by AL-Darbi, et al. [2002] using a rotating cylinder electrode (RCE) system. The heat flux from the working electrode to the solution was controlled to be 3.45 KW/m^2. They found that the corrosion potential became more negative (less noble) with heat flux. This finding agreed with the study of Sparrow and Gregg

[1959] for RCE; it was found that the corrosion potential values under the heat transfer conditions were more negative than the corresponding values under the isothermal condition.

Damborenea et al. [1987] made new contribution to corrosion rate calculation from polarization curves. The Butler-Volmer equation analysis was used to develop a new calculation method which analyses the data corresponding to intermediate values of anodic and cathodic polarization in 2M HCl solution. The solutions were maintained at 278, 288, 298, and 308 K. They calculated steel corrosion in 2M HCl solution.

Silverman [2004] studied the rotating cylinder electrode for examining velocity-sensitive corrosion of the laboratory devices available for examining the effects of single-phase fluid flow on corrosion; the rotating cylinder electrode was probably one of the simplest devices to construct and operate under defined hydrodynamics in the turbulent flow regime and studied the effect of surface roughness on corrosion. Silverman was serving of a variety of corrosion-related studies using the rotating cylinder electrode to provide an overview of the large number of applications of this technology and a source for further reading. He found that simulation the velocity sensitive, mass transfer influenced corrosion mechanism in other geometries should be possible when the hydrodynamic and mass transfer boundary layers are fully developed and there is no separation of boundary layer.

Zhang et. al. [2007] developed a mechanistic model is to predict the general corrosion rate at the top of pipe line. This model covered the three main processes involved in the top-of-the line corrosion phenomena: the dropwise condensation, the behavior of the chemistry in the condensed water, and the corrosion at the steel surface. The dropwise condensation process was modeled based on the heat and mass-transfer theory and was used to predict the condition rate. They studied the effect of heat flux on the dropwise from changing the wall temperature.

3.3 Friction Factor in Smooth and Rough Tubes

The Fanning friction factor is the relation between the wall shear stress and kinetic energy of flow and is defined as **[Thomson, 2000]**:

$$f = \frac{\tau w}{\frac{1}{2}\rho u^2} \qquad \text{… (3.1)}$$

Nikuradse [1932] from experimental data obtained the following equation:

$$\frac{1}{\sqrt{f}} = 4\log\left(Re\sqrt{f}\right) - 0.4 \qquad \text{… (3.2)}$$

This equation is valid to Re of 3200000 for turbulent flow of fluids in smooth tubes. It is superior to any other correlation now in existence, although simpler correlations such as Blasius [1931] have been proposed:

$$f = 0.0079\ Re^{(-1/4)} \qquad \text{… (3.3)}$$

This is used to predict friction factor for smooth pipe for Re 3000 to 100000 **[Welty et. al., 2001; Brodkey and Hershey, 1989]**. Also, an empirical equation relating friction factor and Re was presented by Drew et. al. [1932] this equation holds for Re of 3000 to 3000000.

$$f = 0.0014 + 0.125\ Re^{-0.32} \qquad \text{… (3.4)}$$

Chen [1985] has developed an explicit friction factor equation which is valid for all regions of turbulent flow with an accuracy of about ±8%:

$$f = 0.0791\left[\frac{1}{Re^{0.83}} + 0.11\left(\frac{e}{d}\right)\right]^{0.3} \qquad \ldots (3.5)$$

It is found experimentally that for commercial steel pipe $e=4.572\text{x}10^{-2}$ mm and for cast iron pipe e=0.2591 mm **[Brodkey and Hershey, 1989]**.

3.4 Mass Transfer

Many investigators over years ago have interested in the theoretical development of an accurate mass transfer correlation as a function of Reynolds number and Schmidt number.

The Friend-Metzner [1958] used an equation of substantially different form in order to correlate over wide range of Sc for smooth tube. The mass transfer correlation is **[Brodkey and Hershey, 1989]**:

$$Sh = \frac{Re\,Sc\left({}^{f}/_{2}\right)}{1.2+11.8\left({}^{f}/_{2}\right)^{1/2}(Sc-1)\,Sc^{-1/3}} \qquad \ldots (3.6)$$

The authors demonstrated the applicability of equation (3.6) to turbulent mass transfer in tubes for Sc up to 3000. Znad [1996] analyzed the mass transfer coefficient for rotating cylinder electrode in turbulent flow conditions using experimental data of other investigators .He obtained the following relation for mass transfer coefficient:

$$Sh = 0.38073\sqrt{\frac{f}{2}}Re^{0.834}Sc^{0.334} \qquad \ldots (3.7)$$

For $Sc < 10^4$ and $Re=10^4$-10^6. The following correlation for the mass transfer has been proposed by Berger and Hau [1977] for fully developed region:

$$Sh = 0.0165Re^{0.86}Sc^{0.33} \qquad \ldots (3.7)$$

Eisenberg, et al. [1954] proposed the following correlation for calculating the mass transfer coefficient for polished rotating cylinder.

$$Sh = 0.0791\, Re^{0.7} Sc^{0.336} \qquad \ldots (3.8)$$

Shaw and Hanraty [1977] studied the influence of Sc on the rate of mass transfer between turbulently flowing fluid and pipe wall using electrochemical method and proposed the following equation for mass transfer coefficient in terms of Sc and friction factor:

$$\mathrm{Sh} = 0.0889 \sqrt{(\mathrm{f}/2)}\, \mathrm{Re}\, \mathrm{Sc}^{0.246} \qquad \ldots (3.9)$$

3.5 Heat Transfer

There are many correlations presented to describe heat transfer coefficient for turbulent flow. The form of heat transfer equation was derived through dimensional analysis; the results can be expressed as **[Brodkey and Hershey, 1989]**:

$$\mathrm{Nu} = \frac{\mathrm{hd}}{\mathrm{K_T}} = \mathrm{aRe^bPr^c} \qquad \ldots (3.10)$$

Where a, b and c are empirical constants, Eq. (3.10) is widely used for all fluids except liquid metals. The form of Dittus-Bolter [1930] correlation which is based on equation (3.10) is:

$$\mathrm{Nu} = \frac{\mathrm{hd}}{\mathrm{K_T}} = 0.023\mathrm{Re^{0.8}Pr^n} \qquad \ldots (3.11)$$

where n has values of 0.4 for heating and 0.3 for cooling. In this equation all physical properties are taken at the mean bulk temperature of the fluid $\frac{T_i+T_o}{2}$, where T_i and $T_o$are the inlet and outlet temperatures, Eq. (3.11) is valid for Re > 10000 and Pr lying between 0.7 and 160 **[Coulson and Richardson, 1998]**.

Friend-Metzner [1958] used an equation of substantially different form in order to correlate the heat transfer coefficient over wide range of Pr. Their correlation of heat transfer for 0.5< Pr < 600 and Re > 10000 for pipe flow is:

$$\mathrm{Nu} = \frac{\mathrm{RePr}\left({}^{f}/{}_{2}\right)\left(\mu_b/\mu_w\right)^{0.14}}{1.2+11.8\left(\frac{f}{2}\right)^{1/2}(\mathrm{Pr}-1)\mathrm{Pr}^{-1/3}} \qquad \ldots (3.12)$$

CHAPTER FOUR

THEORETICAL WORK AND ANALYSIS

This chapter describes the theoretical methods followed in this thesis. The theoretical methods involve the use of proposed equations to obtain the results for various values of Re, temperatures, pH, surface roughness, ant heat flux, and comparison with other experimental results to provide information to fill identified gaps in knowledge and to verify the defined hypotheses. The results will be presented in the subsequent chapters.

4.1 Activation and Diffusion Control

4.1.1 Equilibrium Potential

The potential of any two half-cell reactions can be calculated using the following equation (4.1), where the EMF series is written as reduction reactions **[Peabody, 2001]**

$$E = E^{\circ}_{(\text{reduction})} - E^{\circ}_{(\text{oxidation})} \qquad \dots (4.1)$$

The EMF series is calculated for the reactants at unit activity. These potentials shift as a function of concentration according to the Nernst equation. For any electrochemical reaction

$$E = E^{\circ} - \frac{RT}{nF}\ln\left(\frac{a_{\text{red}}}{a_{\text{oxid}}}\right) \qquad \dots (4.2)$$

Since it is more convenient to work with logarithms to the base 10, the value of the coefficient RT/F is multiplied by the conversion factor 2.303 as equation (4.3) **[Uhlig and Winston, 2008]**.

$$E = E^{\circ} - \frac{2.303RT}{nF}\log\left(\frac{a_{\text{red}}}{a_{\text{oxid}}}\right) \qquad \dots (4.3)$$

in which E is the cell potential, R is the gas constant (8.314 J/K .mol), T is the absolute temperature (K), F is Faraday's constant (96487 coulomb/equiv.). Hydrogen ion activity is commonly expressed, for convenience, in terms of pH, defined as **[Soren, 1909]**:

$$\mathrm{pH} = -\log[\mathrm{H}^+] \qquad \ldots (4.4)$$

$$2\mathrm{H}^+ + 2\mathrm{e}^- \rightarrow \mathrm{H}_2 \qquad \ldots (4.5)$$

The standard potential for this reaction is equal to zero at all temperatures. Hence,

$$\mathrm{E}_{\mathrm{H}_2} = \frac{\mathrm{RT}}{2\mathrm{F}} \ln \frac{\mathrm{P}_{\mathrm{H}_2}}{(\mathrm{H}^+)^2} \qquad \ldots (4.6)$$

where $\mathrm{P}_{\mathrm{H}_2}$ the fugacity of hydrogen in atmospheres and H^+ is the activity of hydrogen ions. With the pressure of hydrogen equal to 1 atm and temperature 25 ºC, equation (4.6) becomes

$$\mathrm{E}_{\mathrm{H}_2} = -0.0592\mathrm{pH} \qquad \ldots (4.7)$$

4.1.2 Tafel Equation (Tafel Constants)

In activation polarization the overvoltage (η) increases with current density i, in accord with the Tafel equation **[Uhlig and Winston, 2008]**:

$$\eta = \beta \log \frac{\mathrm{i}}{\mathrm{i_o}} \qquad \text{(for general)} \qquad \ldots (4.8)$$

$$\eta_a = \beta_a \log \frac{\mathrm{i_a}}{\mathrm{i_o}} \qquad \text{(for anode reaction)} \qquad \ldots (4.9)$$

$$\eta_c = \beta_c \log \frac{\mathrm{i_c}}{\mathrm{i_o}} \qquad \text{(for cathode reaction)} \qquad \ldots (4.10)$$

where β is Tafel slopes and $\mathrm{i_o}$ exchange current density, they are constants for a given metal and environment and are both dependent on temperature, i is the rate of oxidation or reduction in terms of current density. The Tafel coefficient that can be obtained from the slope of a plot of η against log i, with the intercept yielding a value for i_o **[Roberge, 2000]**; Tafel slopes are determined from the following equations **[Fontana and Greene, 1984]**:

$$\beta_a = 2.303\frac{RT}{\alpha nF} \qquad \text{(for anode reaction)} \qquad \ldots (4.11)$$

$$\beta_c = -2.303\frac{RT}{(1-\alpha)nF} \qquad \text{(for cathode reaction)} \qquad \ldots (4.12)$$

By using natural logarithm Tafel slopes in equation (4.11) and (4.12) become:

$$b_a = \frac{RT}{\alpha nF} \qquad \text{(for anode reaction)} \qquad \ldots (4.13)$$

$$b_c = -\frac{RT}{(1-\alpha)nF} \qquad \text{(for cathode reaction)} \qquad \ldots (4.14)$$

The term α is approximately 0.4 – 0.6 for Fe, Ni, Cu, Hg, and several other metals **[Uhlig and Winston, 2008]**.

4.1.3 Exchange Current Density

The effect of changing pH is to change the value of the exchange current density of iron ion as follows **[Nesic et. al., 1996]**:

$$\frac{\partial \log i_0^{Fe}}{\partial pH} = \frac{\log i_{0(2)}^{Fe} - \log i_{0(1)}^{Fe}}{pH_2 - pH_1} = 1 \qquad \ldots (4.15)$$

The effect of changing pH is to change the value of the exchange current density of hydrogen ion as follows **[Nesic et, al., 1996]**:

$$\frac{\partial \log i_0^{H^+}}{\partial pH} = \frac{\log i_{0(2)}^{H^+} - \log i_{0(1)}^{H^+}}{pH_2 - pH_1} = -0.5 \qquad \ldots (4.16)$$

The temperature dependence of the exchange current density was modeled with an Arrhenius-type relation **[Nesic et. al., 1996]**:

$$\frac{i_0}{i_0^{ref}} = e^{-\left(\frac{\Delta H}{R}\right)}\left[\frac{1}{T} - \frac{1}{T_{ref}}\right] \qquad \ldots (4.17)$$

The enthalpy of activation for the H^+ reduction reaction is $\Delta H_{[H^+]}$ = 30 kJ/mol, and for iron $\Delta H_{[Fe^{+2}]}$ =26.25 kJ/mol for temperature range 20 to 60 °C **[Nesic et. al., 1996]**.

4.1.4 Current Density and Electrode Area

The anodic and cathodic sides of a reaction can be studied individually by using some well-established electrochemical methods in which the response of a system to an applied polarization, current or voltage is studied. A general representation of the polarization of an electrode supporting one redox system is given in the Butler-Volmer equation (4.18) **[Roberge, 2000]**.

$$i_{reaction} = i_0 \left\{ \exp\left(\alpha_{reaction} \frac{nF}{RT} \eta_{reaction} \right) - \exp\left[-(1 - \alpha_{reaction}) \frac{nF}{RT} \eta_{reaction} \right] \right\} \quad \dots (4.18)$$

where $i_{reaction}$ = anodic or cathodic current $\alpha_{reaction}$= charge transfer barrier or symmetry coefficient for the anodic or cathodic reaction, close to 0.5 **[Roberge, 2000]**:

$\eta_{reaction}$=$E_{applied}$ - E_{eq}, i.e., positive for anodic polarization and negative for cathodic polarization. $E_{applied}$ is the electrode potential relative to the standard hydrogen electrode SHE, Volte, E_{eq} is the equilibrium potential (Volt) and i_0 is the exchange current density, (A/cm^2). When $\eta_{reaction}$ is anodic (i.e., positive), the second term in the Butler-Volmer equation becomes negligible and i_a can be more simply expressed by Equation (4.19) **[Roberge, 2000]**.

$$i_a = i_{0,a} e^{(E - E_{eq,a}/\beta_a)} \quad \dots (4.19)$$

When $\eta_{reaction}$ is cathodic (i.e., negative), the first term in the Butler-Volmer equation becomes negligible and i_c can be more simply expressed by Equation (4.20).

$$i_c = i_{0,c}\left(\exp^{-(E - E_{eq,c}/\beta_c)} \right) \quad \dots (4.20)$$

when the area of the cathode equals the area of the anode I can be replaced by i which may be regarded as the criterion for the uniform corrosion of a single metal **[Shreir, 1994]**. However, if the area of the anode is smaller or greater than that of the cathode, anodic reaction is **[Cifuentes, 1987]**:

$$I_a = i_{0,a}A_a\exp\left[\frac{\alpha_a n_a F}{RT}\left(E_a - E_{eq,a}\right)\right] \qquad \ldots (4.21)$$

or

$$I_a = i_{0,a}f_a\exp\left[\frac{\alpha_a n_a F}{RT}\left(E_a - E_{eq,a}\right)\right] \qquad \ldots (4.22)$$

and the cathodic rate:

$$I_c = i_{0,c}A_c\exp\left[-\left(\frac{\alpha_c n_c F}{RT}\right)\left(E_c - E_{eq,c}\right)\right] \qquad \ldots (4.23)$$

or

$$I_c = i_{0,c}f_c\exp\left[-\left(\frac{\alpha_c n_c F}{RT}\right)\left(E_c - E_{eq,c}\right)\right] \qquad \ldots (4.24)$$

And the area fractions are:

$$f_a = \frac{A_a}{A_T} \qquad \ldots (4.25)$$

$$f_c = \frac{A_c}{A_T} \qquad \ldots (4.26)$$

where A_a and Ac are the anodic and cathodic electrode areas respectively and A_T is the summations of anode and cathode area, and f_a and f_c are the anodic and cathodic electrode area fractions.

4.1.5 Current Density Equivalent to a Corrosion Rate of 1 gmd

The corrosion rate of a metal in terms of weight loss per unit area (gmd) or rate of penetration (mmy^{-1}) can be calculated from Faraday's law if the current density is known **[Shreir, 1994]**.

$$\frac{m}{S} = \frac{M \times i \times t}{n \times F} \qquad \ldots (4.27)$$

Since ($m = \rho \times S \times d$), then from equation (4.27)

$$\rho S d = \frac{M \times i \times S \times t}{n\,F} \quad \text{or} \quad \rho d = \frac{M \times i \times t}{n\,F} \qquad \ldots (4.28)$$

and from equation (4.28) the rate of penetration (d/t) when i is in ($A\ m^{-2}$) is given by

$$\frac{d}{t}=\frac{M\times i}{\rho\, n\, F} \qquad (\text{m.day}^{-1}) \qquad \ldots (4.29)$$

To convert rate of penetration into weight loss per unit area per unit time

$$\text{g.m}^{-2}.\text{day}^{-1}=\rho\times\frac{d}{t}=\frac{M\,i}{n\,F} \qquad \ldots (4.30)$$

The following symbols and units have been adopted in deriving these relationships in which it is assumed that corrosion is uniform and the rate is linear, m = Mass of metal corroded (g), M = Molar mass (g.mol^{-1}), n = Number of electrons involved in one act of the corrosion reaction, F = Faraday's constant (96487 C/g.equiv.), i = Current density (A.m^{-2}), t = Time (day), ρ = Density of metal (g.cm^{-3}), S = Area of metal involved (m^{2}), and d = Thickness of metal removed (m). Simple equation to convert millimeters penetration per year **[Shreir, 1994]**:

$$\text{mmy}^{-1}=\frac{365.25}{\rho}\times\text{gmd} \qquad (\rho \text{ in kg m}^{-3}) \qquad \ldots (4.31)$$

4.2 Limiting Current Density

Fick's first law is introduced as **[Brodkey and Hershey, 1989]**:

$$J=-D\left(\frac{\partial C}{\partial x}\right) \qquad \begin{Bmatrix} T = \text{constant} \\ P = \text{constant} \end{Bmatrix} \qquad \ldots (4.32)$$

where J is the transport flux, D is is called the diffusion coefficient, C is the concentration of material which has units of (moles per volume), x is the distance, and P is the pressure. From Fick's first law and equating the transport flux J with the rate of an electrochemical reaction **[Shreir, 1994]**.

$$-D\frac{(C_b-C_s)}{\delta}=\frac{i}{nF} \qquad \ldots (4.33)$$

where C_b solubility of oxygen in water or liquids (shown in table A-3 in appendix A), C_s concentration of ions at the surface, δ the thickness of diffusion layer, n the number of electrons transferred.

$$i = -DzF\frac{(C_b - C_s)}{\delta} \qquad \dots (4.34)$$

The concentration gradient will be a maximum when $C_s = 0$, and this will correspond with the maximum or limiting current density i_L

$$i_L = \frac{-DzFC_b}{\delta} \qquad \dots (4.35)$$

where the mass transfer coefficient is defined as **[Cifuentes, in 1987]**:

$$K = \frac{D}{\delta} \qquad \dots (4.36)$$

Then the limiting current density becomes:

$$i_L = -zFKC_b \qquad \dots (4.37)$$

4.3 Relationships Between Hydrodynamic Parameters

To calculate the overall values of the mass transfer coefficients; relationships between K and other hydrodynamic parameters are expressed in terms of non-dimensional groups as outlined below **[Poulson and Robinson, 1986]**:

$$Sh = \frac{Kd}{D} \qquad \text{(Sherwood number)} \qquad \dots (4.38)$$

$$Re = \frac{d\rho u}{\mu} \qquad \text{(Reynolds number)} \qquad \dots (4.39)$$

$$Sc = \frac{\mu}{D\rho} \qquad \text{(Schmidt number)} \qquad \dots (4.40)$$

where K is the mass transfer coefficient ($m.\ s^{-1}$), d is the tube diameter, D is the diffusivity of the relevant species, u is the velocity (m/s), μ is the solution viscosity (Pa/s), and ρ is the solution density (kg/m^3).

4.4 The Mass Transfer Coefficient

The mass transfer coefficient can be calculated from Sherwood number in the case of turbulent regime.

$$K = \left(\frac{D}{d}\right) Sh \qquad \dots (4.41)$$

4.4.1 Smooth Pipe

For smooth pipe the friction factor is calculated from Blasius correlations **[Blasius, 1913]**:

$$f = 0.0079Re^{(-1/4)} \qquad \dots (4.42)$$

This equation used to predict friction factor for smooth pipe for Re 3000 to 100000 **[Welty et. al., 2001; Brodkey and Hershey, 1989]**.

Shaw and Hanraty, [1977] proposed the following equation for mass transfer coefficient in terms of Sc and friction factor:

$$Sh = 0.0889 \sqrt{(f/2)}\, Re\, Sc^{0.246} \qquad \dots (4.43)$$

4.4.2 Pipe flow with roughness

Sherwood numbed calculated from Eq. 4.43 for pipe flow in terms of Sc and friction factor **[Shaw and Hanratty, 1977].**

Chen, [1985] developed an explicit friction factor equation for rough surface pipe which is valid for all regimes of turbulent flow with an accuracy of within about ±8%:

$$f = 0.0791 \left[\frac{1}{Re^{0.83}} + 0.11 \left(\frac{e}{d}\right)\right]^{0.3} \qquad \dots (4.44)$$

4.5 Pipe Flow With Heat Flux

Friend-Metzner, [1958] proposed an equation of substantially different form in order to correlate the heat transfer coefficient in smooth pipe over wide range of Pr and Sc. Their correlation of heat transfer for 0.5< Pr < 600 and Re > 10000 for pipe flow is:

$$Nu = \frac{RePr\left(f/2\right)}{1.2+11.8\left(\frac{f}{2}\right)^{1/2}(Pr-1)Pr^{-1/3}} \qquad \dots (4.45)$$

$$\mathrm{Nu} = \frac{hd}{k} \qquad \ldots (4.46)$$

The surface temperature is calculated from heat flux as:

$$T_W = \frac{q_W}{h} + T_b \qquad \ldots (4.47)$$

The film temperature is:

$$T_f = \frac{\mathrm{T_W + T_b}}{2} \qquad \ldots (4.48)$$

Where Pr is the Prandtl number, h is the heat transfer coefficient (Wm $^{-2}$ K^{-1}), T_W is the wall temperature (°C), q_W is the heat flux (W/m^2), T_b is the bulk temperature (°C), and T_f is the film temperature. The mass transfer from Friend-Metzner correlation is

$$Sh = \frac{\mathrm{Re\ Sc}\left(f/_2\right)}{1.2+11.8\left(f/_2\right)^{1/2}(Sc-1)Sc^{-1/3}} \qquad \ldots (4.49)$$

The friction factor is calculated from Blasius correlation as shown in equation 4.42.

4.6 Rotating Cylinder

The mass transfer coefficient can be calculated from correlation of Eisenberg, et al., [1954] for rotating cylinder:

$$Sh = 0.0791\, Re^{0.7} Sc^{0.336} \qquad \ldots (4.50)$$

4.7 Uniform Corrosion

For any corroding metal, the chemical equivalents of metal going into solution at the anodic sites are equal to the chemical equivalents of reduction products produced at cathodic sites. In terms of corrosion current, for a given area of metal surface **[Uhlig and Winston, 2008]**:

$$\sum \mathrm{I}_a = \sum I_c \qquad \ldots (4.51)$$

That is, the anodic and cathodic currents are equal in magnitude, if $A_a = A_c$ that is, if 50% of the surface is anodic and 50% is cathodic.

$$\sum \mathrm{i}_a = \sum i_c \qquad \ldots (4.52)$$

In an aerated aqueous solution, the reduction reaction (cathode reaction) currents equal the oxidation (anodic reaction) currents and Eq. (4.52) becomes:

$$\mathrm{i}_a = i_c + i_L \qquad \ldots (4.53)$$

To determine E_{corr} and $I_{corr,}$ it is possible to solve these problems mathematically, as illustrated in the following transformations. The applied potential is:

$$E = E_{eq} + \beta \log(\mathrm{I}) - \log(\mathrm{I}_\circ) \qquad \ldots (4.54)$$

or

$$\frac{E-E_{eq}}{\beta} = log \frac{I}{I_0} \qquad \ldots (4.55)$$

and the applied current can then be written as

$$I = I_0 exp\left(\frac{E-E_{eq}}{\beta}\right) \qquad \ldots (4.56)$$

At E_{corr}, $I_a = I_c = I_{corr}$ and $E_a = E_c = E_{corr}$, Then one can obtain E_{corr} or I_{corr}:

$$E_{corr} = E_{eq,a} + \beta_a \, log\left(\frac{I_{corr}}{I_{0.a}}\right) \qquad \text{(anode reaction)} \qquad \ldots (4.57)$$

$$E_{corr} = E_{eq,c} + \beta_c \, log\left(\frac{I_{corr}}{I_{0.c}}\right) \qquad \text{(cathodic reaction)} \qquad \ldots (4.58)$$

or

$$\mathrm{I_{corr}} = \mathrm{I_{0,a}} \mathrm{exp}\left(\frac{\mathrm{E_{corr}} - \mathrm{E_{eq,a}}}{\beta_\mathrm{a}}\right) \qquad \text{(anode reaction)} \qquad \ldots (4.59)$$

$$\mathrm{I_{corr}} = \mathrm{I_{0,c}} \mathrm{exp}\left(\frac{\mathrm{E_{corr}} - \mathrm{E_{eq,c}}}{\beta_\mathrm{c}}\right) \qquad \text{(cathodic reaction)} \qquad \ldots (4.60)$$

In aerated neutral or basic aqueous solution the dissolved oxygen affects the reduction reaction then in concentration region, the assumptions in the derivation of the Volmer- Butler equation is the uniformity of concentration near the electrode. This assumption fails at high current densities because migration of ions towards the electrode from the bulk is slow and may become rate determining. A larger overpotential is then needed to produce a given current because the supply of reducible or oxidizable species has been depleted **[Pierre, 2000]**.

For reduction reaction:

$$E_r = E^\circ + \frac{RT}{nF}\ln C_b \qquad \dots (4.61)$$

When passages of external current is made through the cell the interfacial concentration changes to a value of C_S, resulting in change of electrode potential.

$$E_p = E^\circ + \frac{RT}{nF}\ln C_s \qquad \dots (4.62)$$

The concentration overpotential is:

$$\eta_c = E_p - E_r = \frac{RT}{nF}\ln\left(\frac{C_s}{C_b}\right) \qquad \dots (4.63)$$

Deriding Eq. (4.34) by Eq. (4.33):

$$i = i_L\left(1 - \frac{C_s}{C_b}\right) \qquad \dots (4.64)$$

$\frac{C_s}{C_b} = \frac{i}{i_l}$ Then equation (4.64) becomes:

$$i = i_L\left(1 - \frac{i}{i_L}\right) \qquad \dots (4.65)$$

The overpotential becomes:

$$\eta_{conc,c} = \beta_c \log\left(1 - \frac{i}{i_L}\right) \qquad \dots (4.66)$$

Concentration polarization is usually negligible on anodes and usually ignored **[Jones, 1996]**:

$$\eta_a = \eta_{act,c} = \beta_a \log\left(\frac{i_a}{i_0}\right) \qquad \dots (4.67)$$

Total Cathodic Polarization:

$$\eta_c^{total} = \eta_{act,c} + \eta_{conc,c} = \beta_c \log\left(\frac{i_c}{i}\right) + \beta_c \log\left(1 - \frac{i}{i_L}\right) \qquad \ldots (4.68)$$

By combining the laws governing diffusion with the Nernst equation, the following expression can be developed **[Speller , 1935]**

$$\eta_T = E_{corr} - E_{eq} \qquad \ldots (4.69)$$

$$E_{corr} = E_{eq} + \beta_c \log\left(\frac{i_c}{i}\right) + \beta_c \log\left(1 - \frac{i}{i_L}\right) \qquad \ldots (4.70)$$

4.8 Analysis

The above equations were employed to calculate the corrosion rate and corrosion potential for iron corroding in aerated HCl solution for temperatures of 25, 40, and 60 ℃, for pH of 1, 2, and 4, in the turbulent flow for the Reynolds number of 5000, 10000, 20000, 40000, and 60000, the physical properties of solution are presented in table (A-5) in appendix A. The diameter of pipe and rotating cylinder is 0.0255 m, α_{Fe}=0.5 **[Uhlig and Winston, 2008]** and α_{H2}=0.5 **[Nesic et. al., 1996]**, and α_{O2}=0.5 **[Wang and Postlethwaite, 1997]**.

4.8.1General Analysis

i. In all different cases of corrosion the equilibrium potentials is calculated from Nernst equation (4.3) for iron, hydrogen and for oxygen at temperature 25, 40 and 60 $^\circ$C.

ii. Hydrogen ion concentrations with different pH values are calculated using equation (4.4).

iii. Tafel slopes for cathode and anode are determined from equations (4.11) and (4.12) with α_{Fe}=0.5 **[Uhlig and Winston, 2008]** and α_{H2}=0.5 **[Nesic et. al., 1996]**, and α_{O2}=0.5 **[Wang and Postlethwaite, 1997]**.

iv. Changing pH leads to change the value of exchange current density for iron and hydrogen, equation (4.15) is used to calculate the new value of exchange current density for iron and equation (4.16) is used to calculate the new exchange current density of hydrogen. The exchange current density change with temperature (25, 40, and 60 °C) is calculated using an Arrhenius-type relation from equation (4.17). The activation energy (ΔH) for the H^+ reaction is $\Delta H_{[H^+]}$ =30000 J/mol, and for iron $\Delta H_{[Fe^{+2}]}$ = 2625 **[Nesic et. al., 1996]**.

v. The anodic and cathodic currents are estimated from equations (4.21) and (4.23) with A_a=A_c=1m^2. The corrosion current density of iron can be converted to grams per square meter per day (gmd) and millimeters penetration per year (mm/y) by using equations (4.30) and (4.31) respectively.

vi. The mass transfer coefficient (K) is calculated from Sherwood number equation (4.43) then calculated i_L from (K) using Eq. (4.41).

vii. Sherwood number, Reynolds number, and Schmidt number, values from equations (4.38), (4.39), and (4.40) respectively, the diameter is (d=.0255 m), the solution viscosity (μ), and the solution density (ρ), them values from physical properties of water at atmospheric pressure shown in table (A.5),and the value of diffusivity (D) from table (A.2).

4.8.2 Calculations of Mass Transfer Coefficient in Smooth and Rough Pipe Flow

The Sherwood number of smooth pipe is obtained from equation (4.43) and the friction factor from Blasius correlations equation (4.42). For pipe flow with rough surface, the Sherwood number is obtained from equation (4.43), with friction factor correlation from equation (4.44). The values of relative roughness are considered namely, 0.0001, 0.0004, and 0.004.

4.8.3Calculation of Corrosion Under Heat Transfer Flux

The heat flux effect through the surface of the pipe, leads to change the surface temperature which in turn change the oxygen diffusivity as has been mentioned by previous studies **[Mahato et. al., 1968; Raa and Trass, 1964]** and other physical properties such as viscosity and density etc. The film temperature is calculated using equation (4.48), and the wall temperature using equation (4.47). The heat transfer coefficient (h) is calculated from Nusselt number from Friend-Metzner equation (4.45). To obtain the mass transfer coefficient Sherwood number is calculated using equation (4.49) and the friction factor from Blasius correlations in equation (4.42). Four different heat fluxes (3000, 5000, 15000, 30,000 W/m^2) are employed.

4.8.4Calculation of Mass Transfer Coefficient Using Rotating Cylinder of Smooth Surface

From general analysis values needed in this case are obtained. The mass transfer coefficient (K) can be calculated from equation (4.41), Sherwood number depends on the surface (rough or smooth), and the flow region, in rotating cylinder without roughness (smooth surface) the Sherwood number is calculated from equation (4.50).

4.8.5Calculation of Corrosion Current Densities ($I_{corr.}$) and Corrosion Potential ($E_{corr.}$)

To calculate corrosion currents ($i_{corr.}$) for anode or cathode equations (4.21), or (4.23) are used, by use trial and error method by assuming the initial value of corrosion potential ($E_{corr.}$), until the summation of anode currents equal the summation of cathode currents as in equation (4.52), then the right value of corrosion potential (E_{corr}) is obtained and from which corrosion currents ($i_{corr.}$) is obtained. Substituting corrosion potential ($E_{corr.}$) in equation (4.21) and (4.23) to obtain the anodic and cathodic currents. The anodic current is the iron oxidation currents (i_{Fe}) and the cathodic currents are the hydrogen reduction reaction Eq. (2.4) and oxygen reduction reaction Eq. (2.4). Substituting the anodic and cathodic current, equation (4.54) becomes:

$$\mathrm{i_o^{Fe}}\exp\left(\frac{\mathrm{n_{Fe}\times F\times \alpha_{Fe}(E_{corr}-E_{eq}^{Fe}}}{\mathrm{R\times T}}\right) = \mathrm{i_o}^{\mathrm{H^+}/\mathrm{Fe}}\exp-\left(\frac{\mathrm{n_{H_2}\times F\times \alpha_{H_2}(E_{corr}-E_{eq}^{H_2}}}{\mathrm{R\times T}}\right) + n_{O_2}\times F\times C_b\times\frac{D}{d}\times Sh \quad \ldots (4.71)$$

$$\mathrm{i_o^{Fe}}\exp\left(\frac{\mathrm{n_{Fe}\times F\times \alpha_{Fe}(E_{corr}-E_{eq}^{Fe}}}{\mathrm{R\times T}}\right) = \mathrm{i_o}^{\mathrm{H^+}/\mathrm{Fe}}\exp-\left(\frac{\mathrm{n_{H_2}\times F\times \alpha_{H_2}(E_{corr}-E_{eq}^{H_2}}}{\mathrm{R\times T}}\right) + n_{O_2}\times F\times C_b\times\frac{D}{d}\times\left(0.0889\sqrt{(\mathrm{f}/2)}\ \mathrm{Re\ Sc}^{0.246}\right) \quad \ldots (4.72)$$

Table 4-1: Lists the condition that were used for calculating the corrosion currents individual currents, and corrosion potentials in this analysis

Re	5000	10000	20000	40000	60000
T (ºC)	25	40	60	–	–
pH	1	2	4	–	–
e/d	0.0001	0.0004	0.004	–	–
q (W/m^2)	3000	5000	15000	30000	–

CHAPTER FIVE

RESULTS AND DISCUSSION

Chapter five introduced the calculation results under number of variables involved, i.e., Re, temperature, pH, roughness, heat flux, and their interactions. To explain the effect of these variables on corrosion process, the following sequence is followed: section 5.1 explains the effect of Re, temperature, pH, wall roughness, and heat flux, for pipe flow and section 5.2 deals with the effect of Re, temperature, pH, on the rotating cylinder. Also the polarization curves were constructed for various conditions using the proposed theoretical models.

5.1 Pipe Flow

Practical importance of the corrosion of Fe has led to vast literature in the field. In the case of corrosion in aqueous environment the important variables recognized have been the amount of dissolved O_2, temperature, flow conditions, pH, metal composition, duration of exposure, and composition of solution **[Uhlig, 1963]**.

5.1.1 Effect of Reynolds Number

5.1.1.1 Corrosion Rate

The rate of reduction (oxygen reduction) is limited by diffusion from the bulk solution to the electrode surface. Corrosion rates generally increase with increasing velocity due to the depolarizing effect on the cathode. Fig. 5-1 gives the variation of corrosion rate of Fe measured in gram per square meter per day (gmd) with Re at three temperatures in aerated HCl.

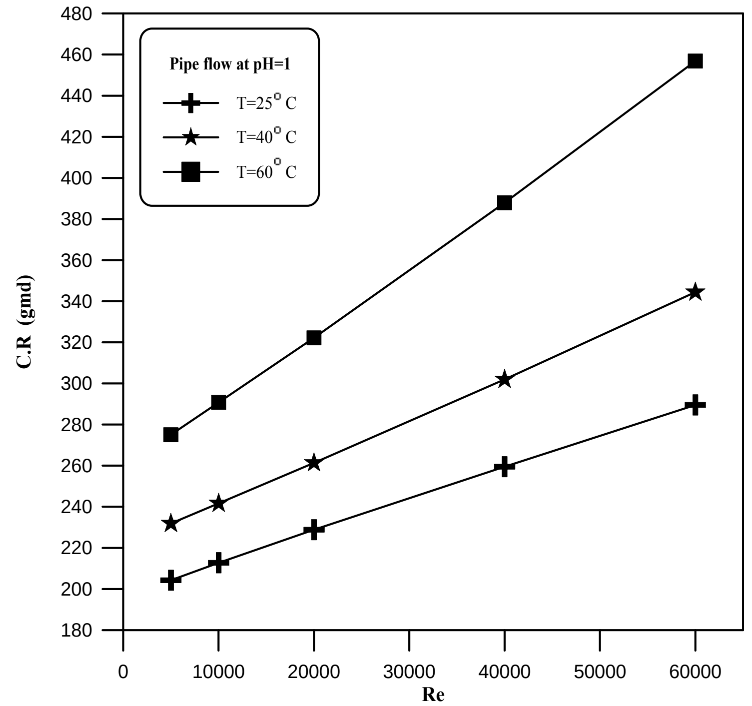

Figure 5-1: Variation of Corrosion Rate of Fe with Re at three temperatures.

The corrosion rate increases with increasing Reynolds number (or velocity) because the increase in O_2 transport to the surface. Within the range investigated, the velocity increases the corrosion rate for all temperatures **[Mahato et. al., 1968; Levlch, 1943]**. Speller and Kendall [1923] found that the rate is low under laminar flow conditions, rapidly increases in the transition range, and more slowly increases under turbulent flow conditions. Butler and Ison [1960] investigated the corrosion of mild steel pipe specimens in flowing water of Teddington (England) mains and presented data for different flow rates and different temperatures. They found that an increase in both speed of flow and temperature promotes the deposition of a protective scale. Other workers tend that the corrosion rate increases by one order of magnitude when the Reynolds number increasing [**Wang and J. Postlethwaite, 1997; Berger and Hau, 1977**]. Fig. 5-2 gives the variation of current density of H_2 with Reynolds number at three temperatures .The rate of hydrogen evolution (hydrogen current) decreased with increasing Reynolds number. This decrease in H_2 current density is because the bulks supply the surface with high rate of oxygen with increasing Reynolds number. Shifting the corrosion potential to more positive leading to decrease the hydrogen evolution rate. The cathodic current for H^+ reaction is negligible compared to that for O_2 reduction in pH ≥4 **[Wang and Postlethwaite, 1997]**. Fig 5-3 shows the variation of current density of H_2 and O_2 with Reynolds number at temperature 25 ºC and pH 4. The sum of currents densities of hydrogen evolution and oxygen reduction represents the cathodic reaction, and when the current density of oxygen increase the current density hydrogen decrease to be equal to the current density of Fe as in equation (6.1)

$$i_{Fe} = i_{H_2} + i_{lim.} \qquad \dots (5.1)$$

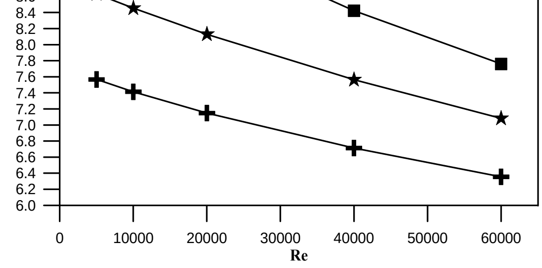

Figure 5-2: Variation of current density of H_2 with Re at three temperatures.

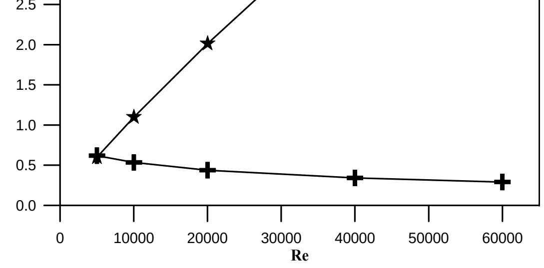

Figure 5-3: Comparison between the current density of H_2 and limiting current density of O_2 at T=25° C and pH=4.

5.1.1.2 Limiting Current Density and Mass Transfer Coefficient

Fig. 5-4 shows the variation of the limiting current density i_L with Re at three temperatures. Increasing Re leads to decrease the thickness of diffusion layer in the wall vicinity which represents the main resistance to oxygen transport; the diffusion layer thickness (δ) is dependent on the velocity of the solution past the electrode surface. As the velocity increases, δ decreases and the limiting current increases **[Steigerwald, 1987]**. At sufficiently high velocities, enough oxygen may reach the surface to cause partial passivity; the rate of oxygen transport is basically function of flow rate, and temperature [**Mahato et. al., 1968; Wormwell, 1946**]. Mahato et. al. [1968] reported that corrosion rates were determined largely by the rate of oxygen supply to the metal surfaces, Hatch and Rice [1945] observed that the change in the oxygen concentration gradient near the metal surface is due to the effect of velocity, since the corrosion of iron in aerated solution is a mass transfer controlled process **[Speller, 1938; Coaen, 1948; Copson, 1952; Btrrler and Stroud, 1965; Whitman et. al., 1924]**. Fig. 5-5 shows the variation of mass transfer coefficient with Re at three temperatures. The values of mass transfer coefficient (k) increased as the flow rate (or Re) increases. Increasing flow turbulence leads to decrease the thickness of the diffusion boundary layer that represents the main resistance to mass transfer, and provide the surface with oxygen leading to increase k, Ross and Badhwar [1965] found that mass transfer coefficient increased as the flow rate increased. This finding is in agreement with previous investigations Speller [1951]; Son and Hanratty [1967].

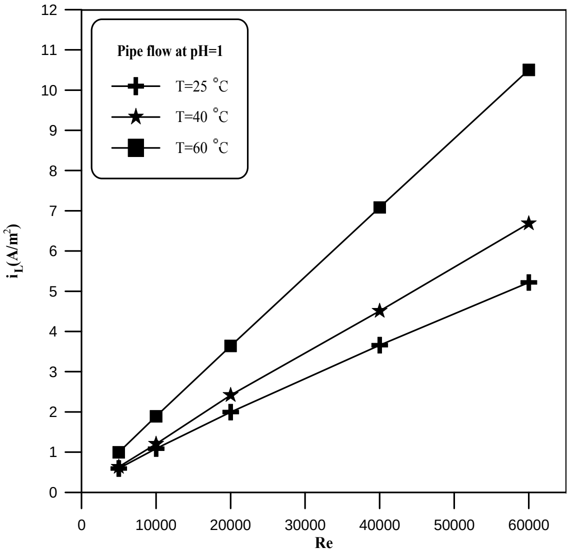

Figure 5-4: Variation of limiting current density with Re at three temperatures.

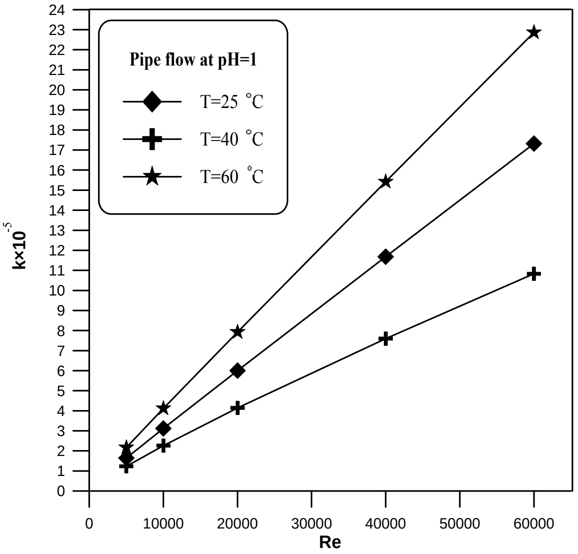

Figure 5-5: Variation of mass transfer coefficient with Re at three temperatures.

5.1.1.3 Corrosion Potential

Fig. 5-6 shows the variation of corrosion potential with Re at three temperatures. It is generally accepted that the corrosion potential of iron is under mixed control of anodic and cathodic processes **[Shreir, 1994; Trethewey and Chamberlain 1996]**. Generally corrosion potential shifts to more positive values with increasing Reynolds number. Ross et, al. [1966] stated that the increase of E_{corr} with Re is due to the increase in oxygen transport to the metal surface and when the system is free from oxygen, Re has no effect on E_{corr}. This finding is in agreement with previous investigations **[Nesic et. al., 1995; Makrides, 1960; Tobias and Nobe, 1975; Chin and Nobe, 1977; Eremais and Prazk, 1973]**. In other words, increasing O_2 transport to the surface leads to shift the potential to more positive because of following reaction:

$$O_2 + 4H^+ + 4e \rightleftharpoons 2H_2O \qquad E^\circ = +1.22 \text{ Volt (SHE)} \quad \ldots (5.2)$$

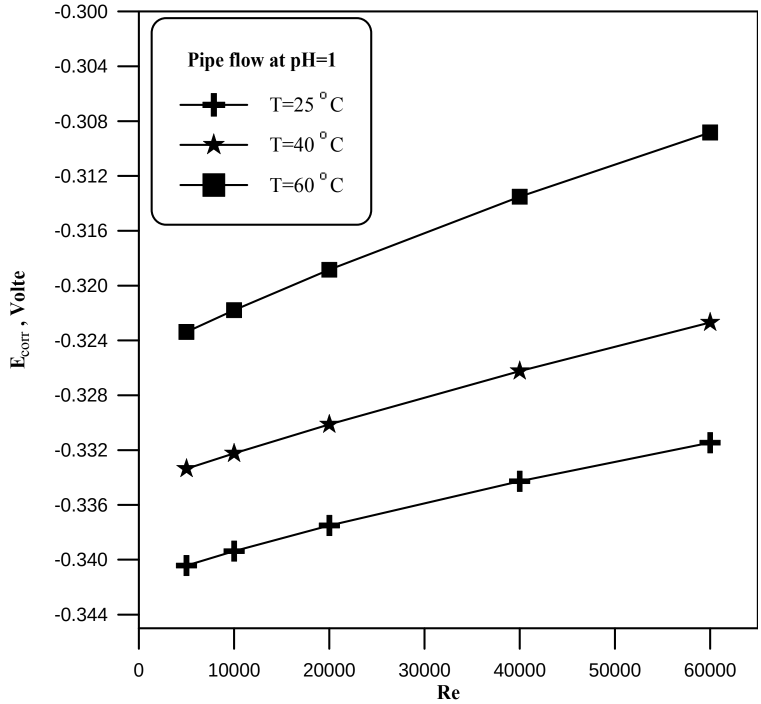

Figure 5-6: Variation of Corrosion Potential with Re at three temperatures.

5.1.2 Effect of Temperature

5.1.2.1 Corrosion Rate

The effects of temperature on a chemical reaction is of practical and theoretical importance. When the temperature rises the corrosion rate increases. This trend is in agreement with revise studies. To explain this variation there are four variables dependedent on temperature which are the exchange current density i_o, the equilibrium potential (E_{eq}), diffusion coefficient of oxygen, the solubility of oxygen. Increasing temperature leads to increase the value of exchange current density i_o according to Arrhenius relation equation 4.17, change the equilibrium potential (E_{eq}) according to Nernst equation 4.3, decrease the equilibrium potential of Fe and H_2 but increase the equilibrium potential of O_2 **[Cifuentes, 1987]**, increase the diffusion rate of oxygen species by increasing the molecular diffusion coefficient (Table A-2 list values of oxygen diffusivity in appendix A), and decreases the oxygen solubility (TableA-3 list values of solubility of oxygen in HCl). Fig. 5-1 shows the effect of temperatures on corrosion rate of Fe variation with Re measured in gram per square meter per day. The rate of corrosion of iron increases with temperature especially in media in which evolution of hydrogen accompanies corrosion, e.g. during corrosion of steel in acids **[Ehteram A. Noor, 2007]**. Temperature effects on acidic corrosion of iron and steel most often in HCl and H_2SO_4 solution had been the object of large number of investigations **[Jiang et. al., 1995; Bentiss et. al.,1999; Popova et. al.,2007; Abd El-Rehim et. al.,2001; Wang et. al., 2003]**. Fig. 5-2 shows the effect of temperature on the current of hydrogen evolution variation with Re. When the temperature increases the current density of hydrogen increases because the temperature effect on the exchange current, equilibrium potential, diffusion rate of hydrogen, and activation energy of hydrogen. The rate for iron corroding in hydrochloric acid, for example, approximately doubles for every 10 °C rise in temperature **[Uhlig and Winston 2008]**. Increasing temperature leads to increase i_o **[AL-Darbi, 2002]**. For metals that corrode by hydrogen evolution, decreasing hydrogen overpotential is one factor accounting for increase of corrosion as the temperature is raised **[Uhlig and Winston 2008]**.

5.1.2.2 Limiting Current Density

The most pronounced effect of increasing temperature was the increase in the mass transfer controlled i_{lim} which resulted from an increase in the diffusion coefficient (D) (Table A-2 gives values of oxygen diffusivity in appendix A) and decrease in viscosity at higher temperatures (TableA-5 physical properties of water in appendix A). Fig 5-3 shows the temperature effect on limiting current density variation with Re. Speller [1951] found in an open vessel, when allowing dissolved oxygen to escape, the rate increases with temperature to about 80 °C and then falls to a very low value at the boiling point (Fig. 2-7). The low corrosion rate above 80 °C is related to a marked decrease of oxygen solubility in water as the temperature is raised, and this effect eventually overshadows the accelerating effect of temperature alone **[Speller, 1951; Skaperdas and Uhlig, 1942]**.

5.1.2.3 Corrosion Potential

Fig. 5-6 shows the temperature effect on the corrosion potential. Increasing temperature shifts the corrosion potential at which positive direction. This agrees with previous investigators **[Ross et. al., 1966]**. E_{corr} values obey the mixed potential theory; E_{corr} are affected by both the anodic (activation controlled) and cathodic (concentration controlled). The anodic and cathodic processes are stimulated by increasing temperature and velocity **[Shreir, 1994; Steigerwald, 1968]**. The cathodic and anodic partial reaction rate are electrically equivalent at the corrosion potential, the cathodic reaction rate is controlled by the rate of arrival of oxygen at the metal surface and is significantly increases **[Qian and Chagnon, 2001]**. Increasing temperature accelerates the reaction rate and decreases the Tafel constant for anodic dissolution and increases the maximum current density in the active region **[Finley and Myers, 1970; Steigerwald and Greene, 1962; Bonhoeffer, 1955]**.

5.1.3 Effect of pH

5.1.3.1 Corrosion Rate

Figure 5-7 shows the variation of corrosion rate of Fe with Re at three values of pH. For pH values below 4.0, ferrous oxide (FeO) is soluble. Thus, the oxide dissolves as it is formed rather than depositing on the metal surface to form a film. In the absence of the protective oxide film, the metal surface is in direct contact with the acid solution, and the corrosion reaction proceeds at a greater rate than it does at higher pH values **[Beddoes and Parr 1999]**. The corrosion rate for iron as a function of pH is illustrated in Fig. 2-4 obtained by Charng and Lansing [1982]. The corrosion rates of Fe were decreasing with pH increase. Acidic solution is one of the most important factors in corrosion combating **[Uhlig et. al., 1955; Kirby, 1951; Leckie, 1075]**. Fig. 5-8 shows the variation of hydrogen current density with Re at three values of pH. The clear effect of pH appeared on the corrosion current of hydrogen because when hydrogen concentration decreases the current density of hydrogen decreases.

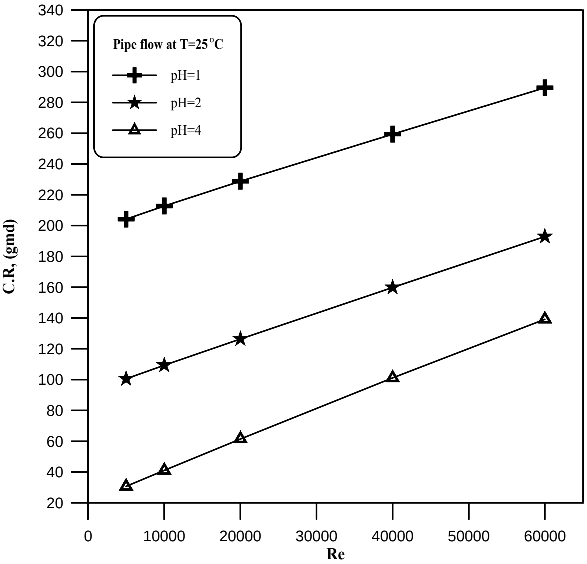

Figure 5-7: Variation of corrosion rate of Fe with Re at three values of pH.

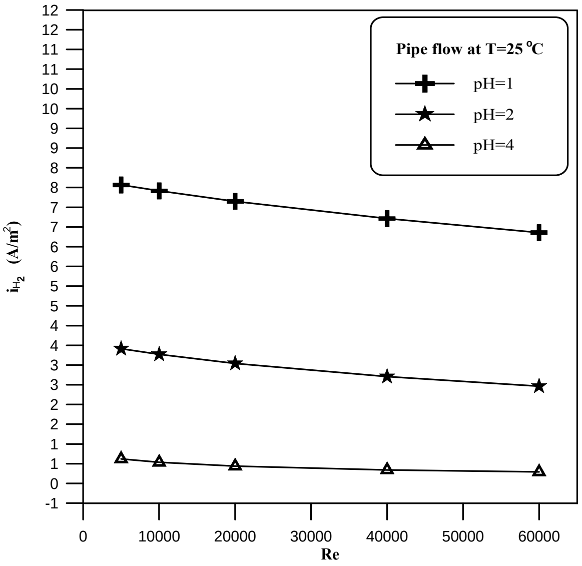

Figure 5-8: Variation of current density of H_2 with Re at three values of pH.

5.1.3.2 Limiting Current Density

Fig 6.9 shows variation of i_L with Re at three values of pH. There is no effect on the limiting current density by increasing or decreasing the pH **[Whitman et. al., 1924]**. In the acid range, pH < 4, oxygen is not controlling, and the corrosion reaction is established, in part, by the rate of hydrogen evolution. The rate becomes sufficiently high in this pH range to make anodic polarization a possible contributing factor (i.e., mixed control) **[Bond, 1958; Whitman et. al., 1923;**

Foroulis and Uhlig; 1964]. The oxygen limiting current is not affected too much by pH because the increase in hydrogen ion concentration has a slight effect on oxygen concentration.

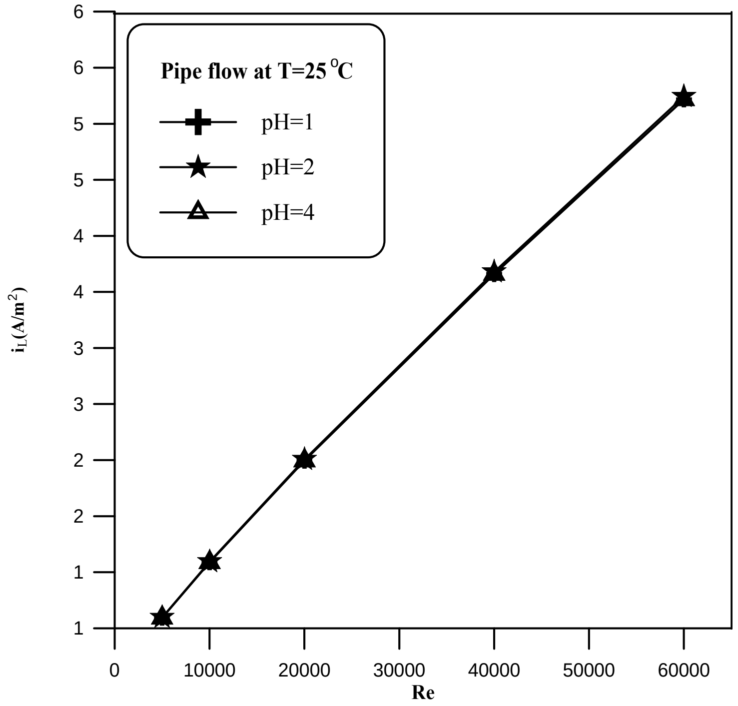

Figure 5-9: Variation of limiting current density with Re at three values of pH.

5.1.3.3 Corrosion Potential

Figure 5-10 gives the variation of corrosion potential with Re at two different values of pH. It is clear that when pH increases corrosion potential shifts to more negative. The decreased corrosion potential of iron as pH increases is not caused by decreased hydrogen evolution alone; in fact, greater accessibility of oxygen to the metal surface on dissolution of the surface oxide favors oxygen depolarization, which is often the more important reason **[Whitman and Russell, 1952; Bond, 1958; Brenan and Trass, 1964]**. Also when hydrogen ion concentration decreses (pH increases), the corrosion potential shifts to equilibrium potential of iron.

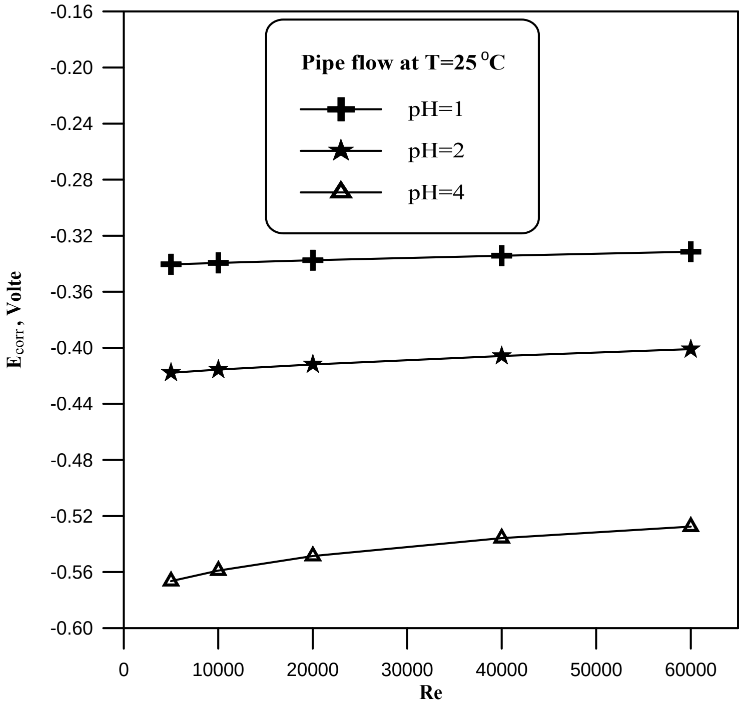

Figure 5-10: Variation of corrosion potential with Re at three values of pH.

5.1.4 Effect of Wall Roughness

5.1.4.1 Corrosion Rate

The corrosion rate is calculated for various values of surface roughness (e/d= 0.0001, 0.0004, and 0.004). Fig. 5-11 shows the variation of corrosion current of Fe with Re at three of relative roughness (e/d) and in smooth pipe. The corrosion rate increases with Re as have been shown. The higher the pipe wall roughness is the higher the corrosion rate. Increasing surface roughness increases the local mass transfer coefficient by increasing the turbulence in the wall vicinity. On the other hand increasing surface roughness leads to increase the surface area between the fluid and pipe wall leading to increases the mass transfer rate. Hence the mass transfer rate increases with the increase in roughness **[Brenan and Trass,**

1964]. For rough pipe, if the Reynolds number was large, the laminar sublayer would be small and roughness would be controlling. On the other hand, if the Reynolds number was low and the sublayer relatively large, then the roughness would be buried in the sublayer, and the pipe would act if it was smooth **[Brodkey and Hershey, 1989**]. In turbulent flow Levich [1962] postulated two zones within the hydrodynamic boundary layer: a damped turbulence layer near the solid interface in which the momentum transfer takes place primarily because of friction, and a turbulent boundary layer beyond where the exchange of momentum occurs entirely by the random eddy movements of turbulent flow. He also stated that diffusion layer is present next to the interface within the hydrodynamic boundary layer in which mass is transported mainly by molecular diffusion. In the corrosion of mild steel pipe in flowing aerated water, the main problem to be resolved is to determine the manner in which the growth of the corrosion product layer and changing surface roughness affect both the hydrodynamics and the transfer of reactants (dissolved oxygen) to the reacting surface. It is accepted that the corrosion of mild steel is controlled here by the rate of cathodic reduction of oxygen and hence by the rate of transport of oxygen from the main stream **[Mahato et. al. 1980]**. King and Broodie [1937]; Litt and Friedlander [1959]; and Meyerink and Friedlander [1962] pointed out that mass transfer is sensitive to surface roughness. Brenan and Trass [1964] studied the effect of surface roughness on the dissolution rate of cinnamic acid, benzoic acid and succinic acid. They observed that mass transfer rate increased by about four times with the increase in roughness. The turbulence in the main stream will be damped down near the solid interface and roughness peaks layer of corrosion products protrode. This finding is in agreement with previous investigations **[Litt and Friedlander, 1959; Meyerink and Friedlander, 1962]**.. In smooth pipe the friction factor depends on the Reynolds number which represented by the Blasius equation (4.42). In case of rough pipe the friction factor is almost dependent on the Reynolds number and the relative roughness of the surface which represented by Kntnasen and Katz [1958].

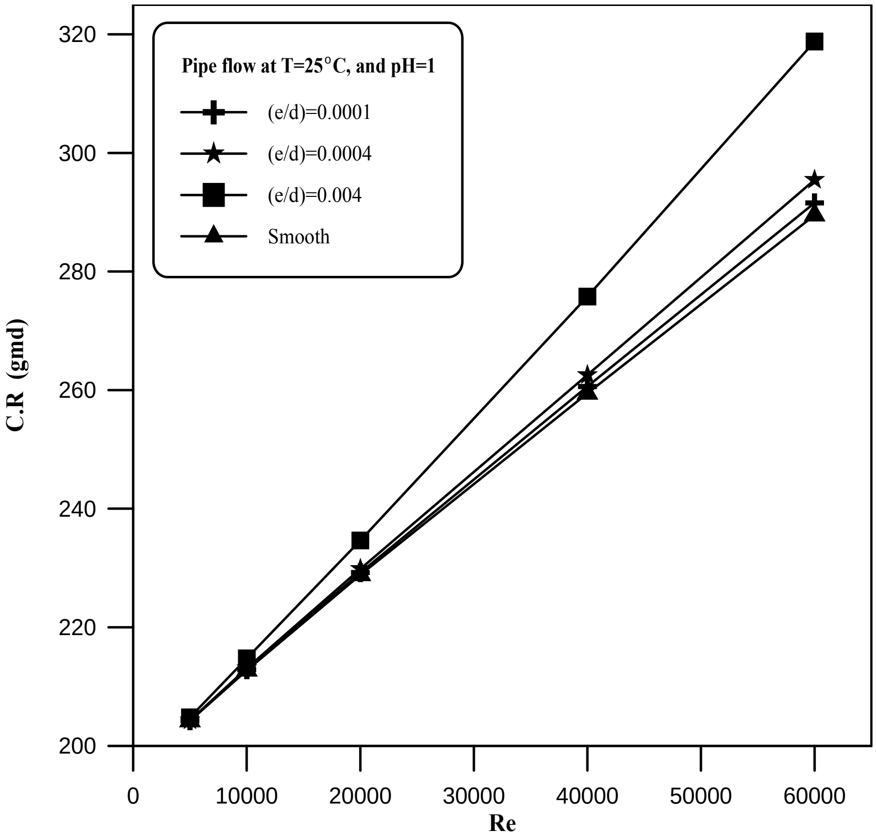

Figure 5-11: Variation of corrosion Rate of Fe with Re in smooth and rough pipe at pH=1.

Fig. 5-12 shows variation of current density of H_2 with Reynolds number at three values of relative roughness (e/d) and in smooth pipe .In the rough surface the supply of oxygen to the surface increases with increasing the relative roughness and Reynolds number by increasing eddy diffusion of oxygen from bulk to the surface, then the corrosion potential shifted to more positive values leading to the current density of hydrogen decreases with increasing relative roughness. It can be seen from Fig. 5-12 that the current density in smooth pipe is greater than rough pipe.

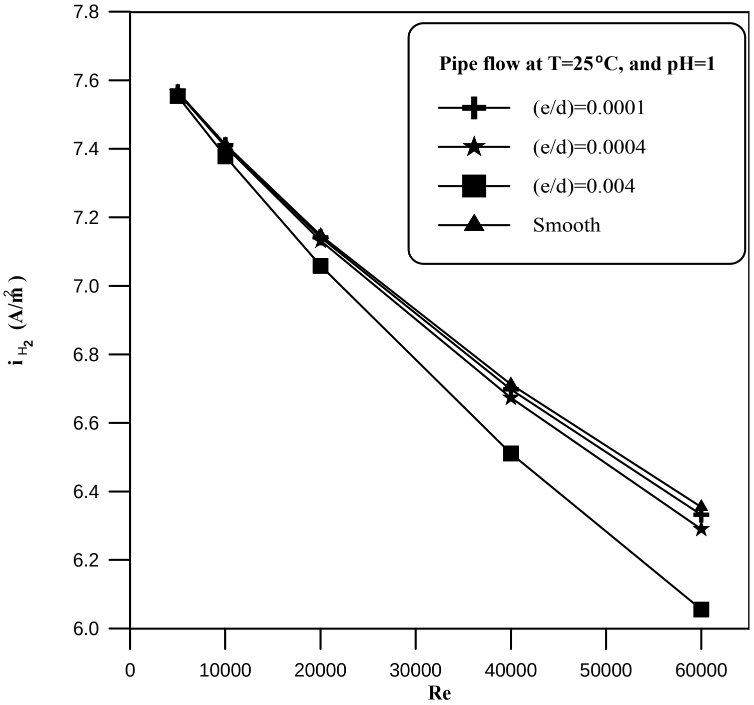

Figure 5-12: Variation current density of H_2 with Re in smooth and rough pipe at pH=1.

5.1.4.2 Limiting Current Density and Corrosion Potential

The limiting current density increases with increase of relative roughness. Fig. 5-13 shows variation of i_L with Reynolds number at three values of relative roughness and in smooth pipe. It is evident that the i_L increases with increasing roughness because in rough pipe the random eddy movement of turbulent flow occurs because of friction effect near the solid interface. This random eddy movement transports the oxygen through the pores to the metal increasing the corrosion rate and the limiting current density.

5.1.4.3 Corrosion Potential

Fig 5-14 shows variation of corrosion potential with Reynolds number at three values of relative roughness and in smooth pipe .The corrosion potential shifts to more positive with increase relative roughness because the large amount of oxygen arriving to the surface **[Edwards et. al., 1978]**. Gabe and Walsh [1984] found that the mass-transfer rate increased in the case of the rough surface. The approach of using the mass-transfer coefficients to relate flow effects between geometrical configurations has been shown to provide reasonable predictions if corrosion is controlled by mass transfer.

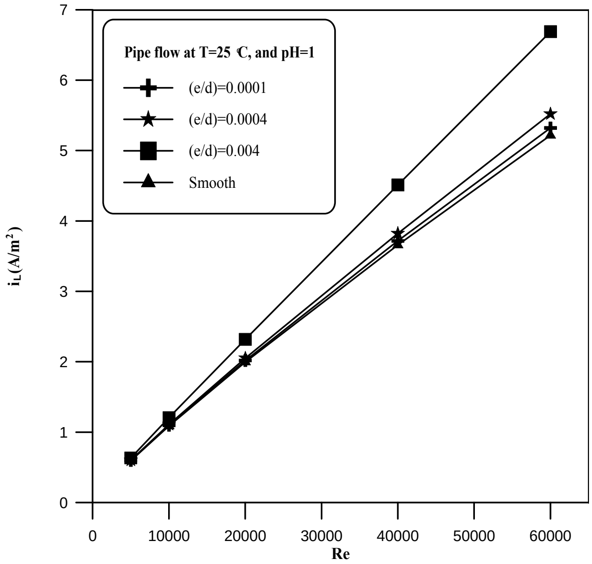

Figure 5-13: Variation of limiting current density with Re in smooth and rough pipe at pH=1.

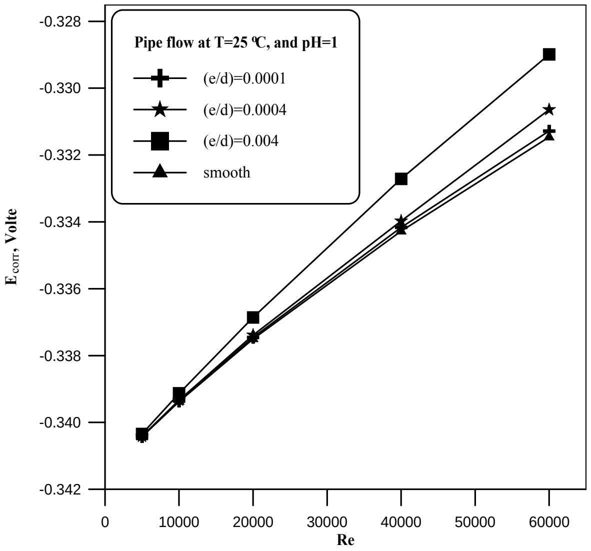

Figure 5-14: Variation corrosion potential with Re in smooth and rough pipe at pH=1.

5.1.4.4 Effect of Temperature on Rough Surface Corrosion

The effect of temperature was explained in section 5.1.2 and shown by Fig. 5-1 to Fig. 5-6. These figures show that temperature affect the corrosion rate, current density of H_2, limiting current density of dissolved O_2, mass transfer coefficient, and corrosion potential variation with Re. There is no effect of temperatures on the friction factor or roughness but its effect appears in the increase of corrosion.

The change in temperature affects the nature of the corrosion reaction because of the significant temperature coefficient for the chemical or physical processes involved in the changes in either or both the reactants and the products. With increase in temperature the solubility of O_2 decreases and the diffusion coefficient of O_2 increases.

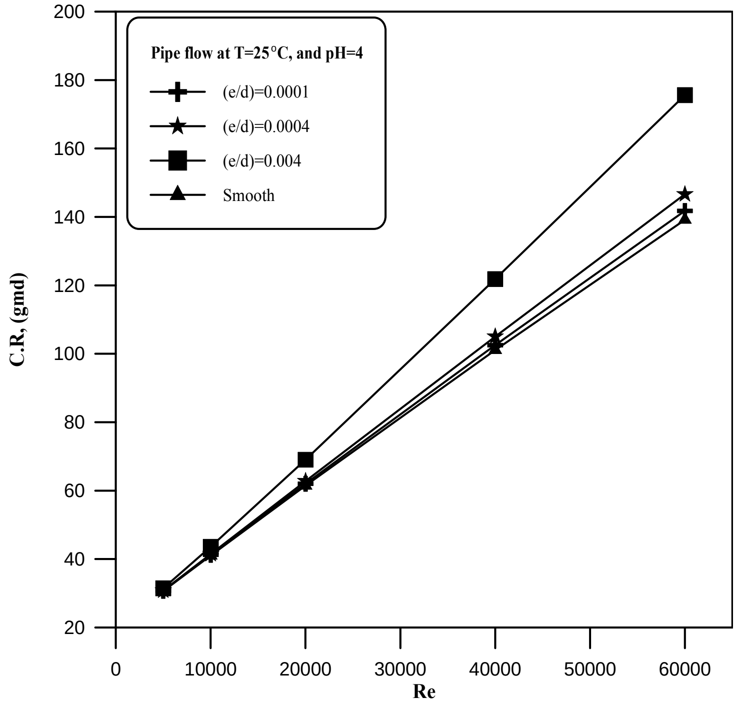

Figure 5-15: Variation of Corrosion Rate with Re in smooth and rough pipe at pH=4.

5.1.4.5 Effect of pH on Rough Surface Corrosion

There is no variation in friction factor with changing pH; the effect of pH on corrosion rate is the increase in pH decrease the corrosion rate. The corrosion rate decreases with increased pH by observing Figs. 6-15 and 6-11. It can be noted that the values of corrosion rate decrease with increase pH. Fig. 5-16 shows variation of current density of H_2 with Re at three values of relative roughness and in smooth pipe. The increased corrosion rate of iron as pH decreases is not caused by increased hydrogen evolution alone; in fact, greater accessibility of oxygen to the metal surface on dissolution of the surface oxide favors oxygen depolarization, which is often the more important reason **[Uhlig and Winston, 2008]**. The current density of H_2 decreases with increasing pH and decreases with roughness.

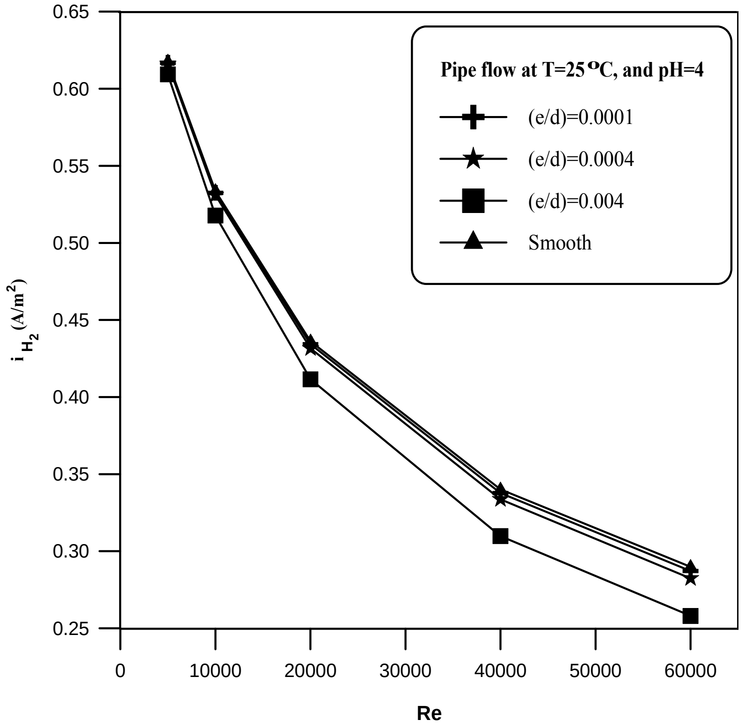

Figure 5-16: Variation of current density of H_2 with Re in smooth and rough pipe at pH=4.

Fig 5-17 gives variation of oxygen limiting current density with Re at three values of relative roughness and in smooth pipe. Limiting current density increases with increased relative roughness, and decreases with increased pH because hydrogen evolution could control the corrosion rate in the absence of oxygen; an increase of corrosion rate with increase [H^+] would be expected for dissolution or diffusion limited current density (oxygen), **[Robertson and Forrest, 1991]**. Fig. 5-18 shows variation of corrosion potential with Re at three values of relative roughness and in smooth pipe for pH = 4. The corrosion potential shifts to passive direction with increase relative roughness. Increase pH shifted corrosion potential to negative direction (decrease corrosion potential).

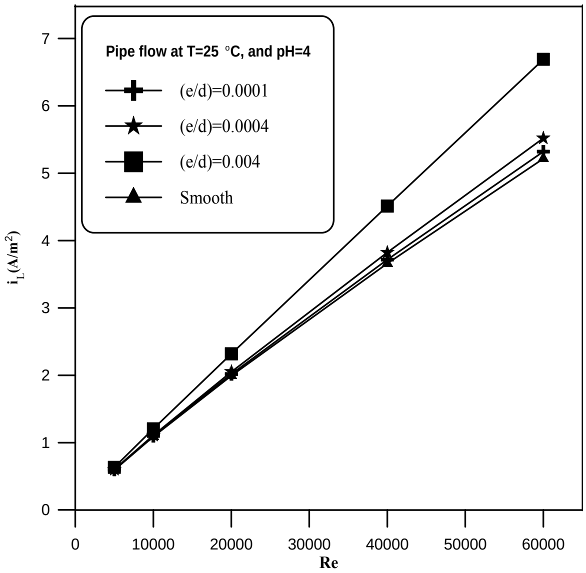

Figure 5-17: Variation of limiting current density with Re in smooth and rough pipe at pH=4.

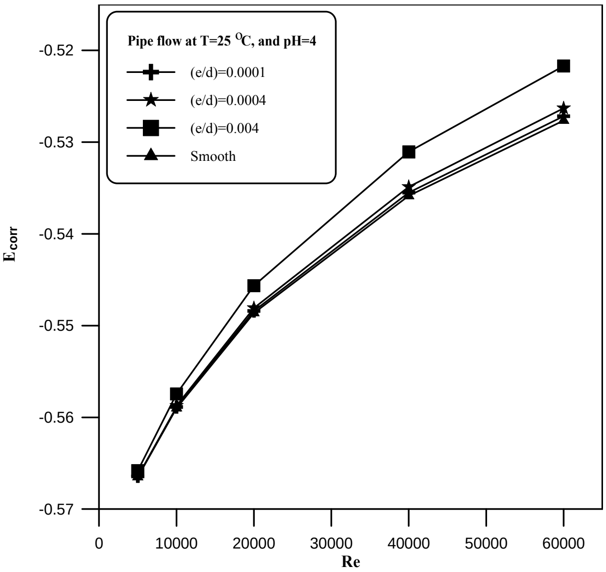

Figure 5-18: Variation of corrosion potential with Re in smooth and rough pipe at pH=4.

5.1.5 Effect of Heat Flux

5.1.5.1 Corrosion rate

Fig 5-19 shows the variation of corrosion rate with Re at four values of heat flux. The effect of heat transfer on corrosion decreases with increased Reynolds number in turbulent flow. It can be noted that at low Re the effect of heat flux is high and this effect decrease with increasing Re, it is nearly disappears at Re=60000. In heat transfer with convection, the fluid properties such as viscosity and density affect the velocity profile, and hence the rates of heat transfer and mass transfer [**Kudryashova and Turkovskaya, 1971**]. The effect of heat flux on the corrosion process is mainly due to its effect on the wall temperature. The wall temperature increases leading to increase the fluid temperature. Increasing surface temperature leads to change the physical properties mainly the viscosity and the diffusivity of oxygen toward the surface. Considerations of temperature effects must be based, of course, on the fact that the solubility of O_2 decreases with increasing temperature while its diffusivity increases; **[Mahato et. al., 1968]**. The corrosion rate in the presence of heat flux is high value at low velocity then become small at higher velocity. This behavior can be interpreted as follows: at low velocity the thickness of momentum sub-layer, diffusion layer and thermal layer in the near wall region is relatively high and when the velocity increases the thickness becomes smaller and smaller leading to decrease the effect of heat flux. Many authors **[Shreir, 1994; Samh, 1994; Atia, 1996; Ross, 1967; Proter et. al., 1968]** attributed the increase in corrosion rate with heat flux to the increase in temperature at the interface between the metal and the solution which has an effect on the diffusion coefficient and viscosity.

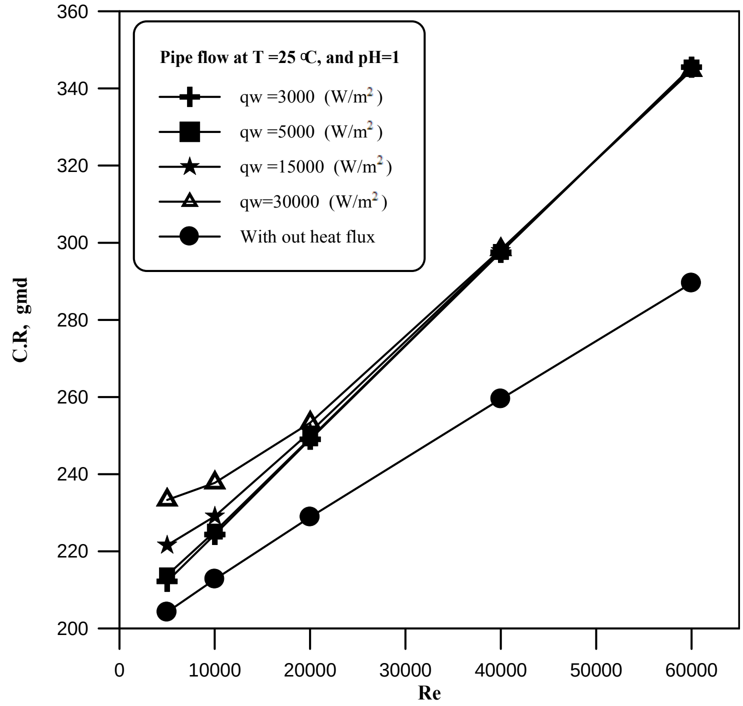

Figure 5-19: Variation of Corrosion Rate with Re under effect of heat flux.

Fig. 5-20 shows variation of current density of hydrogen with Re at four values of heat flux. The current density of hydrogen is affected by increasing oxygen transport to the surface and the limiting current decreases with decreases temperature and the summation of current of hydrogen and limiting current of O_2 equal the anode current of iron. Fig. 5-21 shows variation of wall temperature (or surface temperature T_w) with Re at four values of heat flux. At high Re the surface temperature decreases because high thermal eddy transport between bulk and surface leading to decrease the thickness of thermal sub-layer in the wall vicinity causing high heat transfer rate, as the heat flux increases and since h is slightly affected by heat flux the wall temprature increases.

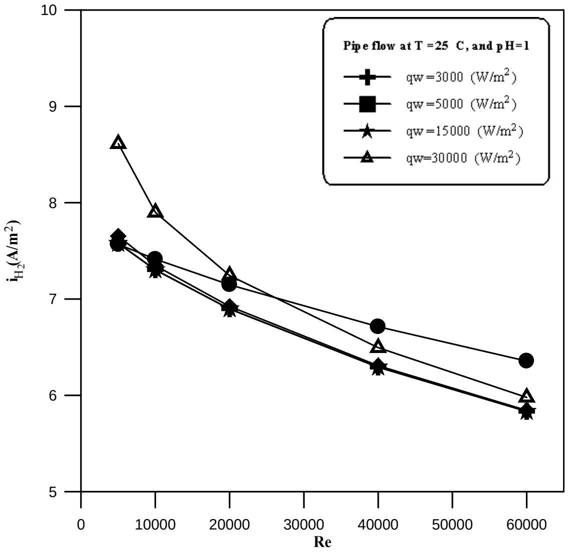

Figure 5-20: Variation of current density of H_2 with Re under effect of heat flux.

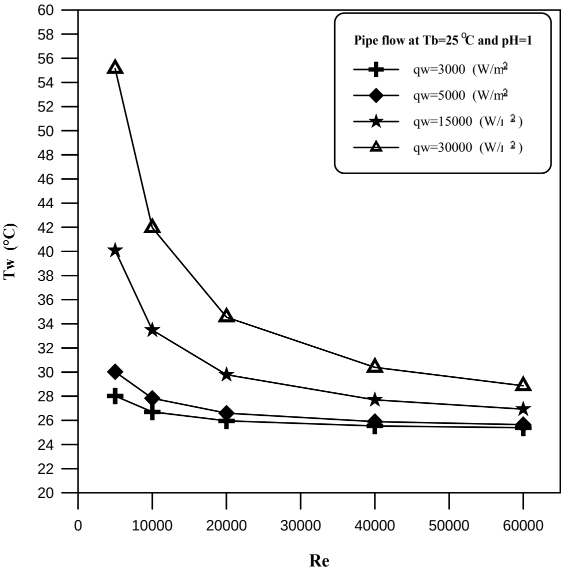

Figure 5-21: Variation of wall temperature with Re under effect of heat flux.

5.1.5.2 Limiting Current Density

Fig. 5-22 gives variation of the limiting current density with Re at four values of heat flux. The limiting current density increases with Re because the high amount of oxygen arrived to the surface. Under effect of heat flux the limiting current density increases when the heat flux increases. Increasing heat flux leads to increases the diffusivity of oxygen and hence increases the corrosion rate **[Zhang et. al., 2007]**.The limiting current density under heat flux effect is higher than under isothermal condition. Jaralla [1984] attributed this tend to the high increase in the solubility of O_2, the large increase in the solubility of the passive film due to the high interfacial temperature under heat transfer condition. The presence of heat flux increases the surface temperature leading to increase the mass transfer rate by increasing molecular diffusion coefficient and thinning the diffusion layer and creation of thermal plumes enhancing the mass transfer rate **[Warrg and Nasiruddin, 1973; Proter et. al., 1968]** .

5.1.5.3 Corrosion Potential

Fig. 5-23 shows variation of the corrosion potential with Re at four values of heat flux. The corrosion potential was shifted to more active values by increasing the temperature of the bulk. The trend agrees with previous work **[AL-Darbi et. al., 2002; Hassan, 2003]**. With increasing Re the corrosion potential shifted to positive direction. Flynn, in 1972 obtained this behavior to higher diffusion under heat transfer condition for Fe .There is an opinion that the rate of nonisothermal corrosion processes limited by kinetic steps is determined by the temperature of the metal wall, but there are no convincing proofs of this **[Flynn, 1972; Brown et. al., 1992]**. The effect of variations of film temperature on the equilibrium potential is shown in appendix D for T_b 25, 40, and 60 ºC from table D-1 to D-12. In addition, the greater the temperature drop, the greater was the change in the dissolution rate caused by the appearance of the temperature drop. Thus, the rate of the anodic process on the heat-transferring surface was not determined simply by its temperature, but depended on the value and direction of the heat flow. Under heat-transfer conditions, an increase in the metal surface temperature leads to increases the temperature of the solution **[Kolotyrkin et. al.,**

1980]. Heat-transfer can be initiated simply by changing the metal temperature since this factor influences the diffusivity and solubility **[Andreev and Kuznetsov, 2002]**. Figures at T_b of 40 and 60 ºC are in appendix D from fig.D-1 to Fig D-14. Ross [1967] suggested that heat transfer might affect the rate of corrosion reaction by influencing the temperature of corroding surface, the solubility and diffusivity of oxygen and the solubility of corrosion products deposits attached to the corroding surface. Ashford et. al. [1974], in their study of corrosion of mild steel under heat transfer conditions in aerated sodium chloride solution by weight loss method, they ascribed the increase in corrosion rate with heat load to the acidic nature of the formed corrosion products.

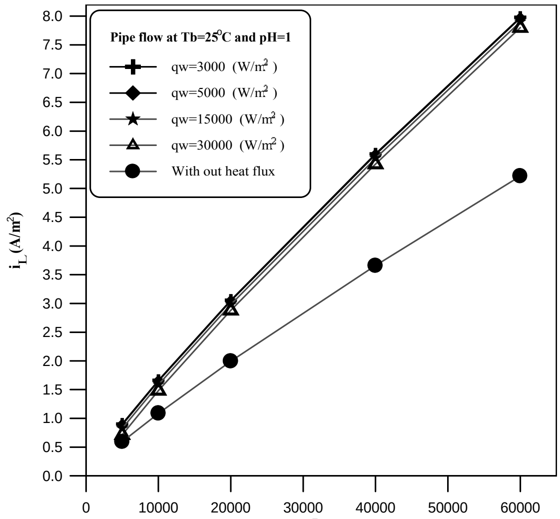

Figure 5-22: Variation of limiting current density

with Re under effect of heat flux.

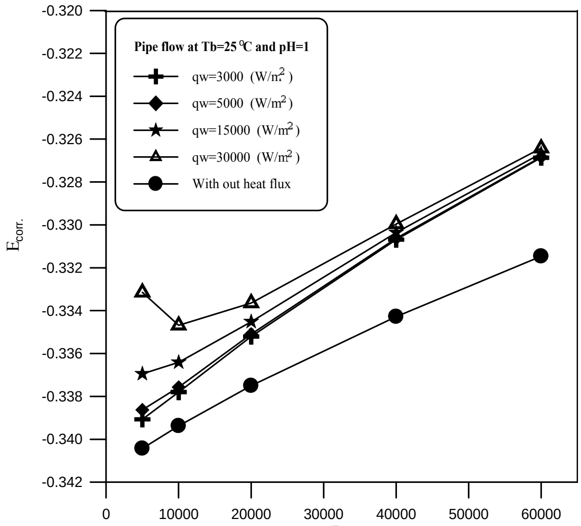

Figure 5-23: Variation of corrosion potential with Re in smooth and rough pipe at pH=1.

5.2 Rotating Cylinder

5.2.1 Effect of Reynolds Number

5.2.1.1 Corrosion Rate

Fig. 5-24 gives the variation of corrosion current measured in ampere per square meter of Fe with Re at three different temperatures. Corrosion rates increase with increasing velocity (Reynolds number or rotational speed). The corrosion rate increases with increasing Reynolds number (or velocity) because the amount of oxygen arrived to the surface increases. In the context of a corrosion study, the rate of mass transport to and from the metal surface is often the factor which governs the rate of corrosion. Significant flow velocities may increase the pitting and crevice corrosion susceptibility of stainless steels in chloride solutions **[Brown et. al., 1992; Roetheli and Brown, 1931]**. Fundamental hydraulic concepts are applied to corrosion and the rate of transfer of interacting chemicals in flow over plates, rotating disks and through pipes. The velocity of the solution, degree of turbulence, geometry of pipes, and other physical factors have a direct influence on the movement of dissolved oxygen and ions throughout the fluid. These factors in turn exert effects on the formation of corrosion products, and on depolarization and thus on the corrosion reaction itself **[Eliassen et al., 1956; Romeo et. al., 1958; Silverman, 2003]**. Fig. 5-25 shows the variation of current density of H_2 with Re at the three different temperatures. The increases in velocity lead to increase amount of oxygen at the surface which affects the current density of H_2 to decrease with increase Reynolds.

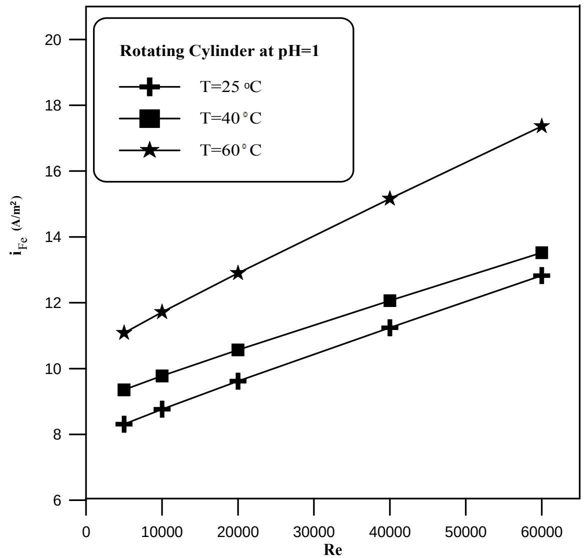

Figure 5-24 Variation of corrosion current Fe with Re at three temperatures.

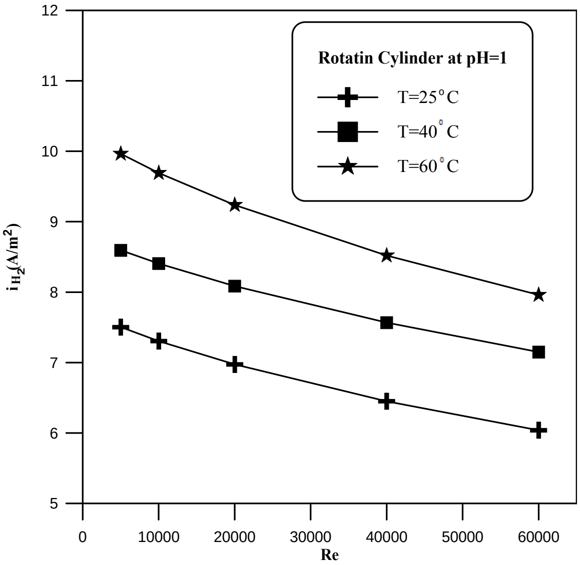

Figure 5-25: Variation of Current density H_2 with Re at three temperatures.

5.2.1.2 Limiting Current Density

Fig 5-26 shows variation of limiting current density with Re at three different temperatures. By increasing the velocity the amount of oxygen increases at the surface of metal which then increases the limiting current density. As the rotation rate increases, the solution flow becomes more complex; while the layer of solution in direct contact with the cylinder continues to cling to the surface [**Eisenberg et. al., 1955**]. Early reports by Eisenberg et. al. [1954] provide the most commonly accepted description for Rotating Cylinder Electrode mass transport; a corrosion process is limited by how fast oxygen can be transported from the solution to the metal surface .Increasing turbulence leads to decrease in the thickness of the viscous sub-layer and the diffusion layer that represents the main resistance to momentum and mass transport respectively **[Poulson and Robinson, 1986; Brodkey and Hershey, 1989]**.

Corrosion rate depends on mass transfer of a reactant to or from the surface, hence the corrosion being sensitive to fluid motion **[Silverman, 2004]**. The increase in oxygen supply from the bulk of the solution to the metal surface leads to high i_L, this behavior is in accordance with mass transfer theory and previous studies, e.g. rotating cylinder [**Vilambi and Chin, 1982; Nesic et. al., 1995; Parshin and Pakhomov, 1982]**, rectangular duct **[Hubbard and E. N. Lightfoot, 1966]**, and rotating disc [**Parshin and Pakhomov, 1982; Zurubin and Zasita, 1965**].

5.2.1.3 Corrosion Potential

Fig. 5-27 gives variation of corrosion potential with Re at three temperatures. Corrosion potential is shifted to more positive values with increasing Re. Ross et. al. [1966] stated that the shifting of corrosion potential with Re is due to the increase in oxygen transport to the metal surface and when the system is free from oxygen the effect of Re on E_{corr} is negligible. The present findings are in agreement with previous work **[Ross et. al., 1966; Tobias and Nobe, 1975; Chin and Nobe, 1977; Eremais and Prazk, 1973]**.

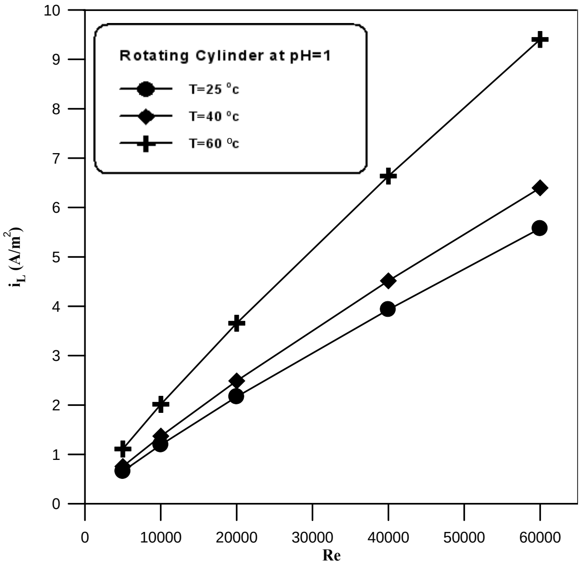

Figure 6-26: Variation of limiting current density with Re at three temperatures.

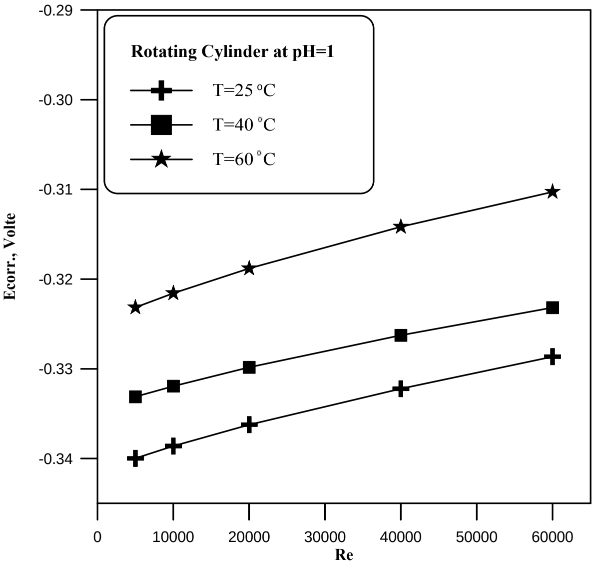

Figure 6-27: Variation of corrosion potential with Re at three temperatures.

5.2.2 Effect of Temperature

5.2.2.1 Corrosion Rate

Fig. 5-24 shows the effect of temperature on corrosion current. Increasing temperature leads to affect two major factors that are the diffusivity of oxygen increases with increasing temperature, and the oxygen solubility decreases with increasing temperature **[Shreir, 1994; Popovers, 2003; Mahato et. al., 1968]**. The effect of temperature is also to change the value of exchange current density i_o according to Arrhenius relation Eq. (4.17) and equilibrium potential (E_{eq}) according to Nernst equation Eq. (4.3). Fig. 5-25 shows the effect of temperature on the current of hydrogen with Reynolds number. When the temperature increasing the current density of hydrogen increases because increasing temperature leads to increase the exchange current density and equilibrium potential.

5.2.2.2 Limiting Current Density

Figure 5-26 shows the effect of temperature on i_{lim} variation with Reynolds number. The increase in the limiting current density with the rising temperature is due to the increased diffusivity of O_2. An other effect of temperature is to decrease the O_2 solubility which leads to decrease the corrosion rate **[Raa and Trass, 1964]**.

5.2.2.3 Corrosion Potential

Figure 5-27 shows variation of corrosion potential with Re at three temperatures. The most likely explanation for shifting corrosion potential to more positive values based on the fact that the solubility of O_2 decreases with increasing temperature while its diffusivity increases **[King et al., 1995; Deslouis et. al., 1988; Dhar et. al., 1985; Sherryl et. al., 2005; Mahato et. al., 1968]**.

5.2.3 Effect of pH

5.2.3.1 Corrosion Rate

Figure 5-28 shows variation of corrosion current measured in ampere per square meter of Fe with Re at three different values of pH. The increase of pH decreases the rate of corrosion because the hydrogen reduction decreases. Long experience has taught value of pH control for corrosion protection, but it has also shown that factors (temperature and velocity etc.) other than pH and dissolved oxygen influence corrosion rates **[Larson, 1975]**. Fig. 5-29 shows variation of current density of H_2 with Re at three different values of pH. The increases in pH decrease the current density of H_2 because the concentration of H^+ decreases with increasing the pH.

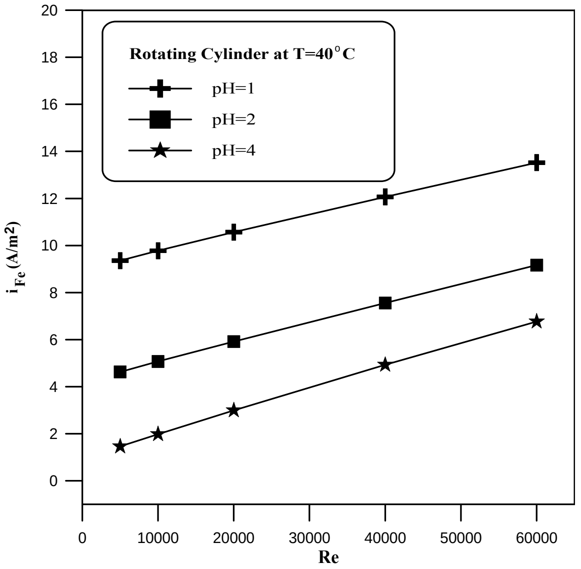

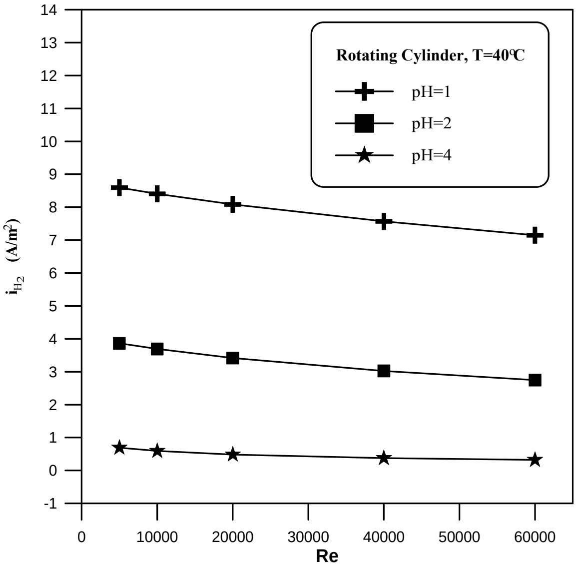

Figure 5-28: Variation of corrosion current of Fe with Re at three pH.

5.2.3.2 Limiting Current Density

Fig. 5-30 shows variation of limiting current density with Re at three pH. There is no effect of pH on the limiting current density of oxygen reduction; it is affected by the flow of fluid and temperature. The change in H^+ concentration has little effect on the O_2 solubility and thus has little effect on the limiting current density.

5.2.3.3 Corrosion Potential

Fig 5-31 gives variation of corrosion potential with Re at three values of pH. The corrosion potential is shifted to more negative direction by increasing pH caused by decreased hydrogen evolution alone; in fact, the increase in oxygen solubility with pH has little effect on corrosion potential **[Shreir, 1994; Mahato et. al., 1980; Smith et. al., 1989; Akimov, 1958; Speller, 1951; Wilson , 1923]**.

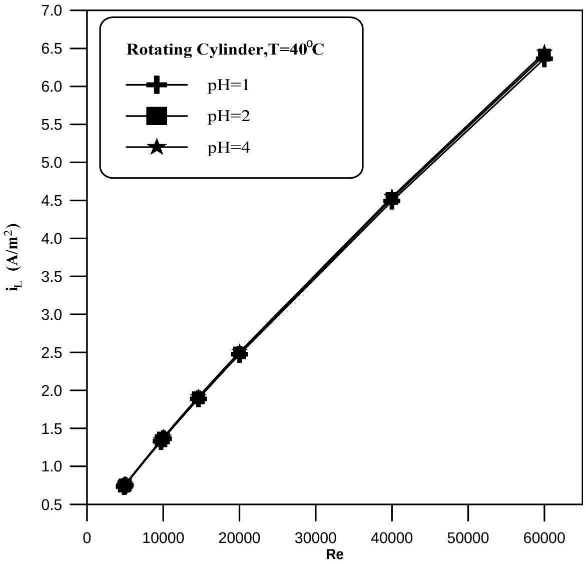

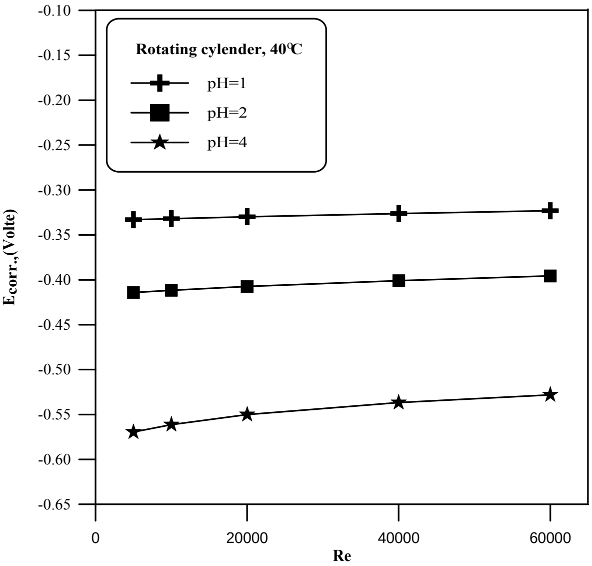

Figure 5-30: Variation limiting current density with Re at three temperatures.

Figure 5-31: Variation of Corrosion Potential with Re at three pH.

5.2.4 Construction of Polarization Diagrams from Proposed Equations

The polarization curves and the mixed potential in a particular environment can be used to determine the magnitude of the corrosion potential or current effects as well as the type of corrosion and the important reason is to know the equilibrium state of the system to understand the various factors that control the rate at which the system tends toward equilibrium, that is, the rate of corrosion. Electron flow occurs between metal surface and surrounding solution. This current flow between the metal and solution causes shifts in potential, because the potentials of the metals and solution approach each other over time. Fig 5-32 shows the polarization curve of rotating cylinder in aerated acid in pH=1 at temperature 25 °C and Re=60000.

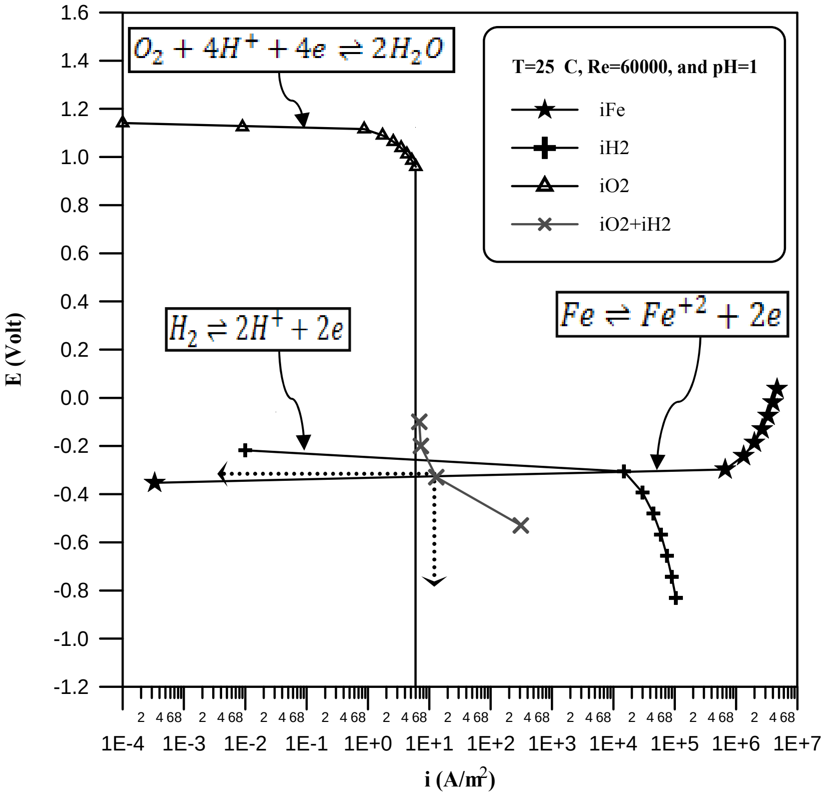

Figure 5-32: Polarization curves of iron rotating cylinder in HCl at T=25 ºC, pH=1 and Re=60000.

In experimentally establishing a polarization diagram, the first measurement is usually that of the corrosion potential, E_{corr}, when the applied current, i_{appl}, is zero as equation (6.2):

$$i_{appl} = i_a - i_c \qquad \dots (5.3)$$

To graph mixed-potential models from activation and concentration controls. Fig. 5-33 shows the polarization curve of rotating cylinder in aerated acid in pH=2 at temperature 25 ºC, and Re=20000. To draw Fe anodic polarization line and H_2 cathodic polarization line using equations 4.59 and 4.60 respectively by assuming different values of corrosion potential.

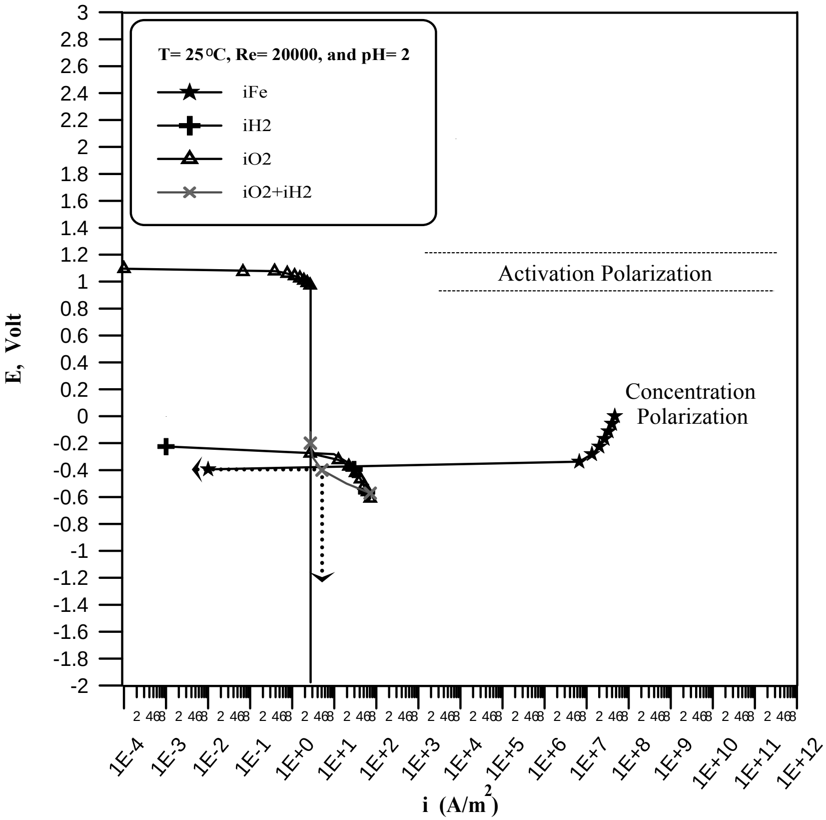

Figure 5-33: Polarization curve of iron rotating cylinder in HCl at T=25 ºC, pH=2 and Re=20000.

The O_2 reduction line includes activation and concentration polarization. Equation 4.67 is used to draw the line under activation control and equation 4.66 to draw the line under concentration control; the polarization curves of O_2 were obtained from equation 4.68. Fig. 5-34 shows the polarization curve of iron rotating cylinder in aerated acid in pH=4 at temperature 25 ºC, and Re=60000.

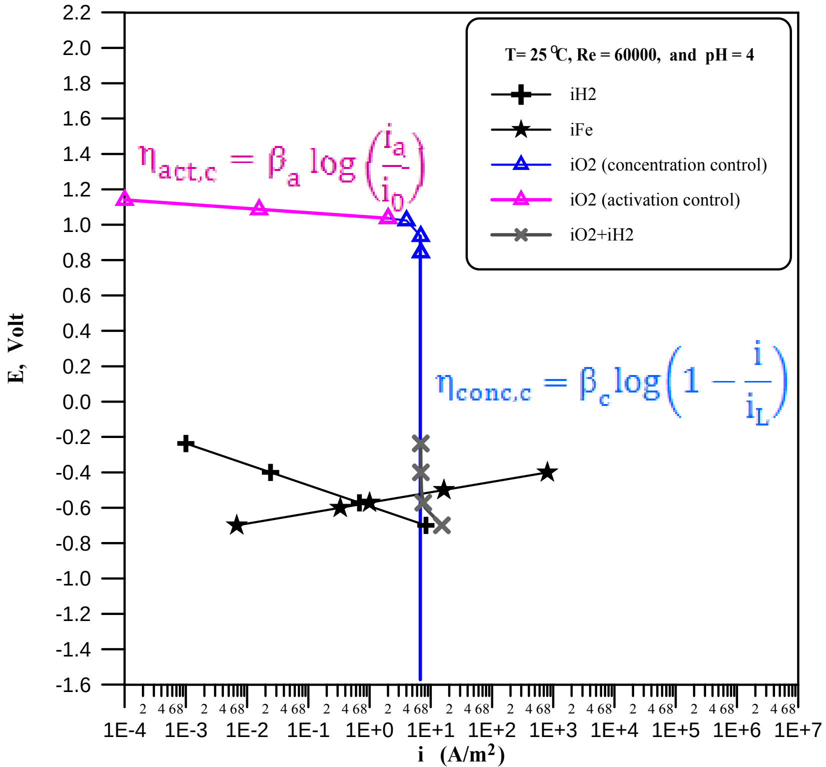

Figure 5-34: Polarization curve of iron rotating cylinder in HCl

T=25 ºC, pH=4 and Re=60000.

It is clear in Figs. 5-32, 5-33, and 5-34 that the current of Fe increase and the potential shifts to more noble but on the contrary in H_2 reaction, the currents densities increases and the potentials shift to more negative valuse. This applies also to O_2 reaction. The i_{corr} value for a particular electrochemical system is derived at the intersection of linearly extrapolated anodic and cathodic current curves. At point of net i_{corr} and E_{corr} the current density of anode (i_{Fe}) equal to cathode current density (i_{H2} + i_{O2}). The corrosion potential is obtained at the point of intersection of the two curves; at this potential the total currents for both reactions are equal **[Stanislaw et al., 1982]**. The plot of the corrosion potential (E_{corr}) versus the logarithm of the corrosion current (i_{corr}) determined by the linear polarization method shows that there is direct proportion between E_a and i_a values of anode (Fe) but there is undirected proportion between E_c and i_c values of cathode (H_2 and O_2) .The corrosion current can be used to determine the corrosion rates through the modified Faradays law **[Pound et al., 1979; Ruperto et al., 2000]**. The effect of Re on iron current is to increase it, and decrease the current density of H_2 but in plotted polarization curve the velocity is constant. The major effect of velocity on current density of oxygen is to supply the surface with oxygen. The cathodic reduction rate is controlled by the rate of arrival of oxygen at the metal surface **[Qian and Chagnon, 2001]**. It is to be noticed from Figs. 5-32 to 5-34 that where pH increased from 1 to 4 the cathodic current decreases while the O_2 cathodic current increases, the limiting current density in Fig. 5-32 is 6.7 while in Fig. 5-34 is about 6.8. Comparing Fig. 5-32, 5-33 and 5-34 indicates that the corrosion current is 12.8, 5.5 and 7.2 respectively, so increasing Re leads to increase the corrosion rate and decreasing pH leads to increase the corrosion rate **[Pierre, 2000]**. The solubility of O_2 decreases with increasing temperature while its diffusivity increases **[Mahato et. al., 1968]**. Fig. 5-35 shows the polarization curve of iron rotating cylinder in aerated acid at pH=1 at temperature 40 ºC, and Re=60000. The difference between polarization curves at 25 ºC and 40 ºC is the corrosion rate increases with increasing temperature **[Finley and Myers, 1970].** This agrees with a number of investigators that have repotted on the anodic polarization behavior of iron in relatively dilute, acid solution **[Bonhoeffer, 1955; Economy et. al., 1961; Steigerwald, and Greene, 1962; Mottern and Myers, 1968]**. Fig. E-1 and Fig. E-2 in Appendex E show the polarization curves of iron rotating cylinder at temperature 40 ºC in aerated acid at pH=2 and 4.

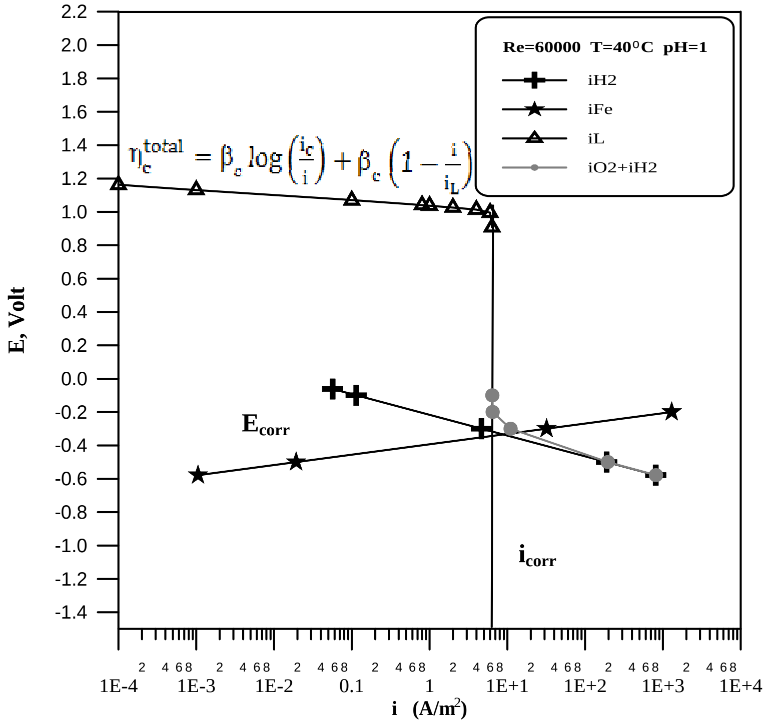

Figure 5-35: Polarization curve of iron rotating cylinder in HCl T=40 ºC, pH=1 and Re=60000.

The corrosion current at 60 ºC is greater than the corrosion rate at tempratures of 25 ºC and 40 ºC for example at Re= 20000 and pH=1 the corrosion rate in temperature 60 ºC is 322.51 gmd, in temperature 40 ºC is 264.18, and temperature 25 ºC is 240.46 . Fig. 5-36 shows the polarization curves of iron rotating cylinder in aerated acid for pH=1 at temperature 60 ºC, and Re=5000. Fig. E-3 and Fig. E-4 in Appendex E show the polarization curve of iron rotating cylinder at temperature 60 ºC in aerated acid at pH=2 and 4. The polarization method is very useful for determing corrosion rates of materials in aqueous media **[Rodney, 1975; Damborenea, 1987]**. The increase of E_{corr} with Re is due to the increase in oxygen transport to the metal surface, as Re (or velocity) increases, i_L increases shifting the intersection point between the cathodic polarization curve of O2 reduction and anodic polarization line of Fe dissolution to more positive potential value.

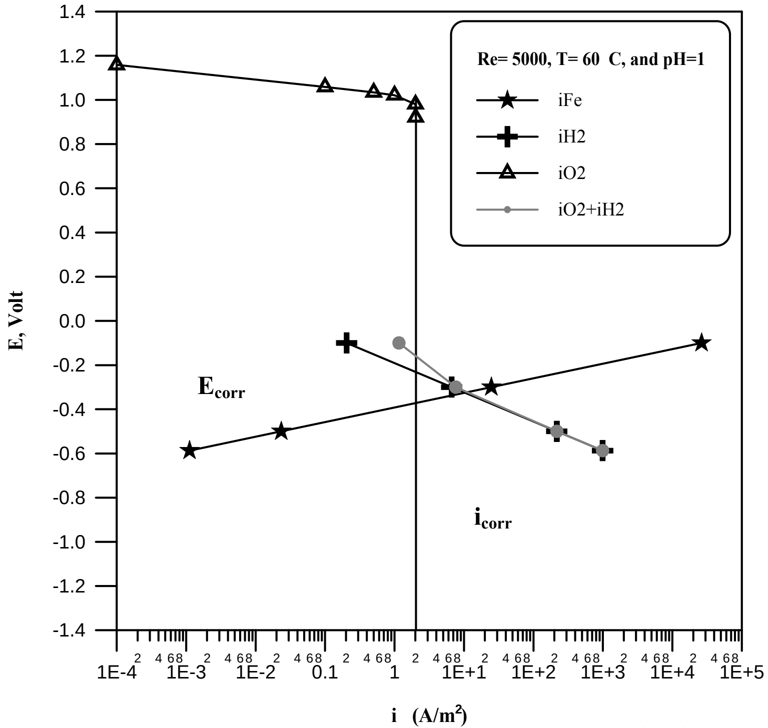

Figure 5-36: Polarization curve of iron rotating cylinder in HCl T=60 ºC, pH=1 and Re=5000.

5.1 Comparison with the Experimental Results

In this section it is aimed to compare the theoretical results of corrosion rate of rotating cylinder obtained from theoritical analysis with experimental results obtained by previous workers concerning the corrosion rates of iron in HCl at different temperatures and pH.

5.3.1 Present Results Comparison with Turki [2009]

Fig. 5-37 reveals the comparison of results of present analysis with Turki, 2009 results at temperature 35 ºC, and pH = 3 in aerated hydrochloric acid solution. It is very good agreement of the theoretical result of present analysis with experimental result of Turki.

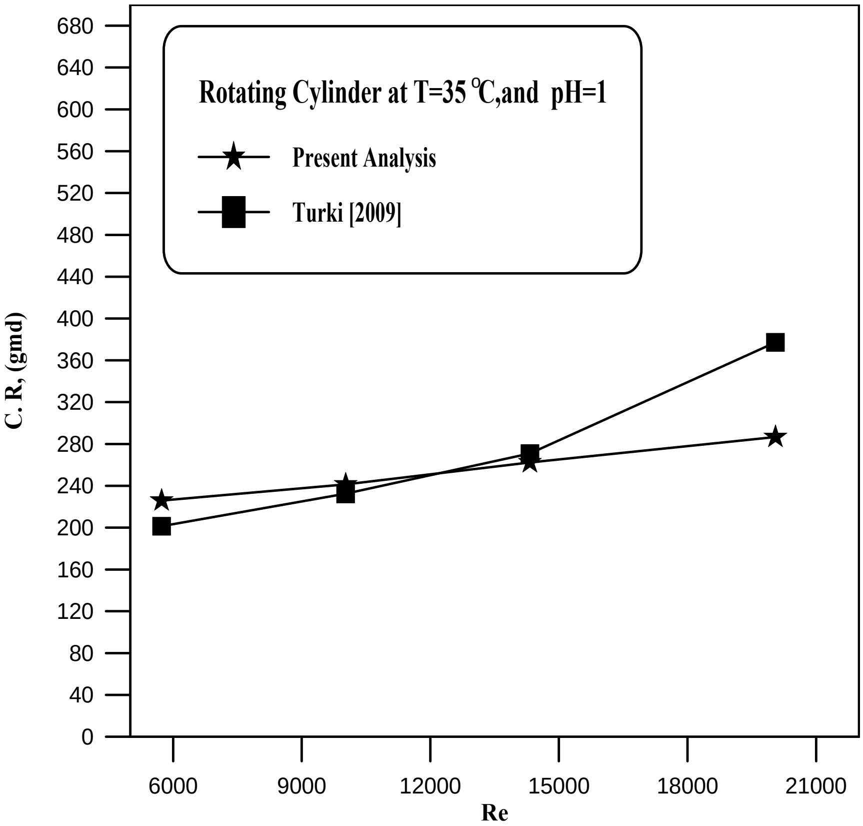

Figure 5-37: Comparison between present analysis and Turki result of rotating cylinder at T=35 ºC and pH=1.

5.3.2 Present Result Comparison with Bahar [2002]

Fig 5-38 shows the comparison between present analysis with Bahar [2002] result. This comparison of rotating cylinder is at temperature 40 ºC and pH=1. It is clear that the present results are in good agreement with experimental results at the specified condation.

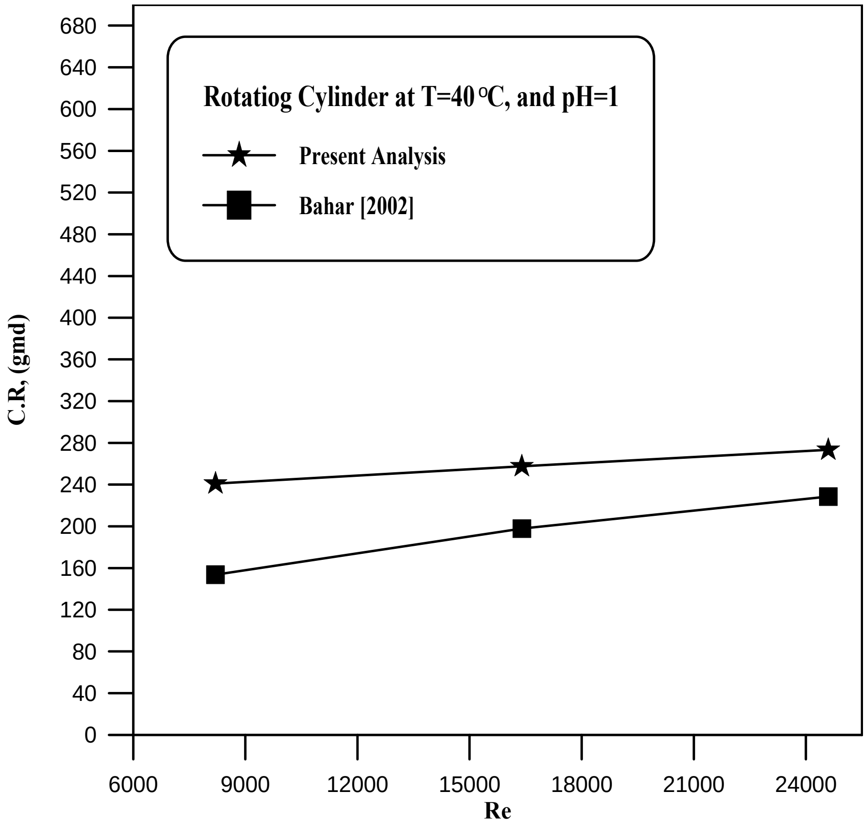

Figure 6-38: Comparison between present analysis and Bahar result of rotating cylinder at T=40 ºC and pH=1.

5.3.3 Present Analysis Comparison with Scheers [1992]

Finger 5-39 shows the comparison between present analysis and Scheers, 1992 results. This comparison gives the corrosion rate of rotating cylinder measured by millimeter per year in acid at temperature 45 ºC and pH= 3. The figure reveals that the theoretical results are in fair agreement with the experimental results but with some deviation at high Re.

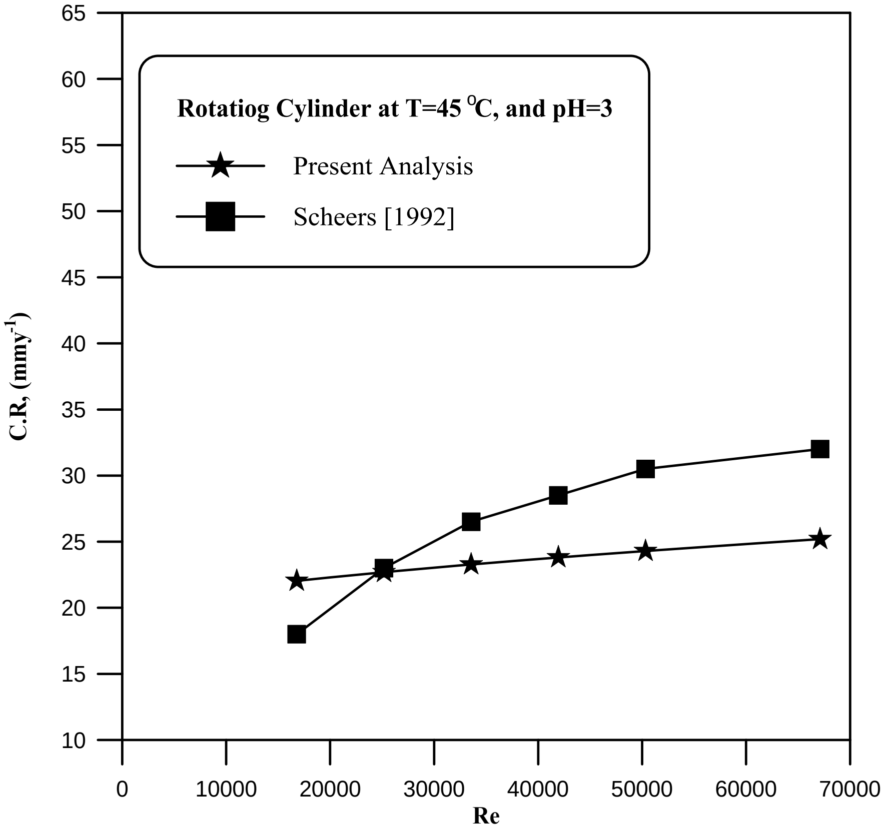

Figure 6-39: Comparison between present analysis and Scheers result of rotating cylinder at T=45 ºC and pH=3.

5.4 Comparison Corrosion Potential in Smooth Pipe Flow and Smooth Surface Rotating Cylinder

Figure 5-40 shows the comparison of corrosion potential in smooth pipe flow and smooth surface rotating cylinder of three temperatures at Re =5000 and pH=1. it is clear that at the same Re (or velocity) for both pipe and rotating cylinder the geometry has no effect on the corrosion potential. This indieates that the corrosion potential is affected by the nature of solution and the type of metal and is not affected by geometry. Figs. C-7 and C-8 (Appendix C) show the comparison of corrosion potential in smooth pipe flow and smooth surface rotating cylinder of three temperatures at pH=2 and 4.

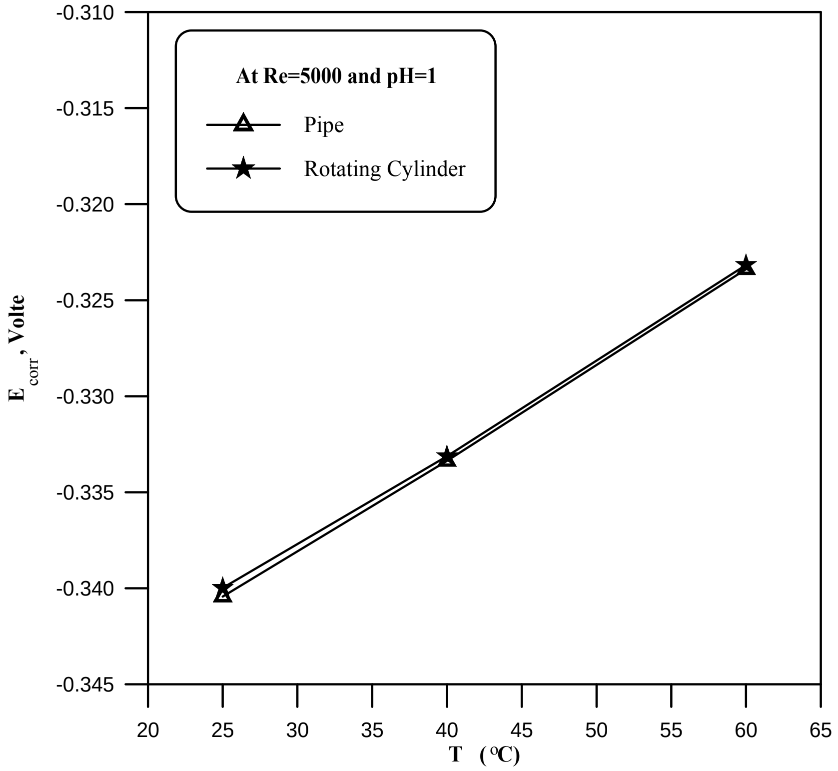

Figure 5-40: The comparison of Corrosion Potential in Smooth Pipe Flow and Smooth Surface Rotating Cylinder of three temperatures at Re =5000 and pH=1.

5.5 Relationships between Rotating Cylinder Corrosion Measurements and Corrosion in Pipe Flow

The main obstacle to relating rotating disk flow to pipe flow is the nonsimilarity of the geometry of the two systems. As has been elaborated by Levich [1962], equating the geometric (equal boundary conditions) and dynamic (equal Reynolds number) characteristics of the systems is sufficient to relate them. Silverman [1988] discussed the corrosion rate relationship between pipes, rotating cylinders, and impinging jets assuming that the process was controlled by diffusion. He demonstrated that mechanisms other than diffusion control were possible. Therefore, a model for different geometries must allow for the possibility of rate control. Silverman [1988] and Nesic et. al. [1997] provided similar information, at least as far as relating mass transfer in the rotating cylinder electrode to mass transfer in a straight pipe section. Liu et. al. [1994] studied the relationship of corrosion in a rotating disk system to that in a turbulent pipe flow system. In the present work, relationships were established between rotating cylinder and pipe flows of carbon steel corrosion. Fig. 5-41 shows the corrosion rate of rotating cylinder and pipe flow with Reynolds number at T=25 °C and pH=1.

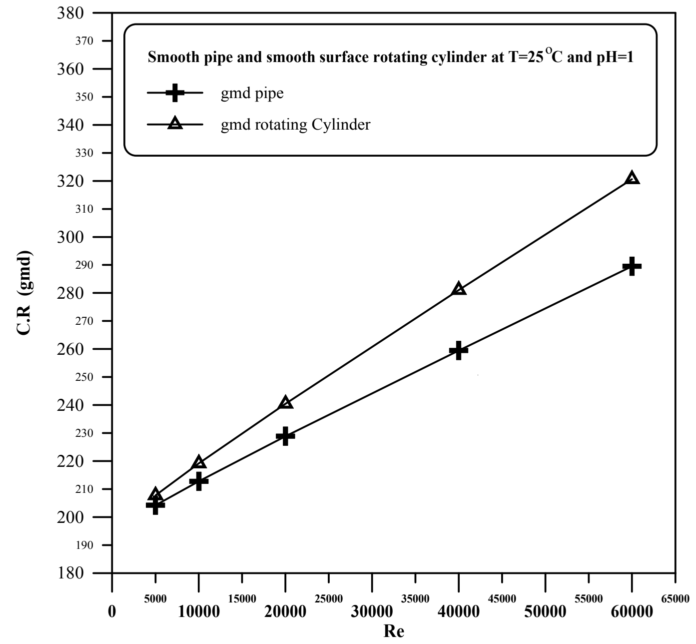

Figure 5-41: The corrosion rate of rotating cylinder and pipe flow various with Reynolds number at T=25 °C and pH=1.

The theoretical results can be applied to any other system in which the corrosion product may form on the corroded surface. The main objective of this work was to determine what kinds of experimental data are relevant in predicting the corrosion rate for pipe flow and rotating cylinder data. By Fick's first law introduced as **[Brodkey and Hershey, 1989]**:

$$\mathrm{j} = -\mathrm{D}\left(\frac{\partial \mathrm{C}}{\partial \mathrm{x}}\right)_{\mathrm{y}=0} \qquad \ldots(5.4)$$

The corrosion rate of rotating cylinder was being equal exactly to the corrosion rate of pipe. Hence, either of this rate could be used in expressing the flux in Equation (5.4). The following expression for mass flux of rotating cylinder (j_R) can be obtained:

$$j_R = \frac{-DC_b}{\delta_R} \qquad \ldots(5.5)$$

The mass flux of pipe flow (j_P) can be obtained:

$$j_P = \frac{-DC_b}{\delta_P} \qquad \ldots(5.6)$$

The following expression for the Nernest diffusion layer of rotating cylinder was obtained by previous workers **[Eisenberg, 1954; Vilambi and Chin, 1982]**:

$$\delta_R = 0.36\left(\frac{d_R}{Re_R^{0.61}}\right) \qquad \ldots(5.7)$$

According to the turbulent boundary layer theory the diffusion layer for pipe is calculated as **[Davies, 1972]**:

$$\delta_P = 44.8\left(\frac{d_P}{Sc^{1/3}\, Re_P^{7/8}}\right) \qquad \ldots(5.8)$$

The next step is the most critical in the model development. To relate the two systems with different flow conditions, fluxes of the two systems are equated. Equal fluxes guarantee that the two systems will have the same corrosion rates. The different flow conditions in the two systems already have been taken into account in the calculation of overall fluxes. From Equations (5.5) and (5.6):

$$Re_P = 247.889\left(\frac{d_P}{d_R}\right)^{(8/7)} \frac{Re_R^{0.6971}}{Sc^{0.38095}} \qquad \ldots(5.9)$$

Where j_R and j_P are the mass flux (mol/m^2.s), for rotating cylinder and pipe flow respectivly, δ_R and δ_P are the diffusion sub-layer thickness (m) for rotating cylinder and pipe flow respectivly, Re_R and Re_P are the Reynolds number (dimensionless) for rotating cylinder and pipe flow respectivly,d_R and d_P are the dimeters (m) for rotating cylinder and pipe flow respectivly, Sc is Schmidt number (dimensionless). For exampel Where the Reynolds numper of rotating cylinder is 10000 and from Fig. 5-41 and Reynolds number of pipe is 14000 and from Eq. (5.9) for Reynolds number of pipe is 15952.77715 because Eq. (5.9) is theoritical equation based on the theoretical correlation of diffusion sub-layer thickness δ. The percentage error of Eq. (5.9) is ٪5.35.

Using statistical analysis the following relation of corrosion rate can be obtained for smooth pipe flow:

$$C.R(gmd) = 10.20697\, Re^{0.208226}\ T^{0.312849}\ pH^{-0.70156} \qquad \dots (5.10)$$

For smooth surface of rotating cylinder the following relation is obtained:

$$C.R(gmd) = 5.53953\, Re^{0.260848}\, T^{0.364818}\, pH^{-0.68343} \qquad \dots (5.11)$$

For rough pipe flow and by using Statstical analysis the fallowing relation can be obtained:

$$C.R(gmd) = 18.2175\, Re^{0.269075}\, T^{0.300839}\, pH^{-0.68342}\, f^{0.224908} \qquad \dots (5.12)$$

Where C.R is the corrosion rate in gram per meter per day (gmd), Re is the Ryenolds number of range 5000-60000, T is the temperture in °C of ring 25-60 °C, and pH of ring 1-4. The correlation coefficint of Eq. (5.10) is R=0.94878, the correlation coefficint of Eq. (5.11) is R=0.9 and the correlation coefficint of Eq. (5.12) is R=0.9468. By using Eq. (5.10) , Eq. (5.11) and Eq. (5.12) one can calculat the corrosion rate without need to the the polarization equations. The percentage error of Eq. (5.10) is ٪6.51. The percent error for Eq. (5.11) is ٪6.31

and the percentage error of Eq. (5.12) is ٪3.74. It is to be noticed from equation (5.10) that the dependence of corrosion rate on the Re is 0.208, the temperature is 0.312, and on pH is -0.702. That means increasing Re and temprature leads to increase the corrosion rate while increasing pH leads to decrease the corrosion rate. Equation (5.11) indicates that the dependence of corrosion rate on Re, temperature and pH for rotating cylinder is close to pipe flow. Eqation (5.12) for rough pipe flow indicates that the friction factor plays important role in increasing the corrosion rate exhibiting dependence of 0.2249. Also from Eqs. (5.10) to (5.12) it can be concluded that the most important factor that affect the corrosion rate for the investigated system within the investigated ranges is the pH or heydrogen concentration.

CHAPTER SIX

CONCLUSIONS AND RECOMMENDATIONS FOR FUTURE WORK

7.1 CONCLUSIONS

1. The polarization equations can be successfully employed to calculate the corrosion rate and corrosion potential for iron in mixed control system that is under both activation and mass transfer control.
2. Corrosion rate of iron for pipe and rotating cylinder generally increases with increasing velocity (Reynolds number), and temperature, while it decreases with increasing pH.
3. Corrosion potential is shifted to more positive (noble) with increasing Re and temperature, while it is shifted to more negative with increasing pH.
4. The higher the pipe wall roughness is the higher the corrosion rate. Increasing surface roughness increases the local mass transfer coefficient by increasing the turbulence in the wall vicinity. The dependence of corrosion rate on rough pipe friction factor is 0.2.
5. Corrosion rate of iron increases with increasing heat flux through pipe wall due to the increased surface temperature which in turn decrease the solution viscosity and increase the oxygen diffusivity. The heat flux effect becomes little with increasing flow rate (Reynolds number).
6. The corrosion rate is obeying the following correlations:
   - For smooth pipe flow:

$$\mathrm{C.R(gmd)} = 10.20697\,\mathrm{Re}^{0.208226}\ \mathrm{T}^{0.312849}\ \mathrm{pH}^{-0.70156}$$

- For smooth surface rotating cylinder:

$$\mathrm{C.R(gmd)} = 5.53953\ \mathrm{Re}^{0.260848}\ \mathrm{T}^{0.364818}\ \mathrm{pH}^{-0.68343}$$

- For rough pipe flow:

$$\mathrm{C.R(gmd)} = 18.2175\ \mathrm{Re}^{0.269075}\ \mathrm{T}^{0.300839}\ \mathrm{pH}^{-0.68342}\ f^{0.224908}$$

7. Comparison between pipe flow and rotating cylinder result show that at the same Reynolds number, temperature, and pH, the corrosion rate in case of rotating cylinder is higher than in pipe flow. Also the corrosion potential does not affect by the geometry of electrode. The Reynolds number for the two geometries are correlated as:

$$Re_P = 247.889\left(\frac{d_P}{d_R}\right)^{(8/7)}\ \frac{Re_R^{0.6971}}{Sc^{0.38095}}$$

7.2 RECOMMENDATIONS FOR FUTURE WORK

The following suggestions are to be considered in greater detail for future work:

1. Carrying out experimental work to investigate the influence of Re, temperature, and pH, on the corrosion rate and compare the results with present theoretical work.
2. Study the effect of temperature higher than 60 °C and pH higher than 4.
3. Carrying out the theoretical study to other metals like Copper and Zinc.
4. Carrying out the theoretical study for galvanic coupling of two metals in aerated acids.

REFERENCE

- Abd El-Rehim S. S., Refaey A. M., Taha F., Saleh M. B. and Ahmed R. A., J. Appl. Electrochem. 2001.
- Akimov G. V., Corrosion- NACE, Vol.14, P.463, 1958.
- AL-Darbi M. M., A. Nouri, and M. R. Islam, Energy Sources, P. 1019-1030, February 2002.
- Andreev N. and Kuznetsov Yu. I., Protection of Metals, Vol. 38, No. 5, P. 399-402, 2002.
- Bahar Sh., Ph.D. Thesis, Dept. Chem. Eng., Al-Nahrain University, Baghdad, 2002.
- Beddoes J. and Parr G. J., Stainless Steels, 3rd Ed., ASM International, Materials Park, OH, 1999.
- Bentiss, M. Traisnel, L. Gengembre and M. Lagrenee, Appl. Surf. Sciences, 152, 1999.
- Berger F.P., and Hau K.-F. F.-L., Int. J. Heat Mass Transfer 20, 1185, 1977.
- Bjorndahl W.D., and Nobe K., Corrosion 40, 82 1984.
- Blasius, Mitt, Forchung Surbocit. VDI BI, 131, P.1, 1913.
- Bond P., Sc.D. thesis, Department of Metallurgy, M.I.T., Cambridge, MA, 1958.
- Bonhoeffer F., corrosion, Vol. 11, P. 32, 1955.
- Brasunas Anton deS. Editor, NACE Basic Corrosion Course, October 1970.
- Brenan W. C. and Trass O., 52nd Nt. Meeting of A.l.Ch.E. 1964.
- Brodkey R. S. and Hershey H. C., “Transport Phenomena”, 2nd Printing, Mc Graw Hill, New York, 1989.

- Brown B.E., Lu H.H., and Duquette D.J., Corrosion–December, P. 970, 1992.
- Btrrler G. and Stroud E. G., J. appl. Chem. 15, 325, 1965.
- Butler G. and Ison H. C. K., J. appl. Chem. 10, 80, 1960.
- Charng T. and Lansing F.,TDA Progress report 42-69, March and April,1982.
- Chen J.J.J., Int. Comm. Heat Mass Trans., Vol. 12, P.219, 1985.
- Chin R.J. and Nobe K., Corrosion J., Vol.33, P.364, 1977.
- Cifuentes, ANTI-Corrosion, November, P.4 to 6, 1987.
- Coaen, J. Electrochem. Soc. 93, 26, 1948.
- Copson H. R., Ind. Engin. Chem. 44, 1745, 1952.
- Coulson M. and Richardson J. F., Chemical engineering, 5th Edition, Butter Worth Heinemann, Britain, 1998.
- Cox L. and Roetheli B. E., Ind. Engng Chem. 23, 1012, 1931.
- Damborenea de J., J. Ruiz, and A. J. Vázquez, Br. Corros. J., Vol. 22, No. 4, 1987.
- David Talbot and James Talbot, Corrosion science and technology, New York Washington London 1998.
- Davies J.T., Turbulence Phenomena, New York, NY: Academic Press, 1972), P. 128, 366-368.
- Deslouis M., Tribollet B., Mengoli G. and Musiani M., J. appl. Electrochem. 18, 374, 1988.
- Dey W. R., M.Sc. Thesis, University of British Columbia 1959.
- Dhar H. P., White R. E., Burnell G., Cornwell L. R., Griffin R. B. and Darby R., Corrosion 41, 317, 1985.

- Dittus F.W. and Bolter L.M., Unv. Calf, Berkeley, Publ. Eng., Vol.2, P.443, 1930.
- Drew T.B., Koo E .C. and Adams W. H. S, Trans. AICHE, Vol. 28, P. 56, 1932.
- Economy G., Speiser R., Beak F. H., and Fontana M. G., Electrochem. Soc., 108, 337, 1961.
- Edwards T. J., Maurer G., Newman J., Prausnitz J.M., A.l.Ch.E. vol. 24, P. 966, 1978.
- Ehteram A. Noor, Int. J. Electrochem. Sci., 2, P. 996 – 1017, 2007.
- Eisenberg M., Tobias C. W., and Wilke C.R., Chem. Eng. Progr. Symp. Ser. 51, 1, 1955.
- Eisenberg M., Tobias C. W., and Wilke C.R., J. Electrochem. Soc., Vol. 101, P.306, 1954.
- Eliassen, Pereda C., Romeo A. J. and Skrinde L T., J. Am. Wat. 14"ks Ass. 48, 1005, 1956.
- Eremais S.A. and Prazk M., Corrosion Sci., Vol.13, P.907, 1973.
- Evans, Ulick R., "An Introduction to Metallic Corrosion", Edward Arnold, London, UK. 1948.
- Evans, Ulick. R., "The Corrosion and Oxidation of Metals", Arnold, London, 1960.
- Finley C. and Myers J. R., Corrosion, Vol. 26, No. 12, December, 1970.
- Flynn C. P. and Greene N. D., London press., 1972.
- Fontana M.G., Greene N.D., “Corrosion Engineering”, 2nd edition, London, 1984.

- Fontana, M. G. and Staehle, R. W., Advances in Corrosion Science and Technology, Plenum Press, New York, 1990.
- Foroulis Z. and Uhlig H., J. Electrochem. Soc. 111, 13, 1964.
- Frank W. J., SPE No. 4064, Humble Oil and Refining Co., 1972.
- Friend W. L. and Metzner A. B., AICHE. J., Vol. 4, No. 4, P. 393, 1958.
- Gabe D.R., Walsh F.C., J. Appl. Electrochem. 14, P. 565, 1984.
- Gabe, D.R, J. Appl. Electrochemical, 4, P. 91, 1974.
- Gerhardus H. Koch, Michiel P.H. Brongers, and Neil G. Thompson, Paul Virmani Y., Payer J.H., July 2002.
- Hasan B. H., Ph.D. Thesis, Dept. Chem. Eng., Saddam University, Baghdad, 1998.
- Hatch B. and Rice O., Ind. Engng Chem. 37, 752 (1945).
- Henry S.D. and Scott W.M., “Corrosion in the Petrochemical Industry”, 1st Edition. ASM International, USA, 1999
- Hoar T. P. and Hines J. G., J. Iron Steel Inst. 182, 124 (1956).
- Hubbard W. and Lightfoot E. N., Ind. Eng. Chem., Vol.5, P.370, 1966.
- Jaralla A. A., Ph.D. Thesis, Dept. Corrosion and Protection Center,. Manchester University, UK, 2002.
- Jiang Z., Wang J., Hau Q. and Huang S., Corros. Sci. 37 1995.
- Jones Denny, “Principles and Prevention of Corrosion”, Prentice-Hall, 1996.
- Jones L. W., “Corrosion and Water Technology for Petroleum Producers”, 1988.
- Kent R., NACE Int. Conf., National Association of Corrosion Engineers, 1987.
- King F., Litke C. D., Quinn M. J. and LeNeveu D. M., Corrosion Science,

Vol. 37. No. 5, P. 833-851, 1995.

- King V. and Broodie S. S., J. Am. chem. Soc. 59, 1375, 1937.
- Kirby, G. N., Chem. Eng., P. 72, Mar. 1951.
- Kntnasen G. and Katz D. L., Fluid Dynamics and Heat Transfer. McGraw-Hill, New York, 1958.
- Kolotyrkin M., Pakhomov V. S., Parshin A. G. and Chekhovskii A. V., Translated from Khimicheskoe Neftyanoe Mashinostroenie, No. 12, pp. 20-22, December, 1980.
- Kruger J., *M.*Sc., Electrochemistry of Corrosion, The Johns Hopkins University, Baltimore, MD 21218, USA, April 2001.
- Kudryashova T. I. and Turkovskaya A. V., Translated from Khimicheskoe i Neftyanoe Mashinostroenie, No. 12, P. 25-27, December, 1971.
- Landrum James R., Designing for Corrosion Control, November 1, 1994, TM-584C Revision C, This manual provides guidelines for the control of corrosion of materials in facilities, systems, and equipment at the John F. Kennedy Space Center (KSC), Florida.
- Larson, T. E. Corrosion by Domestic Waters. Illinois State Water Survey, Urbana, Bulletin 59, 1975.
- Leckie, H. P., Corrosion Eng., P. 157-159, Vol.22, 1975.
- Levich V.G., Physicochemical Hydrodynamics (Englewood Cliffs, NJ: Prentice-Hall,), P. 61-78, 1962.
- Levlch V. G., Acta Phychim. USSR 19, 117, 1943.
- Litt M. and Friedlander S. K., A.I.Ch.E. J15, 483, 1959.
- Liu G., Tree D.A., and High M.S., Corrosion Science, Vol. 50, No. 8, 1994.

- Mahato B.K., Stewrd F.R., and Shimlit L. W., Corrosion Sciences, No. I, Vol.8, P.737, 1968.
- Mahato K., Cha C. Y. and Shemilt U W., Corrosion Sciences, Vol. 20, P. 421 to 441, 1980.
- Mahato K., Voora S. K. and Shemilt L. W., Corrosion Science, No. П, Vol. 8, 173 to 193, 1968.
- Makrides A.C., J. Electrochem. Soc., Vol. 107, P. 869, 1960.
- Mears R. B. and Brown R. H., J. Electrochem. Soc. 97, 75, 1950.
- Meyerink E. S. C. and Friedlander S. K., Chem. Engng Sci. 17, 121, 1962.
- Mottern M. M. and Myers J. R., Corrosion, 24, 197, 1968.
- Mor E. D. and Beccaria A. M., Corrosion, Vol. 31, No.8, P.275, Aug, 1975
- Nesic N., Pots B.F.M., Postlethwaite J., and Trevenot N., J. Corrosion Science and Eng., Ph. D. Study, Vol.1, Paper 3, 1995.
- Nesic N., Solvi G.T., Skjerve S., Br. Corros. J. 32, 4, P.269, 1997.
- Nesic S., Postlethwaite J., and Olsen, Corrosion, Science, Vol. 52, No. 4, P. 280-294,April 1996.
- Nesic S., Solvi G.T., Skjerve S., Br. Corros. J. 32, 4, P. 269, 1997.
- Nikurdse, VDI- Forschungsheft, 356, 1932.
- Peabody A.W., edited by Ronald, L. Bianchetti, “Control Of Pipeline Corrosion”, Second Edition South Creek Drive Houston 2001.
- Perry, R. H ,and Green ,D. W , “Chemical Engineers Handbook”, 8th edition, Mc Graw Hill ,United states ,2008
- Popova, Christov M. and Vasilev A., Corros. Sci. 49 2007.
- Popova, Sokolova E., Raicheva S. and Christov M., Corros, Sci. 45 2003.
- Postlethwaite, Fiadzigbe E. and Aruliah S., Corrosion 34, 85, 1978.

- Poulson B. and Robinson R., Corrosion Science, Vol. 26, No.4, P.265 to 280, 1986.
- Poulson, Corrosion Science, Vol. 23, No. 1, P. 391, 1983.
- Qian S. Y., and Chagnon N., The National Research Council Canada (NRC) pp.1-12, 4-6 July 2001.
- Raa V. V. and O. Trass, Can. J. chem. Engng42, 95, 1964.
- Revie R. W. and Greene N. D., *Corros. Sci.* 9, 755, 1969.
- Roberge Pierre R., Corrosion Engineering: Principles and Practice 1st edition McGraw-Hill, United States of America 2008.
- Roberge Pierre R., “Handbook of Corrosion Engineering”, Mc Graw-Hill Companies Caracas Lisbon London Madrid Mexico City Milan, 2000.
- Roberge Pierre R., Corrosion Basics, by NACE Press Book, 2006.
- Robertson J. and Forrest J. E. Corrosion Science, Vol. 32, No. 5/6, P. 521-540, 1991.
- Rodney L. LeRoy, Corrosion–NACE, Vol. 31, No. 5, May, 1975.
- Roetheli E. and Brown R. H., Ind. Engng. Chem. 23, 1010, 1931.
- Romeo J., Skrinde R. T., and Eliassen R., Proc. Am. Soc. Cir. Engrs. Paper 1702, July, 1958.
- Ross T. K., Br. Corrosion J., No. 2, P.131, 1967.
- Ross T.K. and Badhwar R. K., Corrosion Science, Vol. 5, P. 29 to 38, 1965.
- Ross T.K., Wood G.C., and Mahmud I., J. Electrochem. Soc., Vol. 113, P.334, 1966.
- Ashford J. H., Garsy R., and Mann G. M., Corrosion Science, Vol. 14, P. 515, 1974.

- Seheers P.V., J. S. Afr. Inst. Min. Metall., vol. 92, 110.10. pp. 275-281, Oct. 1992.
- Shaw A. and Hanratty T. J., A.I.CH.E. J., Vol. 23, No. 1, P. 28, 1977.
- Sherryl Robertson, Matthew Jeffrey, Hongguang Zhang, and Elizabeth HO; Metallurgical and Materials Transactions B; 314—Vol. 36B, June 2005.
- Shreir L.L., “Corrosion Handbook”, 2nd Edition, Part 1, Newness-Butter., London, 1994.
- Silverman D.C., Corrosion 44, P. 42, 1988.
- Silverman D.C., Corrosion- NACE 59, 207, 2003.
- Silverman D.C., Corrosion NACE, Vol. 40, No. 5, P. 220, 1984.
- Silverman D.C., Corrosion, Vol. 60, No. 11, November 2004.
- Skaperdas G. and Uhlig H., Ind. Eng. Chem. 34, 748, 1942.
- Smith S. W., Cabe K. M., and Black D.W., Corrosion-NACE, Vol. 45, No. 1, P. 790, 1989.
- Son J.S. and T.J. Hanratty, A.I.Ch.E J. 13,689, 1967.
- Soren Peter Lauritz Sorensen translated from Einführung in die Laborpraxis, 1909.
- Soren Peter Lauritz Sorensen, translated from Einführung in die Laborpraxis, in 1909.
- Sparrow, E. M., and Gregg J. L., ASME Trans. J. Heat Transfer Vol. 81, No. 2, pp. 113-130 in 1959.
- Speller F. N. and Kendall V. V., Ind. Engng Chem. 15, 134, 1923.
- Speller F. N., Corrosion, Causes and Prevention, 3rd edition, Mc Graw-Hill, New York and London, p. 168, 1951.
- Speller F. N., New Engl. War. Wks. Ass. 52, 231, 1938.

- Stanislaw Glab, Gunnar Edwall, and Per- Arne JÖngren, Electrochemical Acta, Vol. 27, No. 5, pp. 581-586, 1982.
- Steigerwald R. F. and Greene N. D., J. Electrochem. Soc. 109, 1026, 1962.
- Steigerwald R. F., Corrosion-NACE, Vol. , P. 1, 1968.
- Steigerwald R., Corrosion, Vol. 13, ASM Handbook, 1987.
- Stern M., Corrosion-NACE, Vol. 13, P.97, 1957.
- Streicher M. A., J. Electrochem. *Soc.* 96, 170, 1949.
- Thomson W. J., Introduction to Transport Phenomena, 1st Edition, Prentice Hall PTR, New Jersey, 2000.
- Tobias R.F. and Nobe K., J. Electrochem. Soc., Vol. 22, P.65, 1975.
- Trethewey K.R., and Chamberlain J., Corrosion for Science and Engineering, 2ed edition, 1996.
- Turki H. M., Ph.D. Thesis, Dept. Chem. Eng., Al-Nahrain University, Baghdad, 2009.
- Uhlig H. H., Corrosion Hand Book. Johan Wiley and Sons, Inc, 1976.
- Uhlig H., Triadis D., and Stern M., J. Electrochem. Soc. 102, P. 59, Feb. 1955.
- Uhlig, H. H. (Ed.) "The Corrosion Handbook" .Wiley. New York and Chapman and Hall, London, 1948.
- Uhlig. H. H., Winston Revie. R, Corrosion and Corrosion Control: An Introduction to Corrosion Science and Engineering, 4th, Canada, 2008.
- Vermilyea, D. A., Proc. 1st International Congress on Metallic Corrosion, London, 1982.
- Vilambi N.R.K. and Chin D.T., Electrochemical. Soc., Vol. 134, No.1, P.2501, 1982.

- Wang H.-L., Fan H.-B. and Zheng J.-S., Mater. Chem. Phys. 77, 2003.
- Wang Y. and Postlethwaite J. Corrosion Science, Vol. 39, No. 7, P. 1265-1283, 1997.
- Wang Y., Postlethwaite J. and Bergstrom D.J., J. of Applied Electrochemistry 26, 471, 1996.
- Welty J. R., Wicks C. E., and Rorrer G., Fundamentals of Momentum, Heat, and Mass Transfer, 4th Edition, John Wiley and Sons, United States of America, 2001.
- West J.M., Electrode Deposition and Corrosion Processes, D.Van Nostrand comp. Lim., London, 1976.
- Whiteman G. E., Russel R. P. and Altieri V., Ind. Engng. Chem. 16, 665, 1924.
- Whitman W. , R. Russell , C. Welling , and J. Cochrane , Ind. Eng. Chem. 15 , 672, 1923 .
- Proter D. T., Donnimirska M., Wall R., Corrosion Science, Vol. 8, P. 833,1968.
- Warrg A. A. and A. Nasiruddin K., Electrochem. Acta., Vol. 18, P. 619, 1973.
- Whitman W. and Russell R., Ind. Eng. Chem. 17, 348, 1925.
- Samh S. A., Ph. D. Thesis, Dept. of Chem. Eng., University of Technology, Baghdad, 1994.
- Atia M. A., Ph.D. Thesis, Dept. Chem. Eng., Saddam University, Baghdad, 1996.
- Wilson E., Industrial and Engineering Chemistry, Vol. 15, No. 2, P.127, 1923.

- Wormwell F. J., Iron Steel Inst. 154, 219, 1946.
- Zhang Z., Hinkson D., Singer M., Wang H., and Nesic S., Corrosion Science, Vol. 63, No. 11, P. 1051-1062, 2007.
- Znad H. T., Analysis of Mass Transfer Coefficient under Turbulent flow Conditions Using LCDT, M.Sc. Thesis, Saddam University, Baghdad, 1996.
- Zurubin P.I and Zasita Metallov, Vol. No. 3, P. 279, 1965.

Appendix A

Table A-1: Atomic Weight of Metal; Density of Metal **[Mor and Beccaria, 1975]**.

Metal	Atomic Weight of Metal	Density of Metal (kg/m^3)
Fe	55.847	7833

Table A-2: Values of oxygen Diffusivity **[Perry, 2008]**.

T(ºC)	**D$_o$ x 10^9 (m^2/s) (pure water)**
10.0	1.54
15.0	1.66
16.0	1.87
20.0	2.01
22.0	2.24
25.0	2.41
29.6	2.49
30.0	2.80
37.0	3.0
40.0	3.55
50.0	4.20
55.0	4.50
60.0	5.70

Table A-3: Solubility of oxygen in HCl (mol/m^3) **[Shreir, 1994]**.

pH T °C	1	2	4
25	0.1248	0.125555	0.126
40	0.1190133	0.11976333	0.1202133
60	0.1	0.10075	0.1012

Table A-4: Exchange Current Density**[Pierre, 2001; Uhlig and Winston, 2008];** and Standard Potential at 25 °C**[Uhlig 2008]**.

Metal	**Exchange Current Density(A/m^2)**	**Metal**	**Standard Potential(Volte)**
Fe^{+2}/Fe	10^{-4}	Fe	-0.44
H^{+}/Fe	10^{-3}	H_2	0.0
OH^{-}/O_2	10^{-7}	O_2	1.229

Table A-5: Physical Properties of Water at Atmospheric Pressure **[Perry, 2008].**

T (°C)	Cp (kJ/kg. °C)	ρ (kg/m^3)	μ×10^4 (kg/m.s)	k$_T$ (W/m. °C)	Pr
0.00	4.225	999.8	17.9	0.566	13.25
4.44	4.208	999.8	15.5	0.575	11.35
10.0	4.195	999.2	13.1	0.585	9.40
15.56	4.186	998.6	11.2	0.595	7.88
21.11	4.179	997.4	9.80	0.604	6.78
26.67	4.179	995.8	8.60	0.614	5.85
32.22	4.174	994.9	7.65	0.623	5.12
37.78	4.174	993.0	6.82	0.630	4.53
43.33	4.174	990.6	6.16	0.637	4.04
54.44	4.179	985.7	5.13	0.649	3.30
60.0	4.179	983.3	4.71	0.654	3.02
65.55	4.183	980.3	4.30	0.659	2.73
71.11	4.186	977.3	4.01	0.665	2.53

Appendix B

Table B-1: The comparison between present analysis and Scheers result of corrosion rate of rotating cylinder in acid at temperature 45 ºC and pH 3 **[Scheers, 1992]**.

u ($m.s^{-1}$)	Re	Present Corrosion Rate (mmy^{-1})	Scheers Corrosion Rate (mmy^{-1})
0.5	16779.66	22.02779	18
0.75	25169.49	22.68958	23
1.25	33559.32	23.26898	26.5
1.5	41949.15	23.81092	28.5
2	50338.98	24.28547	30.5

Table B-2: The comparison between present analysis and Bahar result of corrosion rate of rotating cylinder in acid at temperature 40 ºC and pH 1 **[Bahar, 2002]**.

Re	i_{Fe} Present Analysis (A/m^2)	i_{Fe} Bahar(A/m^2)	Present Corrosion Rate (gmd)	Bahar Corrosion Rate (gmd)
8199.5	9.632375	6.32017	240.8508	158.538
16399.1	10.29429	7.9077	257.4016	197.727
24598.6	10.92841	9.13579	273.2572	228.438

Table B-3: The comparison between present analysis and Turki result of corrosion rate of rotating cylinder in acid at temperature 35 ºC and pH 1 **[Turki, 2009]**.

Re	Present Corrosion Rate (gmd)	Turki Corrosion Rate (gmd)
5729	225.8536	201.3369
10025.78	241.318	232.3151
14322.55	262.3049	270.8047
20051.58	286.5935	377.1662

Appendix C

Graphs of Effect wall Roughness at T=25 and pH=4

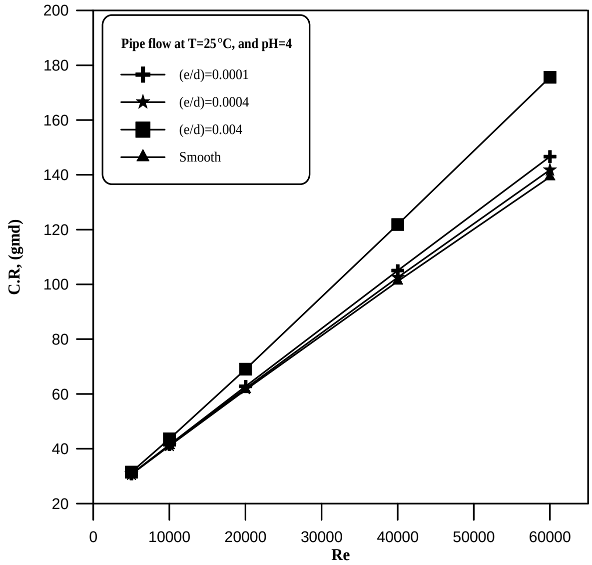

Figure C-1: Variation of Corrosion Rate with Re in smooth and rough pipe at pH=4.

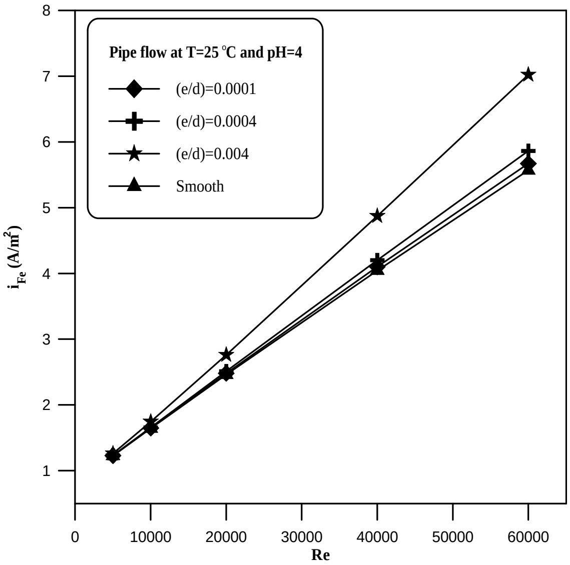

Figure C-2: Variation of Corrosion Rate with Re in smooth and rough pipe at pH=4.

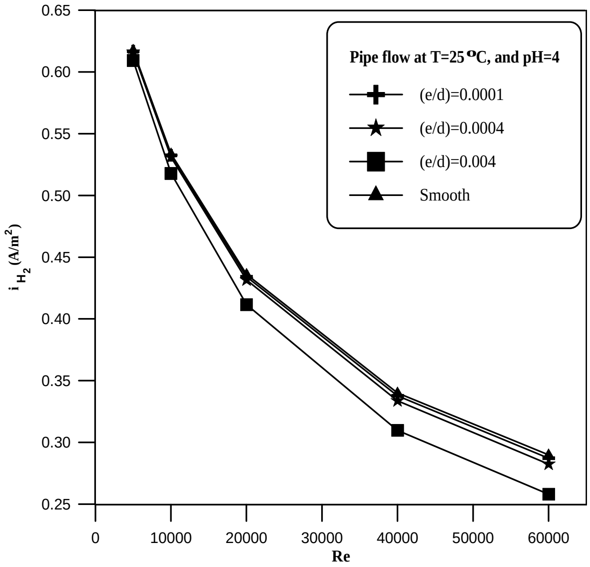

Figure C-3: Variation of current density of H_2 with Re in smooth and rough pipe at pH=4.

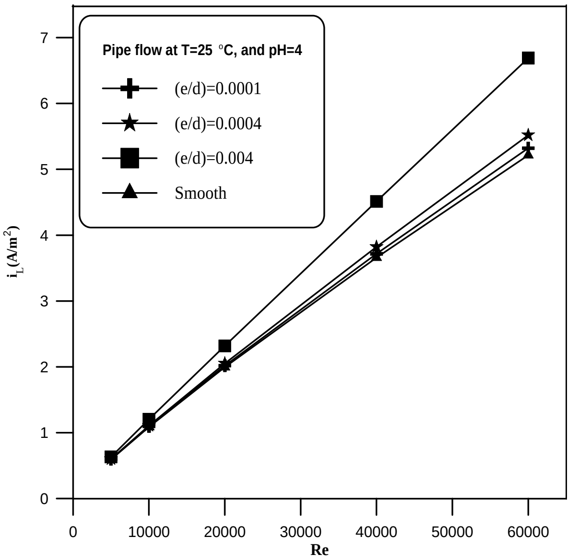

Figure C-4: Variation of limiting current density of H_2 with Re in smooth and rough pipe at pH=4.

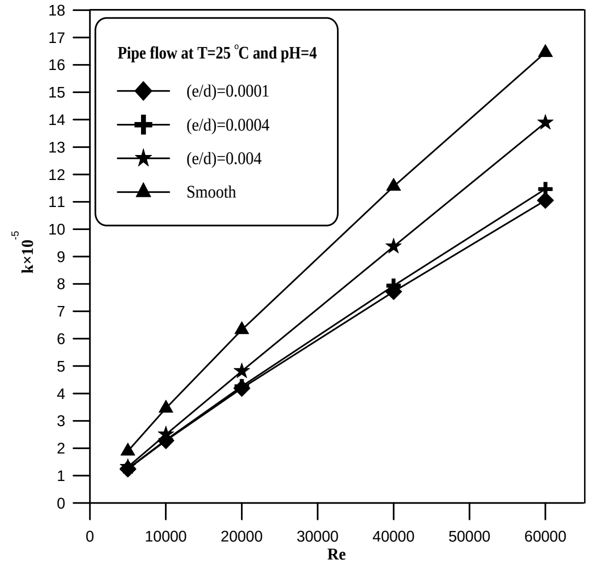

Figure C-5: Variation of mass transfer coefficient with Re in smooth and rough pipe at pH=4.

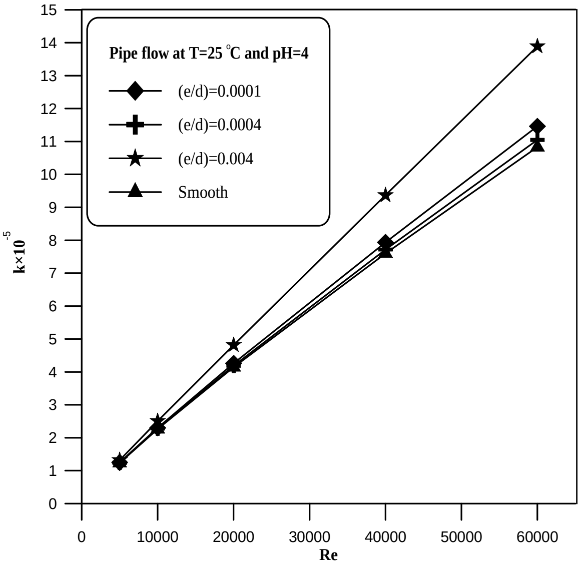

Figure C-6: Variation of mass transfer coefficient with Re in smooth and rough pipe at pH=4.

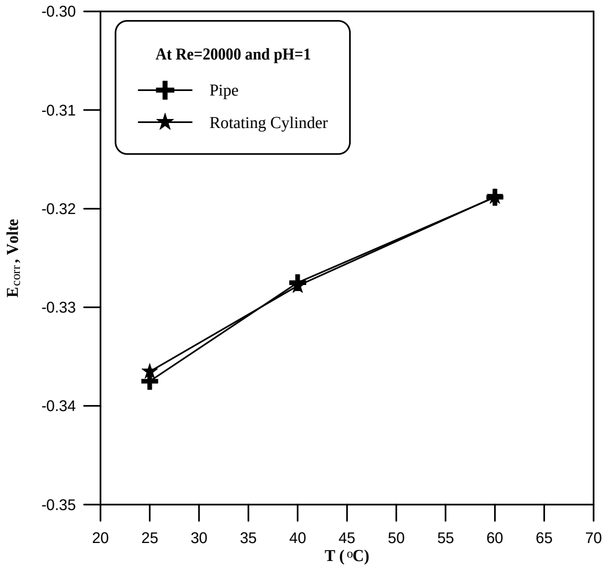

Figure C-7: The comparison of Corrosion Potential in Smooth Pipe Flow and Smooth Surface Rotating Cylinder of three temperatures at Re =20000 and pH=1.

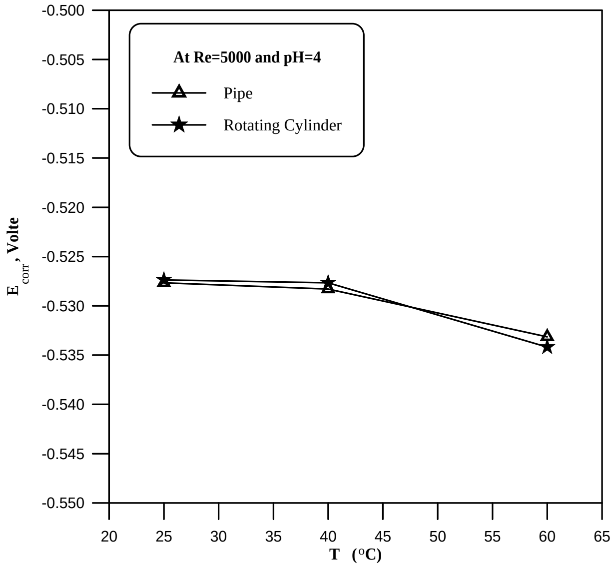

Figure C-8: The comparison of Corrosion Potential in Smooth Pipe Flow and Smooth Surface Rotating Cylinder of three temperatures at Re =5000 and pH=4.

Appendix D

D.1 Results of Effect Heat Transfer

Table D-1: Pipe flow under q_w=3000 W/m^2 at T_b=25 ˚C, pH=1, in aerated solutions.

Re	T_w °C	$I_{oFe}\times10^3$(A/m^2)	$I_{oH2}\times10^2$(A/m^2)	E_{eqFe}	$E_{eqH2}\times10^2$
5000	28.01512	1.005345	3.361009	-0.5723955	-5.942439
10000	26.69551	1.003009	3.272785	-0.5721039	-5.929348
20000	25.95511	1.001696	3.224137	-0.5719402	-5.922002
40000	25.53899	1.000957	3.197065	-0.5718482	-5.917875
60000	25.38601	1.000686	3.187157	-0.5718144	-5.916357

Table D-2: Pipe flow under q_w=5000 W/m^2 at T_b=25 ˚C, pH=1, in aerated solutions.

Re	T_f °C	$I_{oFe}\times10^3$(A/m^2)	$I_{oH2}\times10^2$(A/m^2)	E_{eqFe}	$E_{eqH2}\times10^2$
5000	27.5126	1.008895	3.499197	-0.5728398	-5.962379
10000	26.41293	1.005011	3.348235	-0.5723537	-5.940561
20000	25.79593	1.002825	3.265939	-0.5720809	-5.928319
40000	25.44916	1.001595	3.220433	-0.5719277	-5.921439
60000	25.32167	1.001143	3.203834	-0.5718713	-5.918909

Table D-3: Pipe flow under q_w=15000 W/m^2 at T_b=25 ˚C, pH=1, in aerated solutions.

Re	T_w °C	$I_{oFe}\times10^3$ (A/m^2)	$I_{oH2}\times10^2$ (A/m^2)	E_{eqFe}	$E_{eqH2}\times10^2$
5000	40.0756	1.026475	4.263195	-0.5750611	-6.062082
10000	33.47755	1.014965	3.747582	-0.5736028	-5.996628
20000	29.77554	1.008455	3.481778	-0.5727846	-5.959902
40000	27.69493	1.004779	3.339423	-0.5723248	-5.939262
60000	26.93003	1.003425	3.288324	-0.5721557	-5.931674

Table D-4: Pipe flow under q_w=30000 W/m^2 at T_b=25 ˚C, pH=1, in aerated solutions.

Re	T_w °C	$I_{oFe}\times10^3$ (A/m^2)	$I_{oH2}\times10^2$ (A/m^2)	E_{eqFe}	$E_{eqH2}\times10^2$
5000	55.15119	1.052325	5.665311	-0. 5783932	-6.211638
10000	41.9551	1.016846	4.420407	-0. 5754765	-6.080728
20000	34.55109	1.008455	3.827748	-0. 5738401	-6.007278
40000	30.38987	1.009538	3.524769	-0. 5729204	-5. 965997
60000	28.86005	1. 006839	3.41853	-0. 5725822	-5. 95082

Table D-5: Pipe flow under q_w=3000 W/m^2 at T_b=40 ˚C, pH=1, in aerated solutions.

Re	T_w °C	$I_{oFe}\times10^3$(A/m^2)	$I_{oH2}\times10^2$(A/m^2)	E_{eqFe}	$E_{eqH2}\times10^2$
5000	43.31484	1.057672	6.003257	-0.5790924	-6.243022
10000	41.87373	1.05524	5.847309	-0.5787739	-6.228726
20000	41.06108	1.053866	5.760857	-0.5785943	-6.22066
40000	40.602	1.053089	5.712483	-0.5784928	-6.21611
60000	40.4325	1.052802	5.69471	-0.5784553	-6.214428

Table D-6: Pipe flow under q_w=5000 W/m^2 at T_b=40 ˚C, pH=1, in aerated solutions.

Re	T_w °C	$I_{oFe}\times10^3$(A/m^2)	$I_{oH2}\times10^2$(A/m^2)	E_{eqFe}	$E_{eqH2}\times10^2$
5000	45.52473	1.061391	6.249059	-0.5795808	-6.264945
10000	43.12289	1.057349	5.982288	-0.57905	-6.241118
20000	41.76847	1.055062	5.836054	-0.5787506	-6.227682
40000	41.00337	1.053768	5.754755	-0.5785815	-6.220092
60000	40.72083	1.05329	5.724972	-0.5785191	-6.217289

Table D-7: Pipe flow under q_w=15000 W/m^2 at T_b=40 ˚C, pH=1, in aerated solutions.

Re	T_w °C	I_{oFe}×10^3(A/m^2)	I_{oH2}×10^2(A/m^2)	E_{eqFe}	E_{eqH2}×10^2
5000	56.57419	1.079793	7.605977	-0.582023	-6.37456
10000	49.36866	1.06783	6.696375	-0.5804304	-6.303078
20000	45.30542	1.061023	6.284301	-0.5795324	-6.26277
40000	43.01001	1.057158	5.969989	-0.579025	-6.239998
60000	42.16249	1.055728	5.878285	-0.5788377	-6.23159

Table D-8: Pipe flow under q_w=30000 W/m^2 at T_b=40 ˚C, pH=1, in aerated solutions.

Re	T_w °C	I_{oFe}×10^3 (A/m^2)	I_{oH2}×10^2 (A/m^2)	E_{eqFe}	E_{eqH2}×10^2
5000	73.14838	1.106798	10.08789	-0.5856863	-6.538981
10000	58.73733	1.083358	7.898036	-0.5825011	-6.396019
20000	50.61085	1.069902	6.846444	-0.580705	-6.315401
40000	46.02003	1.062223	6.305274	-0.5796903	-6.269859
60000	44.32499	1.059374	6.114608	-0.5793157	-6.253044

Table D-9: Pipe flow under q_w=3000 W/m^2 at T_b=60 ˚C, pH=1, in aerated solutions.

Re	T_w °C	I_{oFe}×10^3(A/m^2)	I_{oH2}(A/m^2)	E_{eqFe}	E_{eqH2}×10^2
5000	63.84569	1.123856	0.1201532	-0.5880506	-6.645103
10000	62.19471	1.121242	0.1169969	-0.5876857	-6.628724
20000	61.25484	1.119751	0.1152305	-0.587478	-6.6194
40000	60.7188	1.1189	0.1142329	-0.5873595	-6.614083
60000	60.51931	1.118583	0.1138633	-0.5873154	-6.612103

Table D-10: Pipe flow under q_w=5000 W/m^2 at T_b=60 ˚C, pH=1, in aerated solutions.

Re	T_w °C	$I_{oFe}\times10^3$(A/m^2)	I_{oH2}(A/m^2)	E_{eqFe}	$E_{eqH2}\times10^2$
5000	66.40948	1.127902	0.1251917	-0.5886173	-6.670536
10000	63.65784	1.123559	0.1197906	-0.5880091	-6.643239
20000	62.0914	1.121079	0.1168017	-0.5876629	-6.6277
40000	61.19799	1.11961	0.1151244	-0.5874694	-6.618837
60000	60.86551	1.119133	0.1145051	-0.5873919	-6.615537

Table D-11: Pipe flow under q_w=15000 W/m^2 at T_b=60 ˚C, pH=1, in aerated solutions.

Re	T_w °C	$I_{oFe}\times10^3$(A/m^2)	I_{oH2}(A/m^2)	E_{eqFe}	$E_{eqH2}\times10^2$
5000	79.22844	1.147886	0.1530291	-0.5914506	-6.797705
10000	70.97353	1.135063	0.134586	-0.589626	-6.715813
20000	66.27421	1.127689	0.1249216	-0.5885874	-6.669194
40000	63.59398	1.123458	0.1196676	-0.587995	-6.642605
60000	62.59653	1.121879	0.1177588	-0.5877745	-6.632711

Table D-12: Pipe flow under q_w=30000 W/m^2 at T_b=60 ˚C, pH=1, in aerated solutions.

Re	T_w °C	$I_{oFe}\times10^3$(A/m^2)	I_{oH2}(A/m^2)	E_{eqFe}	$E_{eqH2}\times10^2$
5000	98.15483	1.176664E	0.2031015	-0.5956337	-6.985461
10000	81.76448	1.151792	0.1590888	-0.592011	-6.822863
20000	72.43823	1.137351	0.1377195	-0.5899498	-6.730343
40000	67.12155	1.129022	0.1266212	-0.5887747	-6.67760
60000	65.14371	1.125906	0.122683	-0.5883375	-6.657979

D.2 Graphs of Effect Heat Transfer

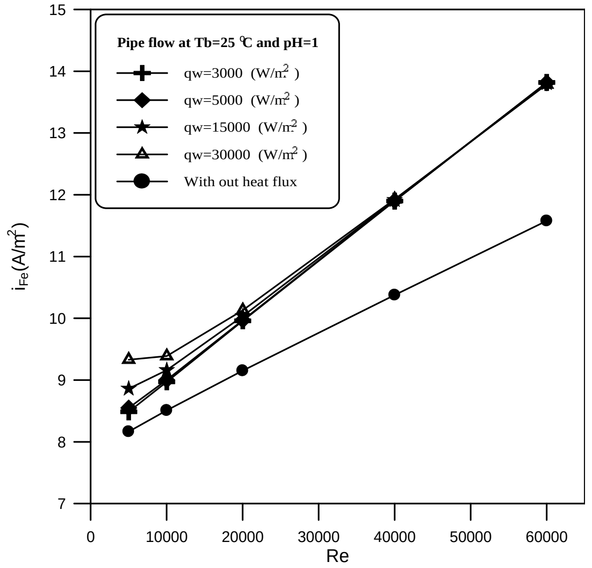

Figure D-1: Variation of Corrosion Rate with Re under effect of heat flux in T_b=25 ºC.

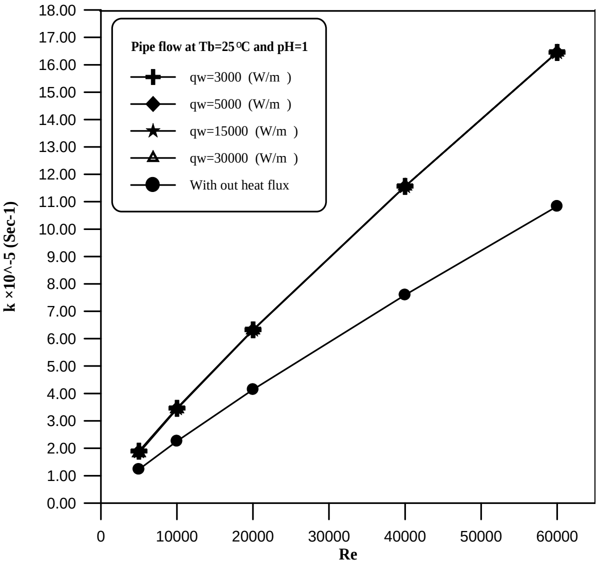

Figure D-2: Variation of mass transfer coefficient with Re under effect of heat flux in T_b=25 ºC.

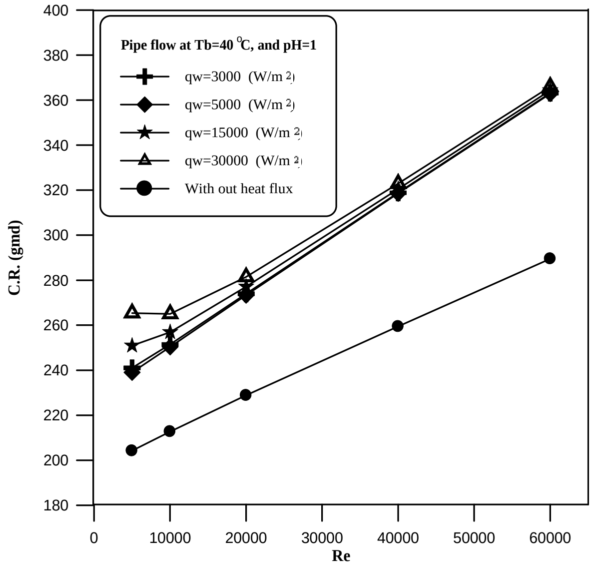

Figure D-3: Variation of Corrosion Rate with Re under effect of heat flux at T_b=40 ºC.

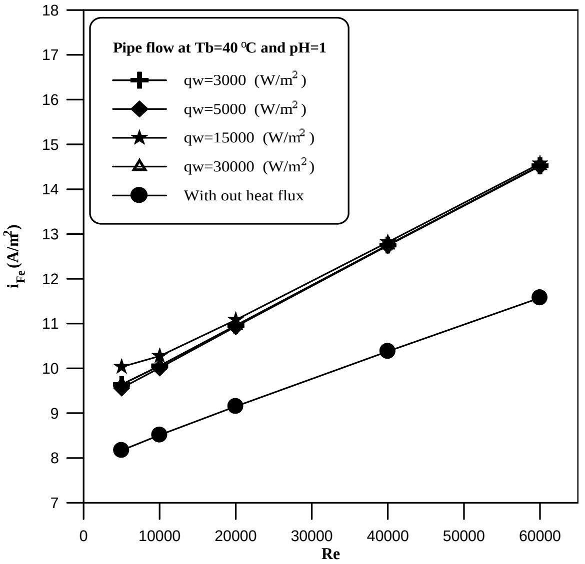

Figure D-4: Variation of Corrosion current with Re under effect of heat flux at T_b=40 ºC.

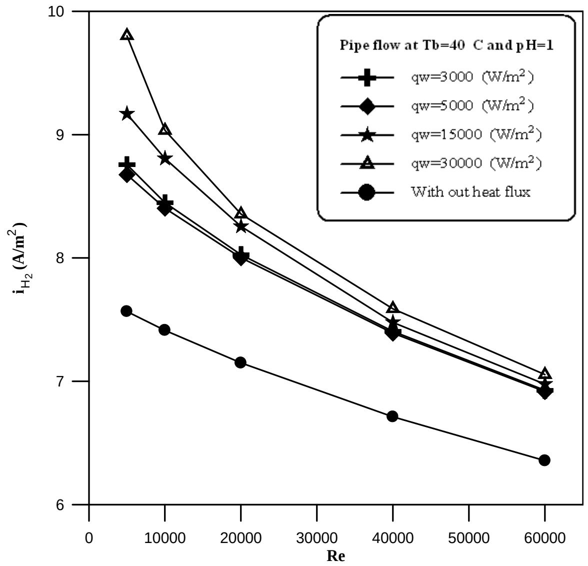

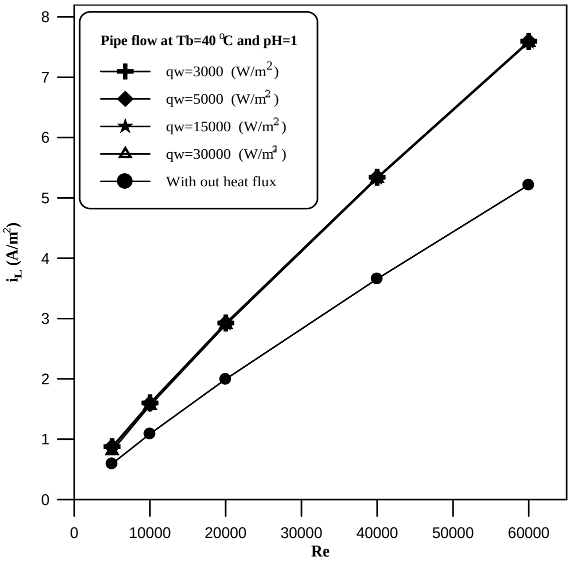

Figure D-5: Variation of current density of H_2 with Re under effect of heat flux at T_b=40ºC.

Figure D-6: Variation of limiting current density with Re under effect of heat flux at T_b=40ºC.

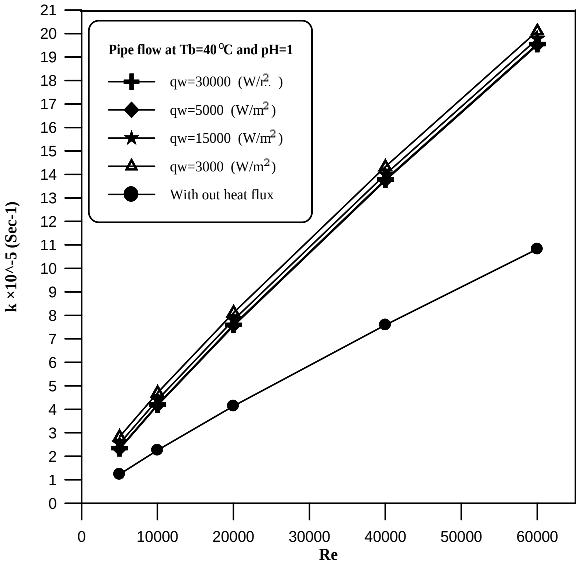

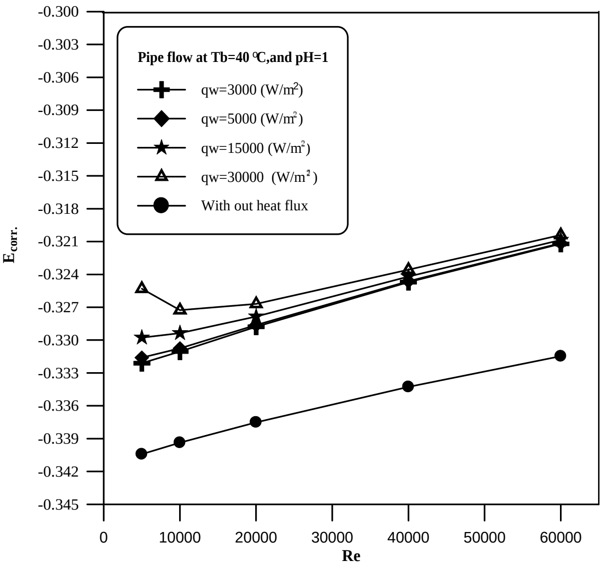

Figure D-7: Variation of mass transfer coefficient with Re under effect of heat flux in T_b=40 ºC.

Figure D-8: Variation of corrosion potential with Re under effect of heat flux in T_b=40 ºC.

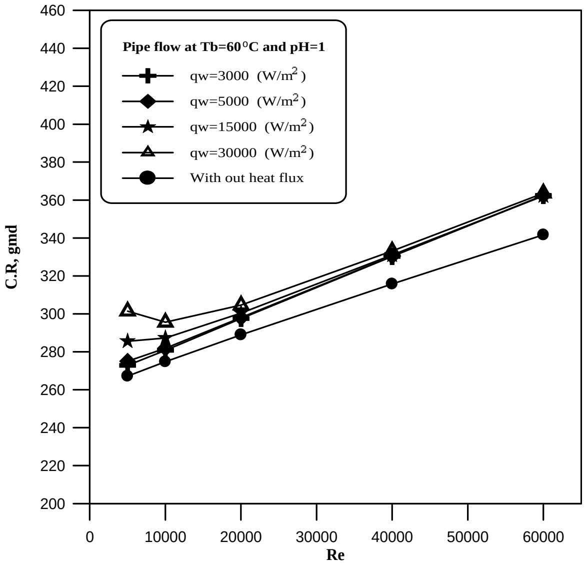

Figure D-9: Variation of Corrosion Rate with Re under effect of heat flux at T_b=60 ºC.

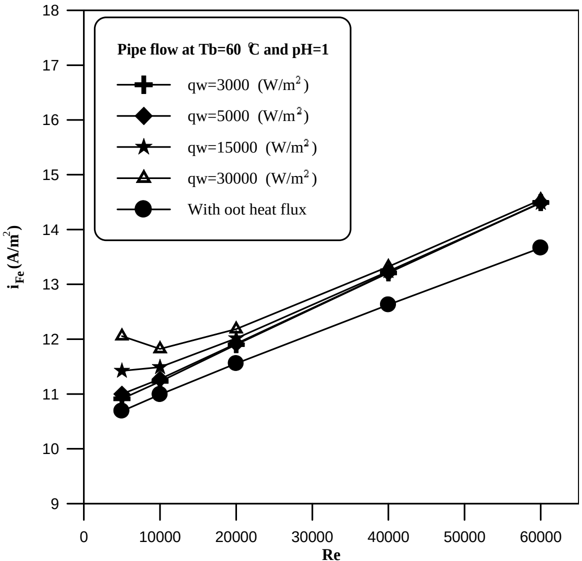

Figure D-10: Variation of corrosion current with Re under effect of heat flux at T_b=60 ºC.

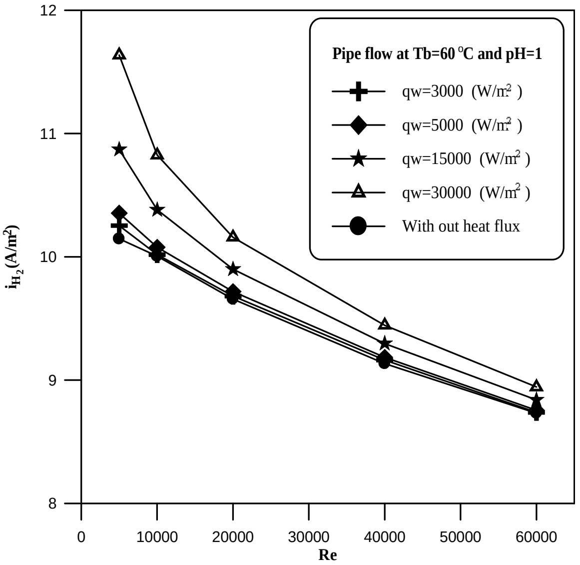

Figure D-11: Variation of current density of H_2 with Re under effect of heat flux at T_b=60 ºC.

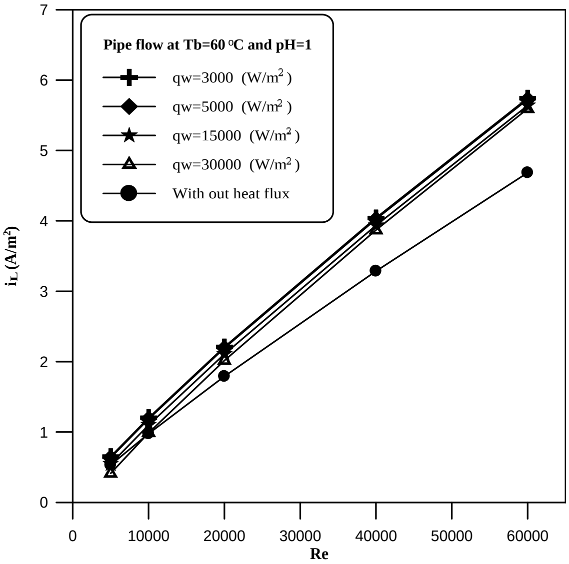

Figure D-12: Variation of limiting current density with Re under effect of heat flux at T_b=60 ºC.

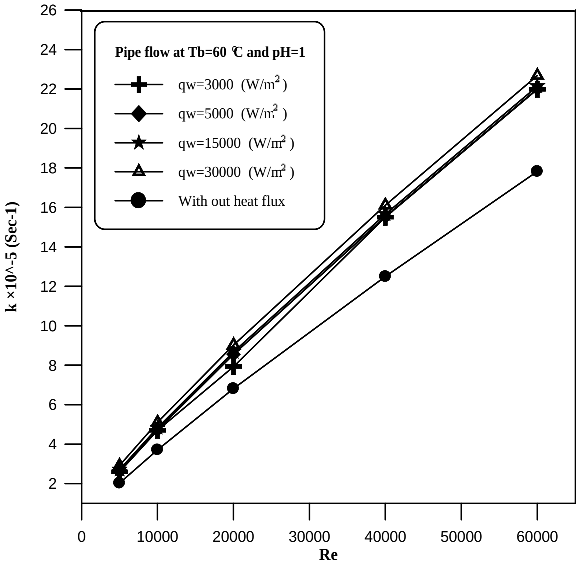

Figure D-13: Variation of mass transfer coefficient with Re under effect of heat flux in T_b=60 ºC.

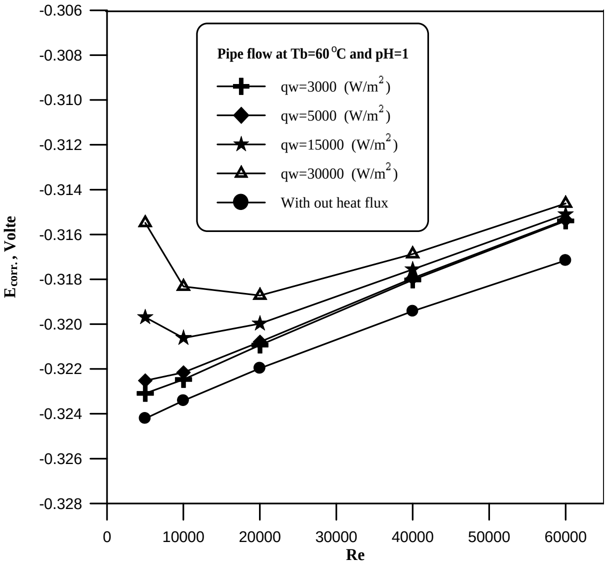

Figure D-14: Variation of corrosion potential with Re under effect of heat flux in T_b=60 ºC.

Appendix E

Graphs of Polarization Curve of Rotating Cylinder

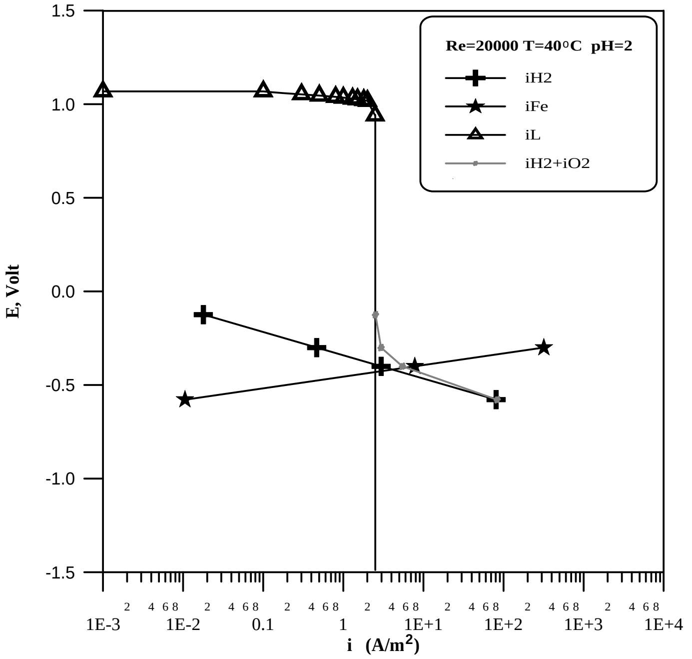

Figure E-1: Polarization curve of iron rotating cylinder in HCl at T=40 ºC, pH=2 and Re=20000.

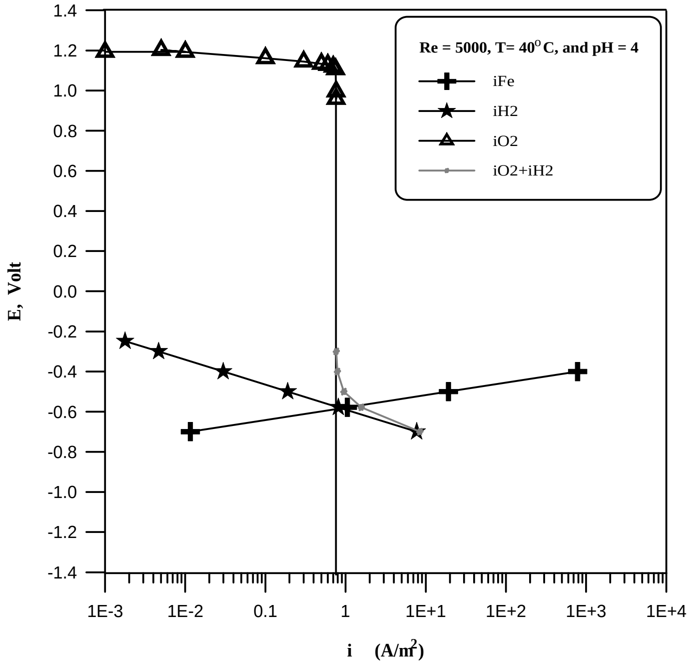

Figure E-2: Polarization curve of iron rotating cylinder in HCl at T=40 ºC, pH=4 and Re=5000.

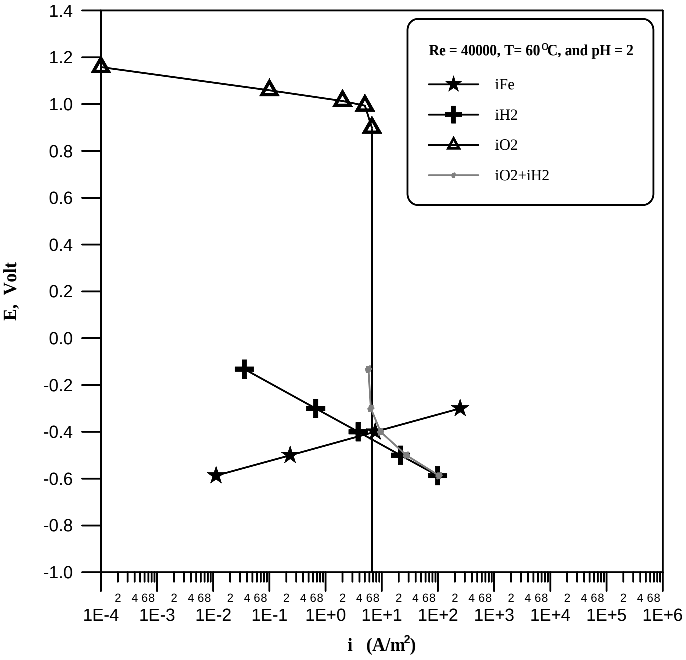

Figure E-3: Polarization curve of iron rotating cylinder in HCl at T=60 ºC, pH=2 and Re=40000.

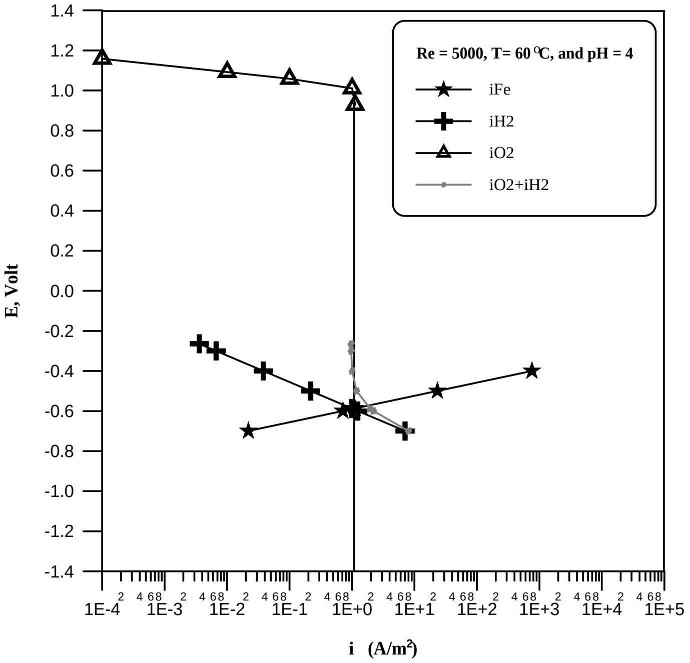

Figure E-4: Polarization curve of iron rotating cylinder in HCl at T=60 ºC, pH=4 and Re=5000.

Appendix F

TABLES

The concentration of dissolved $[Fe^{+2}] = 3.5\times10^{-5}M$, $[O_2] = 10^{-10}$ M **[West, 1976]**, and $[H^{+2}] = 10^{(-pH)}$. The standard potentials are -0.44, 0, and 1.229 V for iron, hydrogen, and oxygen respectively, numbers of electrons are $n_{Fe}=2$, $n_{H2}=1$, and $n_{O2}=4$, Alpha values are $\alpha_{Fe}=0.5$ **[Uhlig and Winston, 2008]**, $\alpha_{H2}=0.5$ **[Nesic et. al., 1996]**, the diameter of rotating cylinder and pipe flow is 0.0255 m, and the exchange current density are $i_o^{(Fe^{+2}/Fe)}=10^{-4}$ (A/m^2) at temperature of 25 ºC **[Uhlig and Winston, 2008]**, and $i_o^{(H^{+}/Fe)}=10^{-3}$ (A/m^2) at temperature of 25 ºC **[Roberge, 2000]**.

F.1 Smooth pipe flow

Table F-1: Results of smooth pipe flow at T=25 °C and pH=1 in aerated acid solutions.

Re	$f\times10^3$	$K\times10^5$(m/s)	E_{corr}(V)	i_L(A/m^2)	i_{H2}(A/m^2)	i_{Fe}(A/m^2)
5000	9.406628	1.231248	-0.3404277	0.5930465	7.566024	8.1655
10000	7.91	2.258118	-0.3393763	1.087652	7.412696	8.5082
20000	6.65149	4.141407	-0.3375037	1.994763	7.147281	9.1519
40000	5.593215	7.595374	-0.3342794	3.658411	6.712334	10.376
60000	5.05404	10.83001	-0.3314655	5.216417	6.354453	11.578

Table F-2: Results of smooth pipe flow at T=25 °C and pH=4 in aerated acid solutions.

Re	$f\times10^3$	$K\times10^5$(m/s)	E_{corr}(V)	i_L(A/m^2)	i_{H2}(A/m^2)	i_{Fe}(A/m^2)
5000	9.406628	1.231248	-0.5664995	0.598789	0.6175482	1.2259
10000	7.91	2.258118	-0.5589993	1.09811	0.5336356	1.6417
20000	6.65149	4.141407	-0.5486252	2.013943	0.4360288	2.459
40000	5.593215	7.595374	-0.5358579	3.693588	0.3400532	4.043
60000	5.05404	10.83001	-0.5276475	5.266575	0.2898107	5.5666

Table F-3: Results of smooth pipe flow at T=40 °C and pH=1 in aerated acid solutions.

Re	$f\times10^3$	$K\times10^5$(m/s)	E_{corr}(V)	i_L(A/m^2)	i_{H2}(A/m^2)	i_{Fe}(A/m^2)
5000	9.406628	1.230469	-0.3404248	0.5926716	7.565603	8.1678
10000	7.91	2.25669	-0.3393734	1.086964	7.412283	8.5092
20000	6.65149	4.138788	-0.3375109	1.993501	7.148276	9.1493
40000	5.593215	7.590571	-0.3342765	3.656098	6.71196	10.378
60000	5.05404	10.82317	-0.3314727	5.213119	6.355338	11.575

Table F-4: Results of smooth pipe flow at T=40 °C and pH=4 in aerated acid solutions.

Re	$f\times10^3$	$K\times10^5$(m/s)	E_{corr}(V)	i_L(A/m^2)	i_{H2}(A/m^2)	i_{Fe}(A/m^2)
5000	9.40663	1.230469	-0.566501	0.59837	0.6175719	1.2258
10000	7.91	2.25669	-0.559011	1.097416	0.5337601	1.641
20000	6.65149	4.138788	-0.548637	2.01267	0.4361306	2.4579
40000	5.59322	7.590571	-0.535869	3.691253	0.3401325	4.0411
60000	5.05404	10.82317	-0.527669	5.263246	0.2899309	5.5616

Table F-5: Results of smooth pipe flow at T=60 °C and pH=1 in aerated acid solutions.

Re	$f\times10^3$	$K\times10^5$(m/s)	E_{corr}(V)	i_L(A/m^2)	i_{H2}(A/m^2)	i_{Fe}(A/m^2)
5000	9.406628	2.025587	-0.324212	0.532621	10.14591	10.686
10000	7.91	3.714943	-0.323411	0.976831	10.00526	10.989
20000	6.65149	6.813236	-0.321969	1.791516	9.656994	11.555
40000	5.593215	12.49553	-0.319426	3.285654	9.134	12.626
60000	5.05404	17.817	-0.317163	4.684915	8.73076	13.663

Table F-6: Results of smooth pipe flow at T=60 °C and pH=4 in aerated acid solutions.

Re	$f\times10^3$	$K\times10^5$(m/s)	E_{corr}(V)	i_L(A/m^2)	i_{H2}(A/m^2)	i_{Fe}(A/m^2)
5000	9.406628	1.230469	-0.3404248	0.5926716	7.565603	8.1678
10000	7.91	2.25669	-0.3393734	1.086964	7.412283	8.5092
20000	6.65149	4.138788	-0.3375109	1.993501	7.148276	9.1493
40000	5.593215	7.590571	-0.3342765	3.656098	6.71196	10.378
60000	5.05404	10.82317	-0.3314727	5.213119	6.355338	11.575

F.2 Pipe flow with roughness

F.2.1 Pipe flow with (e/d) =0.0001 at pH=1

Table F-7: Results of pipe flow with (e/d) =0.0001 at T=25 °C and pH=1 in aerated acid solutions.

Re	$f\times10^3$	$K\times10^5$(m/s)	E_{corr}(V)	i_L(A/m^2)	i_{H2}(A/m^2)	i_{Fe}(A/m^2)
5000	9.523718	1.23887	-0.3404248	0.5967261	7.565603	8.1678
10000	8.037794	2.276286	-0.3393634	1.096463	7.410838	8.5125
20000	6.798876	4.187039	-0.3374608	2.016742	7.141311	9.1672
40000	5.772956	7.716449	-0.3341663	3.716729	6.697579	10.422
60000	5.260585	11.04909	-0.3312824	5.321941	6.331847	11.661

F.2.2 Pipe flow with (e/d) =0.0004 at pH=1

Table F-8: Results of pipe flow with (e/d) =0.0004 at T=25 °C and pH=1 in aerated solutions.

Re	$f\times10^3$	$K\times10^5$(m/s)	E_{corr}(V)	i_L(A/m^2)	i_{H2}(A/m^2)	i_{Fe}(A/m^2)
5000	9.523718	1.23887	-0.3404248	0.5967261	7.565603	8.1678
10000	8.037794	2.276286	-0.3393634	1.096463	7.410838	8.5125
20000	6.798876	4.187039	-0.3374608	2.016742	7.141311	9.1672
40000	5.772956	7.716449	-0.3341663	3.716729	6.697579	10.422
60000	5.260585	11.04909	-0.3312824	5.321941	6.331847	11.661

F.2.3 Pipe flow with (e/d) =0.004 at pH=1

Table F-9: Results of pipe flow with (e/d) = 0.004 at T=25 °C and pH=1 in aerated acid solutions.

Re	$f\times10^3$	$K\times10^5$(m/s)	E_{corr}(V)	i_L(A/m^2)	i_{H2}(A/m^2)	i_{Fe}(A/m^2)
5000	10.75077	1.31628	-0.3403447	0.63340033	7.55381	8.1933
10000	9.707752	2.501599	-0.3391331	1.204928	7.377677	8.5892
20000	8.982869	4.812779	-0.33686	2.318138	7.05825	9.3834
40000	8.50655	9.36688	-0.3327144	4.511682	6.510871	11.028
60000	8.314816	13.891	-0.3289893	6.69082	6.055329	12.75

F.2.4 Pipe flow with (e/d) =0.0001 at pH=4

Table F-10: Results of pipe flow with (e/d) =0.0001 at T=25 °C and pH=4 in aerated acid solutions.

Re	f×10^3	K ×10^5(m/s)	E_{corr}(V)	i_L(A/m^2)	i_{H2}(A/m^2)	i_{Fe}(A/m^2)
5000	9.523718	1.238887	-0.5664401	0.6024638	0.6168348	1.2287
10000	8.037794	2.276286	-0.5588899	1.106945	0.5324997	1.6487
20000	6.798876	4.187039	-0.5484056	2.036134	0.4341685	2.4801
40000	5.772956	7.716449	-0.5354981	3.752467	0.3376793	4.1
60000	5.260585	11.04909	-0.5271769	5.373114	0.287167	5.6692

F.2.5 Pipe flow with (e/d) =0.0004 at pH=4

Table F-11: Results of pipe flow with (e/d) =0.0004 at T=25 °C and pH=4 in aerated acid solutions.

Re	f×10^3	K ×10^5(m/s)	E_{corr}(V)	i_L(A/m^2)	i_{H2}(A/m^2)	i_{Fe}(A/m^2)
5000	9.63168	1.245889	-0. 56638	0.605869	0.616114	1.2316
10000	8.196619	2.298665	-0.5587397	1.117828	0.5309445	1.6584
20000	7.029769	4.257542	-0.5480852	2.070419	0.4314679	2.5113
40000	6.102278	7.933492	-0.5348773	3.858014	0.3336216	4.2003
60000	5.660842	11.46173	-0.5263057	5.573776	0.2823366	5.8649

F.2.6 Pipe flow with (e/d) =0.004 at pH=4

Table F-12: Results of pipe flow with (e/d) =0.004 at T=25 °C and pH=4 in aerated acid solutions.

Re	f×10^3	K ×10^5(m/s)	E_{corr}(V)	i_L(A/m^2)	i_{H2}(A/m^2)	i_{Fe}(A/m^2)
5000	10.75077	1.31628	-0.5658092	0.6400995	0. 6093038	1.2593
10000	9.707752	2.501599	-0.5574479	1.216514	0. 5177562	1.744
20000	8.982869	4.812779	-0.5456519	2.340428	0. 4115011	2.7609
40000	8.50655	9.366884	-0.5310621	4.555064	0. 3097353	4.8732
60000	8.314816	13.89108	-0.5216794	6.755155	0. 2580148	7.0227

F.3 Smooth pipe flow in presence of heat flux

F.3.1 Smooth Pipe flow under heat flux with T_b=25 °C

Table F-13: Results of pipe flow under q_w=3000 W/m^2 at T_b=25 ˚C, and pH=1 in aerated solutions.

Re	T_f(°C)	Nu	h(W/m^2.°C)	K×10^5(m/s)	E_{corr}(V)	i_L(A/m^2)	i_{H2}(A/m^2)	i_{Fe}(A/m^2)
5000	26.50706	40.77052	981.223	1.89048	-0.339073	0.9011438	7.576143	8.485773
10000	25.84776	73.06459	1755.043	3.457408	-0.3378013	1.662616	7.302492	8.971794
20000	25.47755	130.2819	3126.026	6.322373	-0.3352078	3.055269	6.89609	9.95911
40000	25.26949	231.4602	5550.335	11.55976	-0.3306916	5.60157	6.291559	11.89788
60000	25.193	323.5065	7755.829	16.45175	-0.3268664	7.980134	5.831763	13.81511

Table -14: Results of pipe flow under q_w=5000 W/m^2 at T_b=25 ˚C, and pH=1 in aerated solutions.

Re	T_f (°C)	Nu	h(W/m^2.°C)	K ×10^5(m/s)	E_{corr}(V)	i_L(A/m^2)	i_{H2}(A/m^2)	i_{Fe}(A/m^2)
5000	27.5126	40.25618	971.6982	1.890748	-0.3386324	0.8891463	7.650867	8.54933
10000	26.41293	72.53802	1745.286	3.458175	-0.337571	1.650513	7.346051	9.002599
20000	25.79593	129.7395	3115.925	6.323378	-0.3350976	3.042908	6.922336	9.970201
40000	25.44916	230.8999	5539.825	11.56085	-0.3306316	5.588844	6.305077	11.90281
60000	25.32167	322.935	7745.058	16.45284	-0.3268364	7.967155	5.8428803	13.81932

Table F-15: Results of pipe flow under q_w=15000 W/m^2 at T_b=25 ˚C, and pH=1 in aerated solutions.

Re	T_f(°C)	Nu	h(W/m^2.°C)	K×10^5(m/s)	E_{corr}(V)	i_L(A/m^2)	i_{H2}(A/m^2)	i_{Fe}(A/m^2)
5000	32.5378	37.54028	919.4478	1.881236	-0.3369494	0.8243499	8.118667	8.860992
10000	29.23878	69.82666	1693.968	3.455967	-0.3364094	1.587142	7.728593	9.160046
20000	27.38777	126.9835	3063.993	6.324954	-0.3345168	2.979421	7.33263	10.03468
40000	26.34747	228.0731	5486.455	11.5643	-0.3303612	5.524224	6.823585	11.91344
60000	25.96501	320.0594	7690.614	16.45684	-0.3266662	7.901533	6.439921	13.820719

Table F-16: Results of pipe flow under q_w=30000 W/m^2 at T_b=25 ˚C, and pH=1 in aerated solutions.

Re	T_f(°C)	Nu	h(W/m^2.°C)	K×10^5(m/s)	E_{corr}(V)	i_L(A/m^2)	i_{H2}(A/m^2)	i_{Fe}(A/m^2)
5000	40.0756	32.90535	823.4221	1.827634	-0.333175	0.712955	8.611623	9.329783
10000	33.47755	65.48501	1608.219	3.432409	-0. 334687	1.483484	7.897569	9.388644
20000	29.77554	122.7035	2981.385	6.316151	-0.333646	2.879039	7.243614	10.13085
40000	27.69493	223. 752	5403.773	11.56311	-0. 329961	5.424235	6.493433	11.92698
60000	26.93003	315.6882	7607.067	16.45822	-0. 326426	7.800851	5.977718	13.78706

F.3.2 Smooth Pipe flow under heat flux with T_b=40 °C

Table F-17: Results of pipe flow under q_w=3000 W/m^2at T_b=40 ˚C, and pH=1 in aerated solutions.

Re	T_f(°C)	Nu	h(W/m^2.°C)	K×10^5 (m/s)	E_{corr}(V)	i_L(A/m^2)	i_{H2}(A/m^2)	i_{Fe}(A/m^2)
5000	41.65742	36.96713	909.764	2.303427	-0.3321129	0.875311	8.674803	9.559606
10000	40.93687	65.21566	1606.124	4.161795	-0.3310514	1.600632	8.402589	10.01033
20000	40.53054	114.9705	2832.633	7.553366	-0.3287819	2.924614	8.001034	10.93031
40000	40.301	202.4461	4989	13.74173	-0.3247064	5.340844	7.389894	12.74049
60000	40.21625	281.6817	6942.239	19.51351	-0.3212116	7.594648	6.916298	14.51461

Table F-18: Results of pipe flow under q_w=5000 W/m^2at T_b=40 ˚C, and pH=1 in aerated solutions.

Re	T_f(°C)	Nu	h(W/m^2.°C)	K×10^5 (m/s)	E_{corr}(V)	i_L(A/m^2)	i_{H2}(A/m^2)	i_{Fe}(A/m^2)
5000	42.76237	37.13507	912.8832	2.342533	-0.3316057	0.873654	8.75653	9.638567
10000	41.56144	65.39209	1609.459	4.202189	-0.3307646	1.599419	8.447923	10.0563
20000	40.88424	115.1551	2836.177	7.595104	-0.3286217	2.923637	8.026278	10.95678
40000	40.50167	202.6389	4992.746	13.78492	-0.3246263	5.339976	7.404988	12.75166
60000	40.36042	281.8792	6946.103	19.55758	-0.3211516	7.593807	6.926332	14.52427

Table F-19: Results of pipe flow q_w=15000 W/m^2 at T_b=40 ˚C, and pH=1 in aerated solutions.

Re	T_f(°C)	Nu	h(W/m^2.°C)	K×10^5 (m/s)	E_{corr}(V)	i_L(A/m^2)	i_{H2}(A/m^2)	i_{Fe}(A/m^2)
5000	48.28709	37.96026	927.9868	2.536852	-0.3297723	0.856693	9.168373	10.03388
10000	44.68433	66.26537	1625.84	4.403395	-0.3293627	1.588254	8.98066	10.27444
20000	42.65271	116.0732	2853.717	7.803369	-0.3278406	2.915748	8.155828	11.08107
40000	41.505	203.5998	5011.374	14.00054	-0.3242057	5.333871	7.477841	12.81694
60000	41.08125	282.8645	6965.345	19.7777	-0.3208511	7.588305	6.976583	14.5724

Table F-20: Results of pipe flow q_w=30000 W/m^2 at T_b=40 ˚C, and pH=1 in aerated solutions.

Re	T_f(°C)	Nu	h(W/m^2.°C)	K×10^5(m/s)	E_{corr}(V)	i_L(A/m^2)	i_{H2}(A/m^2)	i_{Fe}(A/m^2)
5000	56.57419	39.15534	949.1844	2.825111	-0.325317	0.804646	9.802169	10.6137
10000	49.36866	67.5487	1649.508	4.703047	-0.327269	1.555758	9.034546	10.59846
20000	45.30542	117.4342	2879.481	8.114389	-0.326699	2.894609	8.355872	11.25515
40000	43.01001	205.0315	5038.99	14.32313	-0.323575	5.319217	7.587588	12.91471
60000	42.16249	284.3354	6993.968	20.10723	-0.320411	7.576013	7.053512	14.63912

F.3.3 Smooth Pipe flow under heat flux with T_b=60 °C

Table F-21: Results of pipe flow under q_w=3000 W/m^{2}at T_b=60 ˚C, and pH=1 in aerated solutions.

Re	T_f(°C)	Nu	h(W/m^2.°C)	K×10^5 (m/s)	E_{corr}(V)	i_L(A/m^2)	i_{H2}(A/m^2)	i_{Fe}(A/m^2)
5000	61.92284	29.97816	770.8917	2.594005	-0.3230925	0.650291	10.25319	10.91055
10000	61.09735	52.83548	1357.13	4.69954	-0.3224717	1.202858	10.01782	11.22654
20000	60.3594	92.73059	2380.337	7.530859	-0.320938	2.209115	9.680938	11.89914
40000	60.3594	162.2232	4162.634	15.50031	-0.3180309	4.040401	9.161911	13.20805
60000	60.25965	224.7227	5765.574	21.98434	-0.3153973	5.74456	8.737431	14.49099

Table F-22: Results of pipe flow q_w=5000 W/m^2at T_b=60 ˚C, and pH=1 in aerated solutions.

Re	T_f(°C)	Nu	h(W/m^2.°C)	K×10^5 (m/s)	E_{corr}(V)	i_L(A/m^2)	i_{H2}(A/m^2)	i_{Fe}(A/m^2)
5000	63.20474	29.68187	764.6155	2.616251	-0.322522	0.634466	10.35439	10.99791
10000	61.82892	52.52512	1350.515	4.72336	-0.322161	1.186928	10.07728	11.27188
20000	61.0457	92.40529	2373.351	8.555963	-0.320795	2.192779	9.717505	11.91777
40000	60.599	161.8825	4155.26	15.52632	-0.317951	4.023446	9.183969	13.21357
60000	60.43275	224.3728	5757.971	22.0108	-0.315347	5.727163	8.754036	14.4907

Table F-23: Results of pipe flow under q_w=15000 W/m^2at T_b=60 ˚C, and pH=1 in aerated solutions.

Re	T_f(°C)	Nu	h(W/m^2.°C)	K×10^5(m/s)	E_{corr}(V)	i_L(A/m^2)	i_{H2}(A/m^2)	i_{Fe}(A/m^2)
5000	62.61422	28.14656	731.4333	2.705769	-0.3196979	0.545512	10.87058	11.42038
10000	65.48677	50.97164	1316.378	4.829929	-0.3206192	1.100972	10.38089	11.48729
20000	63.1371	90.73003	2337.794	8.673668	-0.319984	2.107193	9.899302	12.01489
40000	61.79699	160.1678	4118.021	15.65168	-0.317561	3.936282	9.2962	13.23645
60000	61.29826	222.6156	5719.677	22.13958	-0.315107	5.638398	8.838821	14.48434

Table F-24: Results of pipe flow under q_w=30000 W/m^2at T_b=60 ˚C, and pH=1 in aerated solutions.

Re	T_f(°C)	Nu	h(W/m^2.°C)	K×10^5(m/s)	E_{corr}(V)	i_L(A/m^2)	i_{H2}(A/m^2)	i_{Fe}(A/m^2)
5000	79.07742	27.00191	709.7638	2.914579	-0.3154822	0.411614	11.63717	12.05441
10000	70.88224	50.00537	1300.542	5.107722	-0.3183261	0.988444	10.82503	11.82133
20000	66.21912	90.18262	2331.226	9.02637	-0.3187266	2.015363	10.15847	12.18291
40000	63.56078	160.2566	4128.208	16.10805	-0.3168741	3.869764	9.444323	13.3209
60000	62.57185	223.3359	5745.647	22.68274	-0.314621	5.592389	8.943779	14.5414

F.4 Rotating cylinder

F.4.1 Rotating cylinder at T=25 ˚C

Table F-25: Results of rotating cylinder at T=25 ˚C and pH=1 in aerated acids solutions.

Re	K × 10^{-5}(m/s)	$E_{corr.}$ (V)	i_L(A/m^2)	i_{H2}(A/m^2)	i_{Fe}(A/m^2)
5000	1.660593	-0.3399871	0.7998463	7.50139	8.308228
10000	3.01404	-0.3386152	1.451752	7.303658	8.764175
20000	5.470598	-0.336232	2.6395	6.972465	9.919549
40000	9.929344	-0.3322266	4.782598	6.44932	11.23994
60000	0.1407211	-0.32808	6.778014	6.037891	12.82355

Table F-26: Results of rotating cylinder at T=25 ˚C and pH=2 in aerated acid solutions.

Re	K × 10^{-5}(m/s)	$E_{corr.}$ (V)	i_L(A/m^2)	i_{H2}(A/m^2)	i_{Fe}(A/m^2)
5000	1.660593	-0.4168529	0.804653	3.350937	4.163508
10000	3.01404	-0.4194059	1.46047	3.173513	4.642067
20000	5.470598	-0.4094328	2.65082	2.900131	5.558488
40000	9.929344	-0.4022887	4.81134	2.523498	7.341519
60000	0.1407211	-0.3967913	6.81874	2.267322	9.094226

Table F-27: Results of rotating cylinder at T=25 ˚C and pH=4 in aerated acids solutions.

Re	K × 10^{-5}(m/s)	$E_{corr.}$ (V)	i_L(A/m^2)	i_{H2}(A/m^2)	i_{Fe}(A/m^2)
5000	1.660593	-0.5631598	0.8075372	0.5786663	1.396161
10000	3.01404	-0.5544079	1.465711	0.4879968	1.963171
20000	5.470598	-0.5430024	2.660322	0.390897	3.060987
40000	9.929344	-0.5296944	4.828586	0.301595	5.19771
60000	0.1407211	-0.5213731	6.843187	0.2564804	7.106956

F.4.2 Rotating cylinder at T=40 ˚C

Table F-28: Results of rotating cylinder at T=40 ˚C, and pH=1 in aerated acids solutions.

Re	$K\times10^5$(m/s)	$E_{corr.}$ (V)	i_L(A/m^2)	i_{H2}(A/m^2)	i_{Fe}(A/m^2)
5000	1.94576	-0.3331261	0.75092	8.592713	9.353535
10000	3.531628	-0.3319345	1.33025	8.404971	9.776063
20000	6.410041	-0.3298405	2.73943	8.084933	10.56534
40000	0.116344	-0.3262656	4.4903	7.566483	12.0628
60000	0.164885	-0.3231915	6.3671	7.14714	13.5191

Table F-29: Results of rotating cylinder at T=40 ˚C and pH=2 in aerated acids solutions.

Re	$K\times10^5$(m/s)	$E_{corr.}$ (V)	i_L(A/m^2)	i_{H2}(A/m^2)	i_{Fe}(A/m^2)
5000	1.94576	-0.4142078	0.7565942	3.863198	4.627458
10000	3.531628	-0.4117359	1.373247	3.690162	5.071608
20000	6.410041	-0.407503	2.492497	3.416543	5.91647
40000	0.1163447	-0.4009849	4.523977	3.023326	7.555556
60000	0.164885	-0.3957778	6.411489	2.745119	9.164615

Table F-30: Results of rotating cylinder at T=40 ˚C and pH=4 in aerated acids solutions.

Re	$K\times10^5$(m/s)	$E_{corr.}$ (V)	i_L(A/m^2)	i_{H2}(A/m^2)	i_{Fe}(A/m^2)
5000	1.94576	-0.5695599	0.7599735	0.6882432	1.457984
10000	3.531628	-0.5613154	1.379381	0.5906931	1.979304
20000	6.410041	-0.5501602	2.50363	0.4803392	2.993232
40000	0.116344	-0.5367191	4.544184	0.3743938	4.92696
60000	0.164885	-0.528151	6.446125	0.3194069	6.769363

F.4.3 Rotating cylinder at T=60 ˚C

Table F-31: Results of rotating cylinder at T=60 ˚C and pH=1 in aerated acid solutions.

Re	$K \times 10^{-5}$(m/s)	$E_{corr.}$ (V)	i_L(A/m^2)	i_{H2}(A/m^2)	i_{Fe}(A/m^2)
5000	2.0738	-0.3231714	0.952571	9.963449	10.91602
10000	3.7641	-0.3215793	1.728954	9.690822	11.41978
20000	6.832	-0.3188155	3.138117	9.235175	12.37329
40000	0.124	-0.3141792	5.695802	8.518414	14.21422
60000	0.1757	-0.310284	8.072228	7.959395	16.03162

Table F-32: Results of rotating cylinder at T=60 ˚C and pH=2 in aerated acid solutions.

Re	$K \times 10^{-5}$(m/s)	$E_{corr.}$ (V)	i_L(A/m^2)	i_{H2}(A/m^2)	i_{Fe}(A/m^2)
5000	2.07383	-0.4089778	0.958743	4.443999	5.402742
10000	3.764081	-0.4057434	1.79849	4.200459	5.998949
20000	6.83195	-0.4003962	3.157893	3.826749	6.984642
40000	0.1240025	-0.3921829	5.731696	3.316454	9.04815
60000	0.1757393	-0.385918	8.123097	2.973462	11.09656

Table F-33: Results of rotating cylinder at T=60 ˚C and pH=4 in aerated acid solutions.

Re	$K \times 10^{-5}$(m/s)	$E_{corr.}$ (V)	i_L(A/m^2)	i_{H2}(A/m^2)	i_{Fe}(A/m^2)
5000	2.07383	-0.5720942	0.962176	0.762437	1.724613
10000	3.764081	-0.5620664	1.746386	0.6401997	2.3865857
20000	6.83195	-0.5491359	3.169758	0.5110467	3.6808047
40000	0.1240025	-0.5341356	5.753232	0.3934968	6.1467288
60000	0.1757393	-0.5247865	8.15362	0.3343406	8.4879606

F.5 Current density equivalent to corrosion rate of 1 gmd and mmy^{-1}

F.5.1 gmd and mmy^{-1} in smooth pipe flow with at T=25 °C and pH=1 and 4

Table F-34: Results of smooth pipe flow at pH=1 in aerated acids solutions.

T (°C)	25		40		60	
Re	gmd	mmy^{-1}	gmd	mmy^{-1}	gmd	mmy^{-1}
5000	204.1737	9.52037	204.2301	9.52317	273.9951	12.4599
10000	212.7075	9.91859	212.7662	9.92138	287.4131	12.8124
20000	228.7726	10.6674	228.7726	10.6674	312.8499	13.4727
40000	259.4825	12.0994	259.4825	12.0994	361.7308	14.7214
60000	289.4206	13.4955	289.4206	13.4955	409.7254	15.9296

Table F-35: Results of smooth pipe flow at pH=2 in aerated acids solutions.

T (°C)	25		40		60	
Re	gmd	mmy^{-1}	gmd	mmy^{-1}	gmd	mmy^{-1}
5000	100.4539	4.684129	115.504	5.38591	134.6891	6.280505
10000	109.3248	5.097776	126.6444	5.905383	147.5332	6.87942
20000	126.3925	5.893637	148.1261	6.907067	172.2594	8.032394
40000	159.837	7.453142	190.2442	8.871019	220.8486	10.29809
60000	192.89	8.994392	231.9618	10.8163	268.8904	12.53826

Table F-36: Results of smooth pipe flow at pH=4 in aerated acids solutions.

T (°C)	25		40		60	
Re	gmd	mmy^{-1}	gmd	mmy^{-1}	gmd	mmy^{-1}
5000	30.6501	1.42919	30.6501	1.42919	43.59792	2.0329
10000	41.03125	1.91326	41.03125	1.91321	60.2298	2.8085
20000	61.45735	2.8657	61.45735	2.86585	92.87504	4.33072
40000	101.044	4.71145	101.044	4.70959	155.6717	7.25883
60000	139.0651	6.48478	139.0651	6.48618	215.8097	10.0631

F.5.2 gmd and mmy^{-1} in pipe flow with relative roughness at T=25°C and pH=1, 2, and 4

Table F-37: Results of pipe flow with relative roughness at pH=1 in aerated acids solutions.

e/d	0.0001		0.0004		0.004	
Re	gmd	mmy^{-1}	gmd	mmy^{-1}	gmd	mmy^{-1}
5000	204.23	9.52317	204.31	9.5269	204.81	9.5502
10000	212.85	9.92511	213.1	9.93677	214.77	10.0146
20000	229.22	10.6884	229.85	10.7178	234.65	10.94164
40000	260.6	12.1516	262.52	12.2412	275.76	12.8585
60000	291.57	13.5958	295.46	13.7772	318.81	14.8659

Table F-38: Results of pipe flow with relative roughness at pH=2 in aerated acids solutions.

e/d	0.0001		0.0004		0.004	
Re	gmd	mmy^{-1}	gmd	mmy^{-1}	gmd	mmy^{-1}
5000	100.49	4.66207	100.572	4.66517	101.16	4.69308
10000	109.49	5.07973	109.709	5.689627	111.47	5.17169
20000	126.83	5.88417	127.531	5.91643	132.75	6.15891
40000	161.088	7.47327	163.238	7.57296	177.79	8.24814
60000	195.23	9.05791	199.624	9.26097	225.45	10.4591

Table F-39: Results of pipe flow with relative roughness at pH=4 in aerated acids solutions.

e/d	0.0001		0.0004		0.004	
Re	gmd	mmy^{-1}	gmd	mmy^{-1}	gmd	mmy^{-1}
5000	30.723	1.4326025	30.795	1.4359599	31.488	1.4682742
10000	41.226	1.9223537	41.468	1.9336381	43.607	2.0333789
20000	62.014	2.8916907	62.793	2.9280152	69.034	3.2190308
40000	102.52	4.7804711	105.03	4.8975115	121.85	5.6818221
60000	141.75	6.609752	146.65	6.8382373	175.6	8.1881655

F.5.3 gmd and mmy^{-1} in pipe flow with relative roughness at T=40°C and pH=1,2, and 4

Table F-40: Results of pipe flow with relative roughness at pH=1 in aerated acids solutions.

e/d	0.0001		0.0004		0.004	
Re	gmd	mmy^{-1}	gmd	mmy^{-1}	gmd	mmy^{-1}
5000	231.21	10.78124	231.36	10.78823	231.81	10.80922
10000	239.78	11.18086	239.96	11.18925	241.66	11.26852
20000	255.97	11.93579	256.54	11.96237	261.35	12.18666
40000	286.98	13.38177	288.91	13.47177	301.96	14.08029
60000	317.48	14.80398	312.39	14.56663	344.37	16.05785

Table F-41: Results of pipe flow with relative roughness at pH=2 in aerated acids solutions.

e/d	0.0001		0.0004		0.004	
Re	gmd	mmy^{-1}	gmd	mmy^{-1}	gmd	mmy^{-1}
5000	113	5.26915	113.04	5.271015	113.63	5.298526
10000	121.94	5.686019	122.12	5.694412	123.9	5.777413
20000	139.07	6.484784	139.74	6.516026	144.86	6.75477
40000	172.8	8.057602	174.93	8.156923	189.33	8.82839
60000	206.51	9.629488	210.77	9.82813	236.22	11.01485

Table F-42: Results of pipe flow with relative roughness at pH=4 in aerated acids solutions.

e/d	0.0001		0.0004		0.004	
Re	gmd	mmy^{-1}	gmd	mmy^{-1}	gmd	mmy^{-1}
5000	33.329	1.554119	33.39	1.556964	34.067	1.588532
10000	43.688	2.037156	43.916	2.047787	46.019	2.14585
20000	64.206	2.993903	64.973	3.029668	71.161	3.318212
40000	104.39	4.867668	106.9	4.984709	123.64	5.765289
60000	143.44	6.688556	148.32	6.916109	177.18	8.26184

F.5.4 gmd and mmy^{-1} in pipe flow with relative roughness at T=60°C and pH=1, 2, and 4

Table F-43: Results of pipe flow with relative roughness at pH=1 in aerated acids solutions.

e/d	0.0001		0.0004		0.004	
Re	gmd	mmy^{-1}	gmd	mmy^{-1}	gmd	mmy^{-1}
5000	274.102	12.78128	274.197	12.78575	275.0603	12.825
10000	287.726	13.4165	288.02	13.4306	290.652	13.553
20000	313.518	14.6192	314.504	14.6652	322.170	15.022
40000	363.517	16.9507	366.703	17.0992	387.761	18.081
60000	413.044	19.2601	419.289	19.5513	456.716	21.296

Table F-44: Results of pipe flow with relative roughness at pH=2 in aerated acids solutions.

e/d	0.0001		0.0004		0.004	
Re	gmd	mmy^{-1}	gmd	mmy^{-1}	gmd	mmy^{-1}
5000	134.78	6.284743	134.88	6.289406	135.73	6.329041
10000	147.79	6.891395	148.05	6.903519	150.66	7.025222
20000	172.92	8.063198	173.89	8.108429	181.45	8.460949
40000	222.63	10.38116	225.84	10.53084	246.94	11.51472
60000	272.29	12.69679	278.63	12.99242	316.15	14.74196

Table F-45: Results of pipe flow with relative roughness at pH=4 in aerated acids solutions.

e/d	0.0001		0.0004		0.004	
Re	gmd	mmy^{-1}	gmd	mmy^{-1}	gmd	mmy^{-1}
5000	43.737	2.039441	43.844	2.04443	44.944	2.095723
10000	60.57	2.824357	60.93	2.841144	64.362	3.001177
20000	93.725	4.370363	95.01	4.430282	104.95	4.893781
40000	158.03	7.368882	162.05	7.556334	188.62	8.795283
60000	220.08	10.26225	227.81	10.6227	273.43	12.74994

F.5.5 gmd and mmy^{-1} in smooth pipe flow under q_W=3000, 5000, 15000, and 30000 W/m^2

Table F-46: Results of Pipe flow under q_W=3000 W/m^2, at pH=1 in aerated acids solutions.

T(°C)	25		40		60	
Re	gmd	mmy^{-1}	gmd	mmy^{-1}	gmd	mmy^{-1}
5000	212.1809	9.8938778	239.0313	11.145884	272.8106	12.721033
10000	224.3335	10.460428	250.3013	11.6714	280.7118	13.089407
20000	249.0332	11.61218	273.3047	12.743882	297.5297	13.873718
40000	297.4981	13.872319	318.5672	14.854806	330.2582	15.399906
60000	345.5373	16.112407	362.9276	16.923297	362.3372	16.895785

Table F-47: Results of Pipe flow under q_W=5000 W/m^2, at pH=1 in aerated acids solutions.

T(°C)	25		40		60	
Re	gmd	mmy^{-1}	gmd	mmy^{-1}	gmd	mmy^{-1}
5000	213.7701	9.968019	241.0057	11.23821	274.9951	12.823152
10000	225.1037	10.496333	251.4509	11.725024	281.8455	13.142565
20000	249.2979	11.62477	273.9667	12.775124	297.9957	13.895634
40000	297.6215	13.877915	318.8464	14.867862	330.3961	15.406434
60000	345.4425	16.107744	363.1693	16.934488	362.3299	16.895319

Table F-48: Results of pipe flow under q_W=15000W/m^2, at pH=1 in aerated acids solutions.

T(°C)	25		40		60	
Re	gmd	mmy^{-1}	gmd	mmy^{-1}	gmd	mmy^{-1}
5000	221.563	10.331264	250.8902	11.698911	285.5587	13.315561
10000	229.046	10.680054	256.9052	11.979622	287.2316	13.393433
20000	250.9101	11.699844	277.0746	12.919675	300.4241	14.008478
40000	297.8872	13.890505	320.4786	14.943868	330.9683	15.433013
60000	345.2491	16.098418	364.3727	16.990443	362.1708	16.887858

Table F-49: Results of pipe flow under q_W=30000W/m^2, at pH=1 in aerated acids solutions.

T(°C) Re	25		40		60	
	gmd	mmy^{-1}	gmd	mmy^{-1}	gmd	mmy^{-1}
5000	233.2847	10.877763	265.3883	12.375041	301.4123	14.054641
10000	237.7565	10.946775	265.0071	12.357322	295.5842	13.78279
20000	253.315	11.812221	281.4273	13.122981	304.6251	14.204788
40000	298.2259	13.906359	322.9232	15.057645	333.0798	15.531402
60000	344.7358	16.075103	366.0409	17.068315	363.5977	16.954538

F.5.6 gmd and mmy^{-1} of Rotating cylinder at pH=1, 2, and 4

Table F-50: Results of rotating cylinder at pH=1 in aerated acids solutions.

T(°C) Re	25		40		60	
	gmd	mmy^{-1}	gmd	mmy^{-1}	gmd	mmy^{-1}
5000	207.74	9.6868422	233.88	10.905741	277.08	12.920142
10000	219.14	10.21842	244.44	11.39815	292.89	13.657356
20000	240.46	11.212564	264.18	12.318619	322.51	15.038526
40000	281.05	13.105261	301.62	14.064433	379.06	17.675433
60000	320.64	14.951329	338.04	15.762685	434.18	20.245659

Table F-51: Results of rotating cylinder at pH=2 in aerated acids solutions.

T(°C) Re	25		40		60	
	gmd	mmy^{-1}	gmd	mmy^{-1}	gmd	mmy^{-1}
5000	104.11	4.8546122	115.71	5.3955161	139.28	6.4945768
10000	116.07	5.4123028	126.81	5.9131051	155.9	7.2695615
20000	138.99	6.4810542	147.94	6.8983895	187.83	8.758446
40000	183.57	8.5598037	188.92	8.8092723	250.08	11.661141
60000	227.39	10.603115	229.15	10.685183	311.1	14.506482

Table F-52: Results of rotating cylinder at pH=4 in aerated acids solutions.

T(°C) Re	25		40		60	
	gmd	mmy^{-1}	gmd	mmy^{-1}	gmd	mmy^{-1}
5000	24.91	1.1615444	36.456	1.6999303	47.318	2.2064215
10000	49.088	2.288956	49.491	2.3077477	67.112	3.1294087
20000	76.538	3.5689397	74.844	3.4899491	105.32	4.9110341
40000	128.52	5.9928418	123.2	5.7447721	177.64	8.2832899
60000	177.7	8.2860877	169.26	7.8925335	246.07	11.474156

F.6 Sample of Calculations

F.6.1 General Calculation

This Sample of Calculations at T=25 °C, pH=1, and Re=10000

$$[H^{+}] = 10^{-pH}$$

$$[H^{+}] = 10^{-1} = 0.1$$

Standard potentials are -0.44, 0, and 1.229 Volt for iron, hydrogen, and oxygen respectively as given in table A-4 in appendix A, numbers of electrons are n_{Fe}=2, n_{H2}=1, and n_{O2}=4, Alpha are α_{Fe}=0.5 **[Uhlig and Winston, 2008]**, α_{H2}=0.5, **[Nesic, et. al., 1996]**, the diameter of rotating cylinder and pipe flow is 0.0255 m, and the exchange current density are $i_o^{(Fe^{+2}/Fe)}=10^{-4}$ (A/m^2) at temperature of 25 ºC **[Uhlig and Winston, 2008]**, and $i_o^{(H^{+}/Fe)}=10^{-3}$ (A/m^2) at temperature of 25 ºC **[Roberge, 2000]** as given in table A-4 in appendix A.

Equilibrium Potential

$$E = E^{\circ} - \frac{2.303RT}{nF}\log\left(\frac{a_{red}}{a_{oxid}}\right)$$

$[Fe^{+2}]$ =3.5×10^{-5}M, $[O_2]$ 10^{-10} M **[west, 1976]**, and $[H^{+2}] = 10^{(-pH)}$

$$E_{eq}^{Fe} = E_{Fe}^{\circ} - \frac{2.303RT}{nF}\log\left(\frac{1}{3.5\times10^{-5}}\right) \Longrightarrow E_{eq}^{Fe} = -0.5717291 \text{ volt}$$

$$E_{eq}^{H_2} = E_{H_2}^{\circ} - \frac{2.303RT}{nF}\log\left(\frac{1}{0.1}\right) \Longrightarrow E_{eq}^{H_2} = -0.059 \text{ volt}$$

$$E_{eq}^{O_2} = E_{O_2}^{\circ} - \frac{2.303RT}{nF}\log\left(\frac{1}{0.1}\right) \Longrightarrow E_{eq}^{O_2} = 1.254678 \text{ volt}$$

Tafel slopes are determined from the following equations:

$$b_a = \frac{RT}{\alpha nF} \Rightarrow b_a = \frac{8.314\times298}{0.5\times2\times96487} \Longrightarrow b_a = 0.02512 \text{ V}\backslash\text{decade}$$

$$b_c = \frac{RT}{(1-\alpha)nF} \Longrightarrow \frac{8.314\times298}{(1-\alpha)nF} \Longrightarrow b_c = 0.01256 \text{ V}\backslash\text{decade}$$

The enthalpy of activation for the H^+ reduction reaction is $\Delta H_{[H^+]} = 30000$ J/mol, and for iron $\Delta H_{[Fe^{+2}]} = 2625$ J/mol for temperatures 20 to 60 °C **[Nesic et. al., 1996]**.

Exchange current density for H_2 **[Nesic et. al., 1996]**:

$$\frac{\partial \log i_o^{H^+}}{\partial pH} = \frac{\log i_{o(2)}^{H^+} - \log i_{o(1)}^{H^+}}{pH_2 - pH_1} = -0.5$$

$$i_{o(2)}^{H^+} = i_{o(1)}^{H^+} \times 10^{-0.5(pH_2-pH_1)} \Longrightarrow i_{o(2)}^{H^+} = 10^{-3} \times 10^{-0.5(1-4)} \Longrightarrow i_{o(2)}^{H^+} = 10^{-1.5}$$

The exchange current density was modeled with an Arrhenius Equation:

$$\frac{i_o}{i_o^{ref}} = e^{-\left(\frac{\Delta H}{R}\right)}\left[\frac{1}{T} - \frac{1}{T_{ref}}\right]$$

$$\frac{i_{o_{H_2}}}{i_{o(2)}^{H^+}} = e^{-\left(\frac{30000}{8.314}\right)}\left[\frac{1}{298} - \frac{1}{298}\right] \Longrightarrow i_{o_{H_2}} = i_{o(2)}^{H^+} = 10^{-1.5} \text{ A/m}^2$$

Exchange current density for Fe **[Nesic et. al., 1996]**:

$$\frac{\partial \log i_0^{Fe}}{\partial pH} = \frac{\log i_{0(2)}^{Fe} - \log i_{0(1)}^{Fe}}{pH_2 - pH_1} = 1$$

$$i_{0(2)}^{Fe} = i_{0(1)}^{Fe} \times 10^{(pH_2-pH_1)} \Longrightarrow i_{0(2)}^{Fe} = 10^{-4} \times 10^{(1-0)}$$

$$i_{0(2)}^{Fe} = 10^{-3} \text{ A/m}^2$$

By Arrhenius Equation:

$$\mathrm{i_{0_{Fe}}} = \mathrm{i_{0(2)}^{Fe}} \times \mathrm{e}^{-\left(\frac{2625}{8.314}\right)\left[\frac{1}{298}-\frac{1}{298}\right]} \Rightarrow \mathrm{i_{0_{Fe}}} = \mathrm{i_{0(2)}^{Fe}} = 10^{-3}\ \mathrm{A/m^2}$$

F.6.2 Smooth Pipe

The Physical Properties of Water at Atmospheric Pressure from table A-5 in appendix A **[Perry, 2008]**. The values of oxygen diffusivity from table A-2 in appendix A **[Perry, 2008]**. The solubility of oxygen in HCl (mol/m^3) from table A-3 in appendix A **[Shreir, 1994]**

$$\mathrm{Sc} = \frac{\mu}{\mathrm{D}\rho} \Rightarrow \mathrm{Sc} = \frac{0.00088}{996\times2.41\times10^{-9}} \Rightarrow \mathrm{Sc} = 366.6117$$

The friction factor equation calculated from Blasius equation:

$$f = 0.0079Re^{(-1/4)} \Rightarrow f = 0.0079 \times 10000^{(-1/4)} \Rightarrow f = 7.9 \times 10^{-3}$$

From Sherwood (Eq. 4.43) number calculate the mass transfer coefficient:

$$\mathrm{Sh} = \frac{\mathrm{K\times d}}{\mathrm{D}} = 0.0889\sqrt{(\mathrm{f}/2)}\ \mathrm{Re\ Sc^{0.246}}$$

$$\mathrm{K} = \left(\frac{\mathrm{D}}{\mathrm{d}}\right) \times 0.0889\sqrt{(\mathrm{f}/2)}\ \mathrm{Re\ Sc^{0.246}}$$

$$K = \left(\frac{2.41\times10^{-9}}{0.0255}\right) \times 0.0889 \times \sqrt{(7.9\times10^{-3}/2)} \times 10000 \times 366.6117^{\,0.246}$$

$$K = 2.25669 \times 10^{-5}\ \mathrm{m/sac}$$

Then the limiting current density is calculated from:

$$\mathrm{i_L} = -\mathrm{zFKC_b}$$

$$\mathrm{i_L} = -4 \times 96487 \times 2.25669 \times 10^{-5} \times 0.1248 \Rightarrow \mathrm{i_L} = 1.086964\ A/m^2$$

To determine $\mathrm{i_{corr}}$ using Eq. (4.59) and (4.60):

$$\mathrm{i_{corr}} = \mathrm{i_o^{Fe}}\exp\left(\frac{\mathrm{E_{corr}}-\mathrm{E_{eq}^{Fe}}}{\mathrm{b_a}}\right) \qquad \ldots (4.59)$$

$$i_{corr} = i_o^{H_2} \exp\left(\frac{E_{corr} - E_{eq}^{H_2}}{b_c}\right) \quad \ldots (4.60)$$

Assume E_{corr}= -0.339 and subs in Eq. (4.59) and Eq. (4.60):

$$i_{Fe} = 10^{-3} \exp\left(\frac{-0.339-(-0.5717291)}{0.02512}\right) \Longrightarrow i_{Fe} = 8.631011837\ A/m^2$$

$$i_{H_2} = 10^{-1.5} \exp\left(\frac{-0.339-(-0.059)}{0.01256}\right) \Longrightarrow i_{H_2} = 7.34886\ A/m^2$$

At E_{corr}, $i_a = i_c = i_{corr}$ and $E_a = E_c = E_{corr}$ then

$$\Sigma i_a = \Sigma i_c \Longrightarrow i_{Fe} = i_{H_2} + i_L$$

$$i_{Fe} - \left(i_{H_2} + i_L\right) = 0 \Longrightarrow 8.631011837 - (7.34886 + 1.086964) = 0.19$$

New E_{corr} is assumed until $\Sigma i_a \cong \Sigma i_c$ then Ecorr will be the true E_{corr} and $i=i_{corr}$. By used trial and error the i_{corr}=8.508236 A/m^2 subs. In equation (4.57) to obtain E_{corr}

$$E_{corr} = E_{eq}^{Fe} + \beta_a \log\left(\frac{i_{corr}}{i_o^{Fe}}\right) \quad \ldots (4.57)$$

$$E_{corr} = -0.5717291 + 2.303 \times 0.02512 \log\left(\frac{8.508236}{10^{-3}}\right)$$

$$E_{corr} = -0.3393763\ \mathrm{V}$$

F.6.3 Rough Pipe

The friction factor equation calculated from Chen equation (Eq. 4.44) by taking the relative roughness of 0.004:

$$f = 0.0791\left[\frac{1}{Re^{0.83}} + 0.11\left(\frac{e}{d}\right)\right]^{0.3}$$

$$f = 0.0791\left[\frac{1}{(10000)^{0.83}} + 0.11(0.004)\right]^{0.3}$$

$$f = 9.707752 \times 10^{-3}$$

$$Sc = \frac{\mu}{D\rho} \Longrightarrow Sc = \frac{0.00088}{996 \times 2.41 \times 10^{-9}} \Longrightarrow Sc = 366.6117$$

The Sherwood number is calculated via Eq. 4.43

$$\mathrm{Sh} = 0.0889\sqrt{(\mathrm{f}/2)}\ \mathrm{Re}\ \mathrm{Sc}^{0.246}$$

$$\mathrm{Sh} = 0.0889\sqrt{(9.707752 \times 10^{-3}/2)}\ \times 10000 \times\ 366.6117^{\ 0.246}$$

Sh=264.6920239

The mass transfer coefficient is calculated from Sherwood number:

$$K = \frac{Sh \times D}{d} \Longrightarrow K = \frac{264.6920239 \times 2.41 \times 10^{-3}}{0.0255}$$

$K=2.51599\times10^{-5}$ m/s

$$\mathrm{i_L} = -\mathrm{zFKC_b}$$

$$\mathrm{i_L} = -4 \times 96487 \times 2.51599 \times 10^{-5} \times 0.1248 \Longrightarrow \mathrm{i_L} = 1.204928 A/m^2$$

Assume E_{corr}= -0.339 and subs in Eq.1 and Eq.2:

$$\mathrm{i_{Fe}} = 10^{-3}\exp\left(\frac{-0.339-(-0.5717291)}{0.02512}\right) \Longrightarrow \mathrm{i_{Fe}} = 8.631011837\ A/m^2$$

$$\mathrm{i_{H_2}} = 10^{-1.5}\exp\left(\frac{-0.339-(-0.059)}{0.01256}\right) \Longrightarrow \mathrm{i_{H_2}} = 7.34886\ A/m^2$$

At E_{corr}, $i_a = i_c = i_{corr}$ and $E_a = E_c = E_{corr}$ then

$$\Sigma i_a = \Sigma i_c \ \Longrightarrow\ i_{Fe} = i_{H_2} + i_L$$

$$i_{Fe} - \left(i_{H_2} + i_L\right) = 0 \Longrightarrow 8.631011837 - (7.34886 + 1.204928\,) = 0.07722$$

Assume new E_{corr} by used trial and error the i_{corr}=8.5892 A/m^2 subs. In Eq. (4.57) to obtain E_{corr}

$$E_{corr} = \mathrm{E_{eq}^{Fe}} + \beta_a \log\left(\frac{i_{corr}}{\mathrm{i_o^{Fe}}}\right) \qquad \dots (4.57)$$

$$E_{corr} = -0.5717291 + 2.303 \times 0.02512 \log\left(\frac{8.5892}{10^{-3}}\right)$$

$$E_{corr} = -0.3391331 \text{ volt}$$

F.6.4 Smooth Pipe Corrosion in Presence of Heat Flux

At T_b=25 ºC, pH=1, Re=10000, and q_w=3000

The physical properties at T=25 are:

Cp = 4.179 kJ/kg.ºC; μ = 8.960431 $\times10^{-4}$ kg/m.s; Pr = 6.129334; k= 0.6109964 W/m.ºC; ρ = 996.2806 kg/m^3

The friction factor is calculated from Blasius equation (Eq. 4.42):

$$f = 0.0079Re^{(-1/4)} \Rightarrow f = 0.0079 \times 10000^{(-1/4)} \Rightarrow f = 7.9 \times 10^{-3}$$

Nusselt number is calculated from Friend-Metzner equation (Eq. 4.45) for 0.5< Pr < 600 and Re > 10000:

$$\mathrm{Nu} = \frac{\mathrm{RePr}\left(^{\mathrm{f}}/_{2}\right)}{1.2+11.8\left(\frac{\mathrm{f}}{2}\right)^{1/2}(\mathrm{Pr}-1)\mathrm{Pr}^{-1/3}}$$

$$\mathrm{Nu} = \frac{10000\times6.129334\times(7.9\times10^{-3}/2)}{1.2+11.8\times(7.9\times10^{-3}/2)^{1/2}(6.129334-1)\times6.129334^{-1/3}}$$

Nu= 73.8452

$$\mathrm{h} = \frac{\mathrm{Nu\,K}}{\mathrm{d}} \Rightarrow \mathrm{h} = \frac{73.8452\times0.6109964}{0.0255} = 1769.379\ \mathrm{W/m^2.{}^{\circ}C}$$

The surface temperature is calculated from heat flux as:

$$T_W = \frac{q_W}{h} + T_b \Rightarrow T_W = \frac{3000}{1769.379} + 25 \Rightarrow T_W = 26.69551\ ^{\circ}\mathrm{C}$$

The film temperature is:

$$T_f = \frac{T_W+T_b}{2} \Rightarrow T_f = \frac{26.69551+25}{2} \Rightarrow T_f = 25.84776\ ^{\circ}\mathrm{C}$$

The physical properties at T=25.84776 °C are:

Cp = 4.179kJ/kg. ºC; μ = 8.777463$\times10^{-4}$ kg/m.s; Pr = 5.987534; k=0.6125212W/m. ºC; ρ = 996.0366 kg/m^3; C_b=0.1245984; D=2.366571$\times10^{-9}$ by Substituting physical properties in Nu equation becomes:

Nu=73.06459 and h= 1755.043W/m^2.°C

$$\mathrm{Sc} = \frac{\mu}{\mathrm{D}\rho} \Rightarrow \mathrm{Sc} = \frac{8.777463\times10-4}{996.0366\times2.41\times10^{-9}} \Rightarrow \mathrm{Sc} = 372.3695$$

The exchange currents densities for H_2 and Fe 3.272785×10^{-2} and 1.003009×10^{-3} respectively.

The equilibrium potential for H_2 and Fe become -5.929348×10^{-2} Volt and -0.5721039 Volt respectively.

The Sherwood number from (Eq. 4.49) is:

$$\mathrm{Sh} = \frac{\mathrm{K}\times\mathrm{d}}{\mathrm{D}} = \frac{ReSc\left({}^{f}/_{2}\right)}{1.2+11.8\left({}^{f}/_{2}\right)^{1/2}(Sc-1)Sc^{-1/3}}$$

$$\mathrm{K} = \left(\frac{\mathrm{D}}{\mathrm{d}}\right)\times\frac{ReSc\left({}^{f}/_{2}\right)}{1.2+11.8\left({}^{f}/_{2}\right)^{1/2}(Sc-1)Sc^{-1/3}}$$

$$K = \left(\frac{2.366571\times10^{-9}}{0.0255}\right)\times\frac{10000\times372.3695\times\left({}^{7.9\times10^{-3}}/_{2}\right)}{1.2+11.8\times\left({}^{7.9\times10^{-3}}/_{2}\right)^{1/2}\times(372.3695-1)\times372.3695^{-1/3}}$$

$$K = 3.457408\times10^{-5}\ \mathrm{m/s}$$

Then the limiting current density is calculated from:

$$\mathrm{i_L} = -\mathrm{zFKC_b}$$

$$\mathrm{i_L} = -4\times96487\times3.457408\times10^{-5}\times0.1248 \Longrightarrow \mathrm{i_L} = 1.662616\ \mathrm{A/m^2}$$

$$\mathrm{b_a} = \frac{\mathrm{RT}}{\alpha\mathrm{nF}} \Rightarrow \mathrm{b_a} = \frac{8.314\times298.84776}{0.5\times2\times96487} \Longrightarrow \mathrm{b_a} = 2.569766\times10^{-2}$$

$$\mathrm{b_c} = \frac{\mathrm{RT}}{(1-\alpha)\mathrm{nF}} \Longrightarrow \frac{8.314\times298.84776}{(1-\alpha)\mathrm{nF}} \Longrightarrow \mathrm{b_c} = 5.13953\times10^{-2}$$

To determine i_{corr} use the equations (4.59) and (4.60) and assume E_{corr}= - 0.3378 and subs in Eq. (4.59) and Eq. (4.60):

$$\mathrm{i_{Fe}} = 1.003009\times10^{-3}\exp\left(\frac{-0.3378-(-0.5721039)}{2.569766\times10^{-2}}\right)$$

$$\mathrm{i_{Fe}} = 9.14276\,\frac{\mathrm{A}}{m^2}$$

$\mathrm{i_{H_2}} = 3.272785 \times 10^{-2} \exp\left(\frac{-0.3378 - (-5.929348\times10^{-2})}{5.13953\times10^{-2}}\right)$

$\mathrm{i_{H_2}} = 7.426774\ A/m^2$

At E_{corr}, $i_a = i_c = i_{corr}$ and $E_a = E_c = E_{corr}$ then

$\Sigma i_a = \Sigma i_c \implies i_{Fe} = i_{H_2} + i_L$

$i_{Fe} - \left(i_{H_2} + i_L\right) = 0 \Rightarrow 9.14276 - (7.426774 + 1.662616) = 0.0533$

By trial and error to find $i_{corr} = 8.971794$ A/m^2 substitution in equation (4.57) to obtain E_{corr}

$$E_{corr} = \mathrm{E_{eq}^{Fe}} + \beta_a\, log\left(\frac{i_{corr}}{\mathrm{i_o^{Fe}}}\right) \qquad \ldots (3)$$

$E_{corr} = -0.5717291 + 2.303 \times 0.02512\, log\left(\frac{8.971794}{10^{-3}}\right)$

$E_{corr} = -0.3378013\ \mathrm{V}$

الخُلاصة

تم أجراء حسابات نظرية بأستخدام برنامج حاسوبي على تاكل انبوب والإسطوانة الدواره من الحديد الكاربوني في حامض الهيدروكلوريك الحاوي على الاوكسجين الذائب تحت ظروف الجريان المضطرب عدد رينولدز 5000, 10000, 20000, 40000, 60000 ودرجة حرارة 25, 40, 60 والاس الهيدروجيني للحامض 1,2,4 تمت دراسة ومناقشة: تأثير عدد رينولد (او السرعة) ,درجة الحرارة ,الاس الهيدروجيني, خشونة السطح (e/d) و الفيض الحراري على معدل التأكل وجهد التأكل.

دلت النتائج على ان الزيادة في عدد رينولدز والحرارة تزيد معدل التأكل وجهد التأكل أما الزيادة في الاس الهيدروجيني تقلل من معدل التأكل وجهد التأكل.

دلت النتائج على ان خشونة السطح او معامل الاحتكاك تزيد من نسبة التأكل وجهد التأكل للانبوب الحديدي.

دلت النتائج على ان الزيادة في الفيض الحراري تزيد من معدل التأكل وجهد التأكل وذلك بسبب تأثيرها على درجة حرارة الجدار التي بدورها تؤثر على حرارة المحلول المار وان التغير بالحرارة يوثر على الخواص الفيرياويه للسائل وبالأخص تؤثر على انتشار الأوكسجين في المحلول وقابلية ذوبانهُ.

تم الأستفادة من النتائج بأدخالها في برنامج (Basic Statistics Tables) واستنتاج موديلات رياضية لحساب معدل التاكل من خلال الظروف التشغيلية:

تم حساب علاقه للانبوب ناعم الجدار والاسطوانه الدواره ناعمة السطح للظروف المذكوة فأعطت العلاقات التاليه على التوالي:

تم الحصول على علاقة لمعدل التأكل للانبوب ناعم الجدار نسبة الخطأ 6.51٪:

$$\mathrm{C.R(gmd)} = 10.20697\ \mathrm{Re}^{0.208226}\ \mathrm{T}^{0.312849}\ \mathrm{pH}^{-0.70156}$$

وللاسطوانه الدواره تم الحصول على العلاقة التاليه وبنسبة خطأ 6.31٪:

$$\mathrm{C.R(gmd)} = 5.53953\ \mathrm{Re}^{0.260848}\ \mathrm{T}^{0.364818}\ \mathrm{pH}^{-0.68343}$$

تم الحصول على علاقه بدلالة معامل الاحتكاك للانبوب الخشن الجدار الداخلي وحساب معدل التأكل بنسبة خطأ 3.74٪:

$$\mathrm{C.R(gmd)} = 18.2175\ \mathrm{Re}^{0.269075}\ \mathrm{T}^{0.300839}\ \mathrm{pH}^{-0.68342}\ f^{0.224908}$$

تم اشتقاق علاقة نظريه تربط عدد رينولد للانبوب مع عدد رينولدز الأسطوانه الدائرة:

$$Re_P = 247.889 \left(\frac{d_P}{d_R}\right)^{\left(8/_7\right)} \frac{Re_R^{0.6971}}{Sc^{0.38095}}$$

نسبة الخطأ لهذهِ المعادلة هي 5.35٪.

شكر وتقدير

بعد شكر الله عز وجل اود أن أتقدم بأسمى أيات الشكر والتقدير للدكتور قاسم جابر محمد مشرفا" والدكتور باسم عبيد حسن مشرفا" لما بذلاه من مجهود لأعطاء هذا الناتج العلمي.

أتقدم بالشكر للدكتور قاسم جابر محمد رئيس قسم الهندسة الكيمياويه

أتقدم بالشكر التقدير الكبيرين الى من كانا الدافع وراء حصولي على شهادة الماجستير امي وابي.

الى من كانوا معي خطوة" بخطوة اخوتي واخواتي.

من رافقوا دربي اصدقائي.

المحاكاة النظرية لدراسة تآكل الحديد في الحوامض الحاوية على الأوكسجين

رسالة

مقدمة الى كلية الهندسة في جامعة النهرين

وهي جزء من متطلبات نيل درجة ماجستير علوم

في الهندسة الكيمياوية

من قبل

إيثار مقصود جسار

(بكالوريوس علوم في الهندسة الكيمياوية ٢٠٠٦)

شوال **١٤٣٠**

أيلول **٢٠٠٩**